

NASA TM X- 70629

X-661-74-27

PREPRINT

A CATALOGUE OF SOLAR
COSMIC RAY EVENTS
IMPS IV AND V
(MAY 1967-DEC. 1972)

M. A. VAN HOLLEBEKE

J. R. WANG

F. B. McDONALD

JANUARY 1974

(NASA-TM-X-70629) A CATALOGUE OF SOLAR
COSMIC RAY EVENTS: IMPS 4 AND 5, MAY
1967 - DECEMBER 1972 (NASA) —
1/3 CSCL 03B

00/29 39397

Reproduced by
NATIONAL TECHNICAL
INFORMATION SERVICE
US Department of Commerce
Springfield, VA 22151

GSFC

GODDARD SPACE FLIGHT CENTER
GREENBELT, MARYLAND

PRICES SUBJECT TO CHANGE

X-661-74-27

A CATALOGUE OF SOLAR COSMIC RAY EVENTS

IMPS IV AND V

(MAY 1967 - DEC. 1972)

M. A. VAN HOLLEBEKE*
J. R. WANG**
F. B. McDONALD

JANUARY 1974

*Department of Physics and Astronomy, University of Maryland, College Park, Maryland

**Now at Department of Physics, Columbia University, New York, New York

GODDARD SPACE FLIGHT CENTER
GREENBELT, MARYLAND

INTRODUCTION

This catalogue of solar cosmic ray events has been prepared for the use of solar physicists and other interested scientists. It contains some 185 solar particle events detected by the Goddard Space Flight Center Cosmic Ray Experiments on IMP's IV and V (Explorer 34 and 41) for the period May 1967 - December 1972. An event is defined as an increase in the flux of 20-80 Mev protons which exceeds 10^{-4} Protons/cm²-sec-sr-MeV and lasts for more than 5 hours. The threshold is a function of the detector sensitivity and background. The minimum increase over this energy range corresponds to about 5% of the total galactic cosmic ray intensity at 1 AU. The data is presented in the form of hourly averages for three proton energy intervals - 0.9 - 1.6 MeV; 6 - 20 MeV and 20 - 80 MeV. In addition the time histories of .5 - 1.1 MeV electrons are shown on a separate scale. To assist in the identification of related solar events, the onset time of the electron event is indicated. The details of the instrumentation and detector techniques are described in Section I. Further descriptions of data reduction procedure and on the time-history plots are given in Section II.

I. Detector System and Satellite Instrumentation

The Cosmic Ray Detector System described here used two dE/dx vs. E telescopes which covered the energy ranges 20 - 80 MeV/nucleon and 4 - 20 MeV/nucleon. The experiments flown on IMP's IV and V were essentially identical.

The dE/dx vs. E telescope is of greatest importance in studying low energy cosmic rays (i.e. < 100 MeV). This device measures two parameters for a given charged particle passing through the telescope which makes it possible to determine the energy of the particle and its charge and mass. A schematic of such a device is shown in Figure 1. The basic features of any such telescope are the three separate detectors labeled A, B, and C in the diagram.

Consider a particle having a trajectory such as the one labeled 2 in the schematic. The range of this particle would be greater than the thickness of A, but less than the thickness of A and B taken together. Such a trajectory may be termed a stopping trajectory as opposed to penetrating trajectories such as the tracks labeled 3 and 4. Detector A is usually about 5 - 10% of the thickness of B. As a charged particle of kinetic energy E penetrates detector A it deposits an amount of energy ΔE . It then enters B and comes to rest giving up the remainder of its kinetic energy ($E - \Delta E$) therein. The energy deposited in each of these detectors produces electrical signals which may be amplified and analyzed. For example, if A and B are made of scintillator material the number of photons emitted will be proportional to the energy deposited and hence can be detected and amplified by means of photomultiplier tubes looking at each detector. The measurement of ΔE and $E - \Delta E$ can indeed determine the charge and mass of the particle. The plots of several of these relations are shown in Figure 2. The solid curves represent the ΔE versus $E - \Delta E$ responses for stopping particles, while the dashed curves show the continuation of the response for penetrating particles. The stopping particle events are identified by the logic requirement ABC. In Figure 1 it is seen that of the four tracks shown only track 2 would satisfy this logical criterion. By restricting the analysis of events to those of stopping particles the following points are noted:

1. The energy falls within the limits defined by the thickness of the two detectors A and B.
2. Analyzed particles must enter the telescope within an aperture cone defined by the diameters and separation of the detectors A and B.
3. Spurious events are kept to a minimum by the anticoincidence requirement on detector C.

4. The particles of different z and m will be easily distinguishable because of their different lines.

It should also be noted that for either stopping or penetrating particles, continuous in-flight calibration of the detectors and their associated electronics is provided because of the unique "endpoint" existing for each stopping particle. This endpoint is defined by the materials and geometry of a particular telescope and must represent a unique incident energy for a given species of particle.

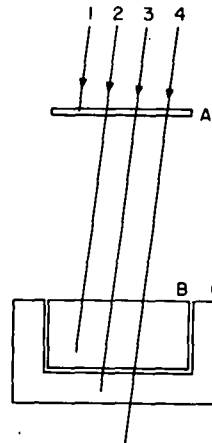


Figure 1. Schematic of ΔE vs. $E - \Delta E$ particle telescope. A denotes detector measuring ΔE and B the detector measuring $E - \Delta E$. C is the anti-coincidence detector.

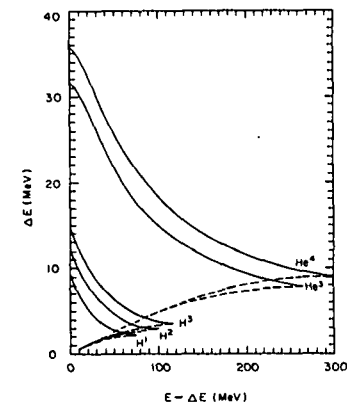


Figure 2. ΔE versus $E - \Delta E$ response curves for hydrogen and helium isotopes for the scintillator telescope used on IMP-IV and IMP-V.

A1. Medium Energy Detector: The thin dE/dx or ΔE element as well as E, ($E - \Delta E$), detector were CsI scintillators with an anti-coincidence plastic scintillator partially enclosing the E detector. It is designed to detect stopping protons and alphas in the 20 - 80 MeV/nucleon range. The axis of the detector is along the spacecraft spin axis which is normal to the ecliptic plane. The dE/dx element is also used as an electron detector over the energy range 0.5 - 1.1 MeV.

A mechanical layout of the MED telescope used in both the IMP-IV and IMP-V experiments is shown in Figure 3. As seen, an incident stopping particle would enter the telescope from the right penetrating the light baffle and passing into the A detector labeled ΔE scintillator in the figure. The particle would continue through the second light baffle and stop in the B detector labeled as the E - ΔE scintillator. Note that each of the three photomultiplier tubes is coupled through the open region adjacent to each of the three detectors. As shown the assembly is very compactly designed with associated high voltage power supplies and pre-amplifiers attached to the photomultiplier housing.

In order to accurately compute the response curve ΔE versus $(E - \Delta E)$ as shown in Figure 2 it is necessary to take into account all of the material in a particle track through the telescope up to but not including the C detector. The aluminum and plastic foam sandwich shown in front of the A detector and the one between the A and B detectors are

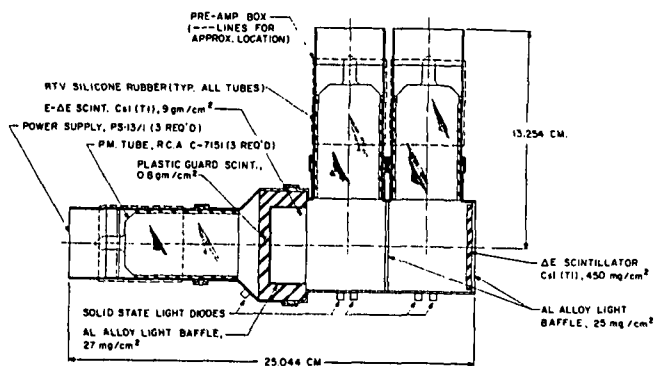


Figure 3. Schematic of IMP scintillator telescope assembly.

primarily responsible for the flattening of the curves at small energies. An average path length of $L/\langle \cos \theta \rangle = 1.02 L$ was used in calculating the detector response.

The geometry factors for varying penetration depths of tracks into the B detector were computed. These are plotted in Figure 4, which has specific incident energies marked along the curve indicating the incident energy of a particle having that geometry factor.

The actual telescope had a threshold for particle detection in the ABC mode of 18.7 MeV/nucleon and the cutoff for the C detector anti-coincidence occurred at 81.6 MeV/nucleon.

The counts of ABC particles were accumulated for 4.48 seconds intervals for IMP-IV and two 4.48 seconds intervals for IMP-V every 2.73 minutes. The relative contribution of the count rate of various species (here protons from 19 to 81.6) and energy spectral information were determined by 1024 channel pulse height analysis performed simultaneously on the output of both CsI scintillators at the rate of 8 times every 2.73 minutes for IMP-IV and 16 times for IMP-V.

A2.

The front detector A from MED telescope provided data for the .5 to 1.1 MeV electrons. MED A is a CsI crystal with a thickness of ~1 cm ecofoam sandwiched in between two ~.0023 cm Al foils. The geometrical factor of MED A is ~60 cm²-ster. The signals from MED A are

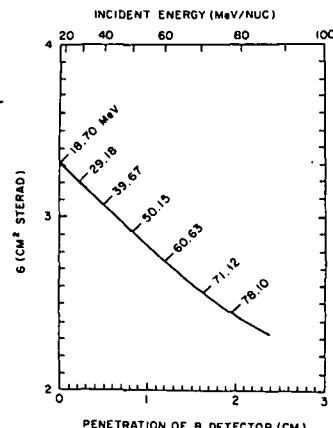


Figure 4. Geometry factor G versus penetration of particle into B detector for IMP scintillator telescope.

amplified and counted via various discriminators levels. There are 4 discriminators for MED A. They are called A0, A1, A2, A3. The corresponding threshold levels in keV are approximately 130, 610, 1260 and 1760 in sequential order. However, because of the thick window in front of the detector, electrons are not detected unless their kinetic energy is ≥ 400 keV. Figure 5 shows the electron detection efficiency for A0-A1. Clearly, the difference in counting rates from A0 and A1 levels is due to electrons in the energy range of ~ 500 -1100 keV. Although the detection efficiency for electrons with energy ≥ 1100 keV is not small, it is neglected because of the steeply falling spectrum for electrons of solar origin.

B1. Low Energy Detector (L.E.D.):

This uses a thin (150 micron) solid state detector for the dE/dx measurement with a thick E - ΔE solid state device. The nominal energy interval for stopping particles extended from 4 to 20 MeV/nucleon. A

schematic of the mechanical design of the telescope assembly is shown in Figure 6. The partial mechanical collimator in front of the dE/dx detector made possible the measurement of 0.6 - 4 MeV proton by single parameter analysis during solar events.

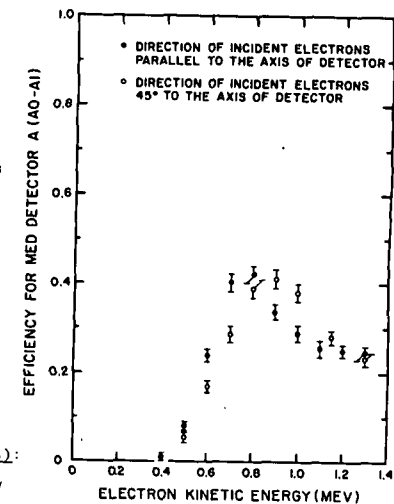


Figure 5. Efficiency for the MED (A-A1) detector.

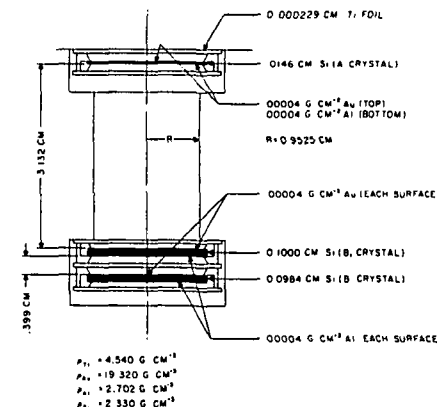


Figure 6. Schematic of IMP-IV solid state detector telescope showing critical dimensions and composition of layers.

The dE/dx or A detector and the E - dE/dx or B detector were mounted in the two ends of a cylindrical plastic scintillator with a plastic plug of the same material after B. The signals from the solid state detectors were fed into charge sensitive preamplifiers since the number of charge pairs created by an ionizing particle would be proportional to the energy it deposited. The plugged end of the C detector was coupled to a photomultiplier. As in the case of the scintillator telescope described above the ABC logic was invoked to discriminate against all but particles coming to rest in detector B after having passed through A.

Note the titanium foil light shield in front of the A detector because of the sensitivity of silicon detectors to light. Also note that each of the silicon detectors has a layer of gold and aluminum on front and back surfaces, respectively. The average obliquity factor for this assembly was $1/\langle \cos \theta \rangle = 1.04$. With this factor applied to the thickness of material shown in Figure 6, the range energy program mentioned in the last section was used to compute the response curves similar of those for MED Figure 2.

Counts of the ABC particle rates were accumulated for a 4.48 seconds interval once every 2.73 minutes. The relative contribution of each count rate of proton within $4.2 \leq E < 19.1$ MeV and energy spectral information were determined by 1024 channel pulse height analysis performed simultaneously on the output of the solid state detectors every 2.73 minutes, 4 times for IMP 4 and 8 times for IMP 5.

B2.

The front dE/dx detector from the LED provided data for the low energy .9 to 1.6 MeV protons. LED A is a totally deflected surface barrier Au-Si detector of thickness ~ 0.0145 cm protected in the front by a .00023 cm Ti foil. The geometric factor for LED A is $\sim 4.25 \text{ cm}^2\text{-ster}$. Protons stopping in this thin detector (or particles penetrating it) were measured by passing the output signal through an eight-level energy threshold discriminator called D1, ..., D8. The energy thresholds in keV for D1, ..., D8 are in sequential order, 6060, 4888, 2580, 1420, 930, 740, 410 and 210 for IMP 4 and slightly different for IMP 5. Data from any one level were accumulated for 4.48 seconds interval once every 2.73 minutes. Since LED A is a thin detector only D8 has enough sensitivity for electron detection. For D7 and higher energy threshold levels, the electron detection was observed to be less than 1%. Therefore, the counting rate D6-D4 free of electron contribution has been used to cover the proton energy range from $\sim .9$ to 1.6 MeV.

Note again that this LED telescope is scanning essentially the ecliptic plane. A complete block diagram of the experiment electronics for both detectors is given in Figure 7.

Satellites

The IMP IV satellite was launched on May 24, 1967 into a high inclination elliptic orbit with initial perigee ~ 270 km and an apogee between 33.4 and 34 earth radii. The spin axis was approximately normal to the ecliptic plane and the orbital period was ~ 104 hours. From January to May 1968 and from February to May 1969 the trajectories of the satellite were in the tail region of the magnetosphere. The experiments providing the data published here performed well from the launch to the date of the spacecraft re-entry on May 3, 1969.

The IMP-V satellite was launched on June 21, 1969 leaving a gap of few important solar events in May and beginning June 1969. The satellite orbit was also elliptic with an apogee from 28.2 to 28.6 earth radii and an initial perigee of ~ 270 km. Again the spin axis is approximately perpendicular to the elliptic plane and the orbital period is ~ 81.5 hours. The periods for which the trajectories of the spacecraft were in the geomagnetic tail are roughly from December through March each year. Except for a period of 2 weeks in March 1970 when the LED data were noisy, all the detectors providing the results published here have functioned well from launch through December 24, 1972, when IMP-V re-entered the Earth's atmosphere.

II. Data Description

We have attempted to identify each discrete event whose intensity above 20 MeV exceeded 10^{-4} Protons/cm 2 -sec-Sr-MeV for a period of more than 5 hours. This requirement for a measurable flux above 20 MeV eliminates most co-rotating events. The plot for each event includes the hourly averages of the three proton energy intervals as well as the .5 - 1.1 MeV electrons.

When possible, the onset time has been defined by the electron component (average velocity $\sim 0.9C$). This time is indicated on the frame by an arrow along with the precision of the measurement. This precision is a function of the rate of increase and the event size. When this time is not available or when the amplitude of the electron intensity increase is too small to be seen on the hourly average plot, the 19-80 MeV proton onset time is indicated.

The proton intensity is plotted in 3 energy ranges, namely: .9 - 1.5 MeV, 6 to 19 MeV, and 19 to 80 MeV on a logarithmic scale from 10^{-5} to 10^4 proton/sec cm 2 -sr-MeV. The logarithmic scale of the .5 to 1.1 MeV electrons intensity is either .5 to 15 electrons/sec cm 2 sr-MeV or 10^{-1} to 10^4 electrons/sec cm 2 -sr MeV depending on the size of each individual event. It was found convenient to standardize at 10 the maximum number of days shown per frame. This time scale shows most of the particle events with a good resolution from the onset of the event until the time when the intensity is back to the galactic level. In those cases where the event lasts longer, the time history is continued on the following page. Also, there are events which start while the particles of the previous event are still present and are being recorded by the detectors. Those "superposed events" are not separated in an independent frame. Rather, they are shown in sequence. If multiple plots are required, then some days from the previous frame may be repeated in order to put the next event in perspective.

For clarity, vertical lines have been drawn to separate each day. It is obvious that twenty four hourly average points for each particle intensity level should be included between two lines - unfortunately, because of telemetry gaps, points are sometimes missing. It should not be any problem to locate those missing points. A period of ~ 8 hours of missing data taken place during the perigee passages of the satellite. Those have been indicated by a heavy horizontal bar on the bottom line of the frame. Note that there can be longer periods of missing .5 - 1.1 MeV electrons near the perigee. Those correspond to trapped electrons in the magnetosphere which have been removed from the plot. Of course, the duration of those periods depends on the satellite trajectory. During a few large events the MED detector was saturated near the intensity maximum. As a result the .5 to 1.1 MeV electrons and the 19 - 80 MeV protons intensities are not available during those saturation periods. This has been indicated on the frame.

As some features in the intensity variations may be due to interplanetary magnetic field perturbations, the often related storm or sudden commencement, when available, has been indicated on the frame. Four isolated micro events with a too short time to be put on an independent frame have been transferred to the end of the catalogue - those events are November 1, 1970; December 6, 1970; January 14, 1971 and July 24, 1971.

An experiment such as this represents the combined efforts of many individuals; in particular, Clro Cancro and Paul Janniche in the design, development and testing of the electronics, and Anthony Flanick and his co-workers for the assembly and test of the detector assemblies. Many of the computer analysis programs were developed by Dr. James H. Kinsey and significant parts of the experiment description were taken from his PhD thesis. We would also like to express our thanks to Miss Kathy Watts for her work in the preparation of this catalogue.

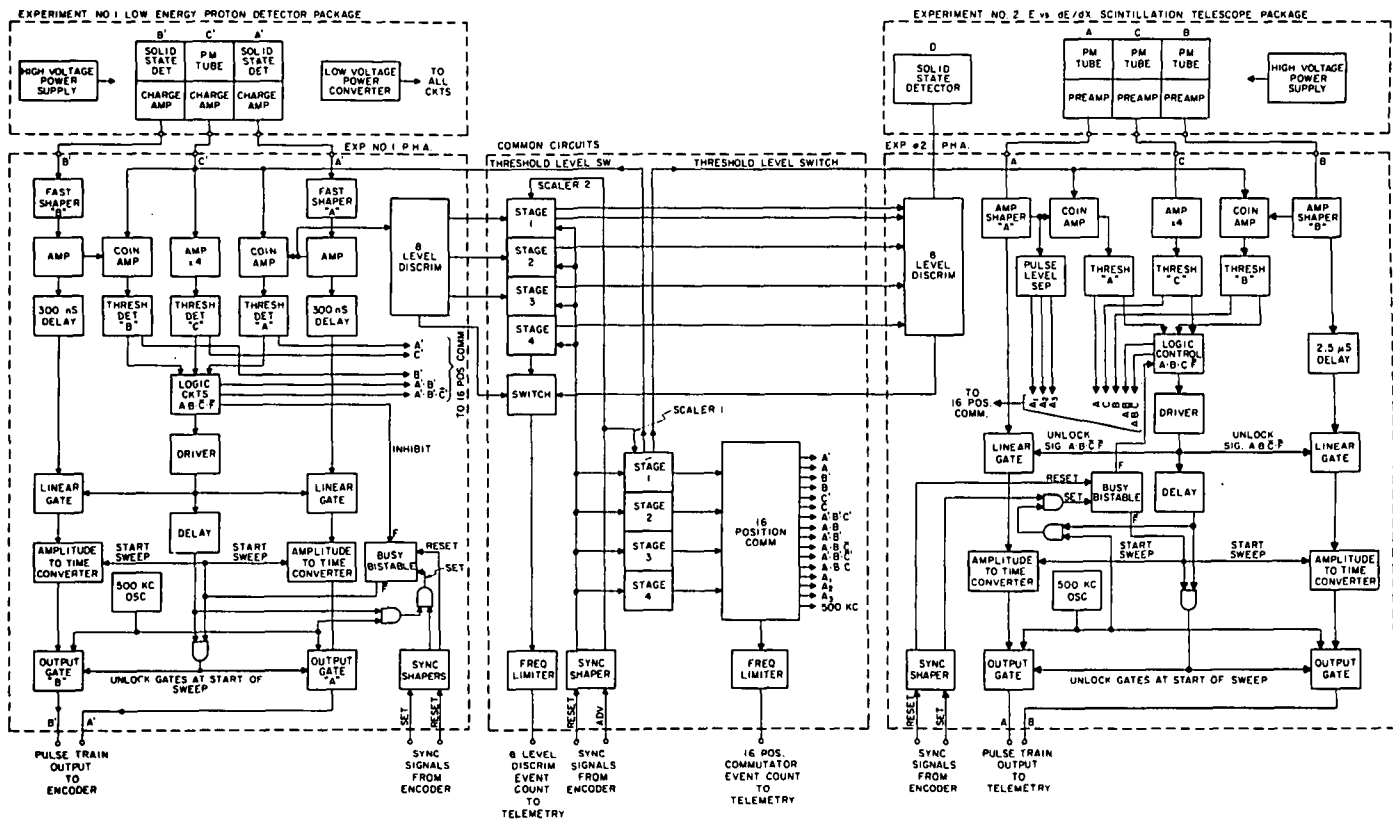
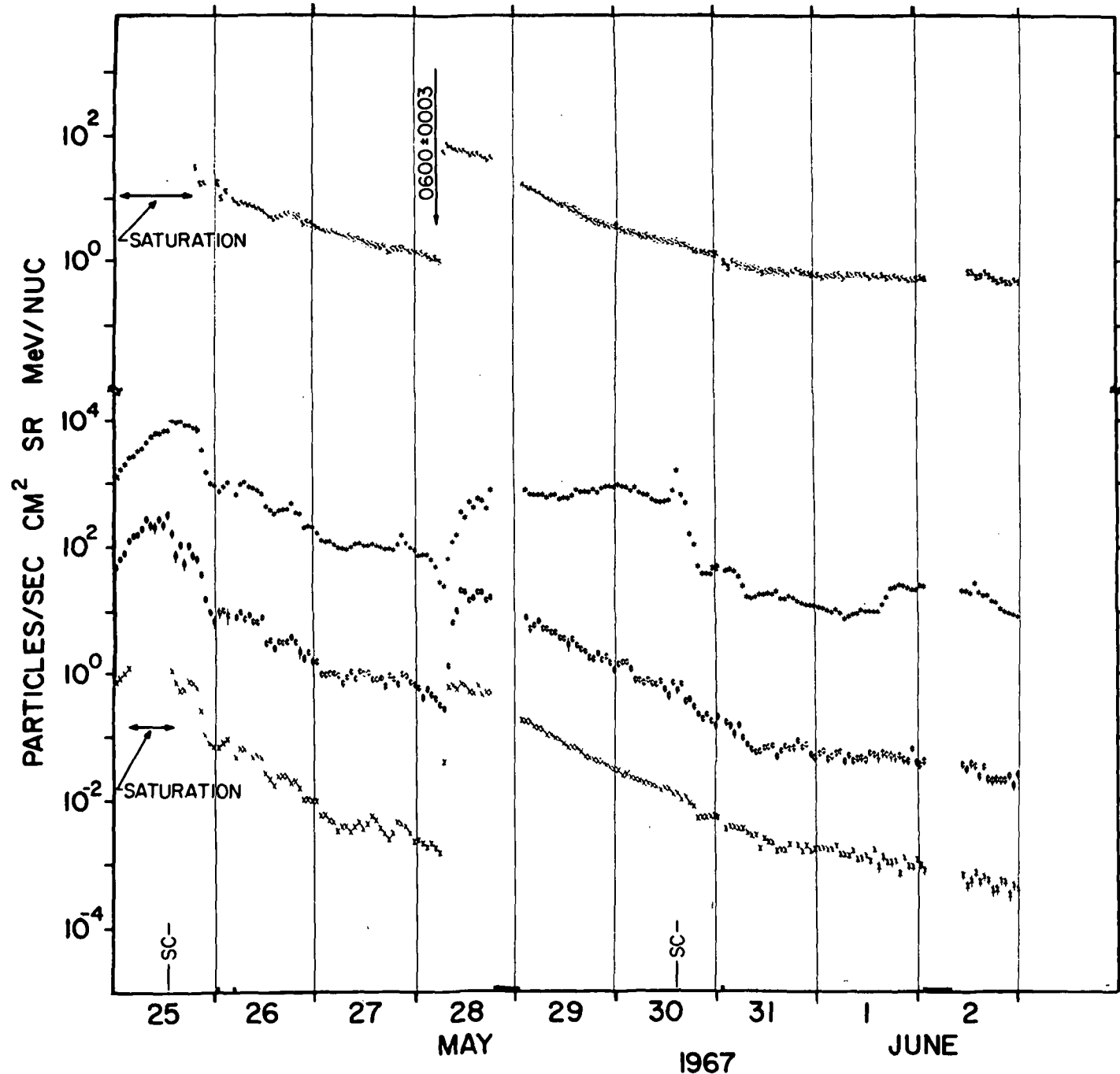


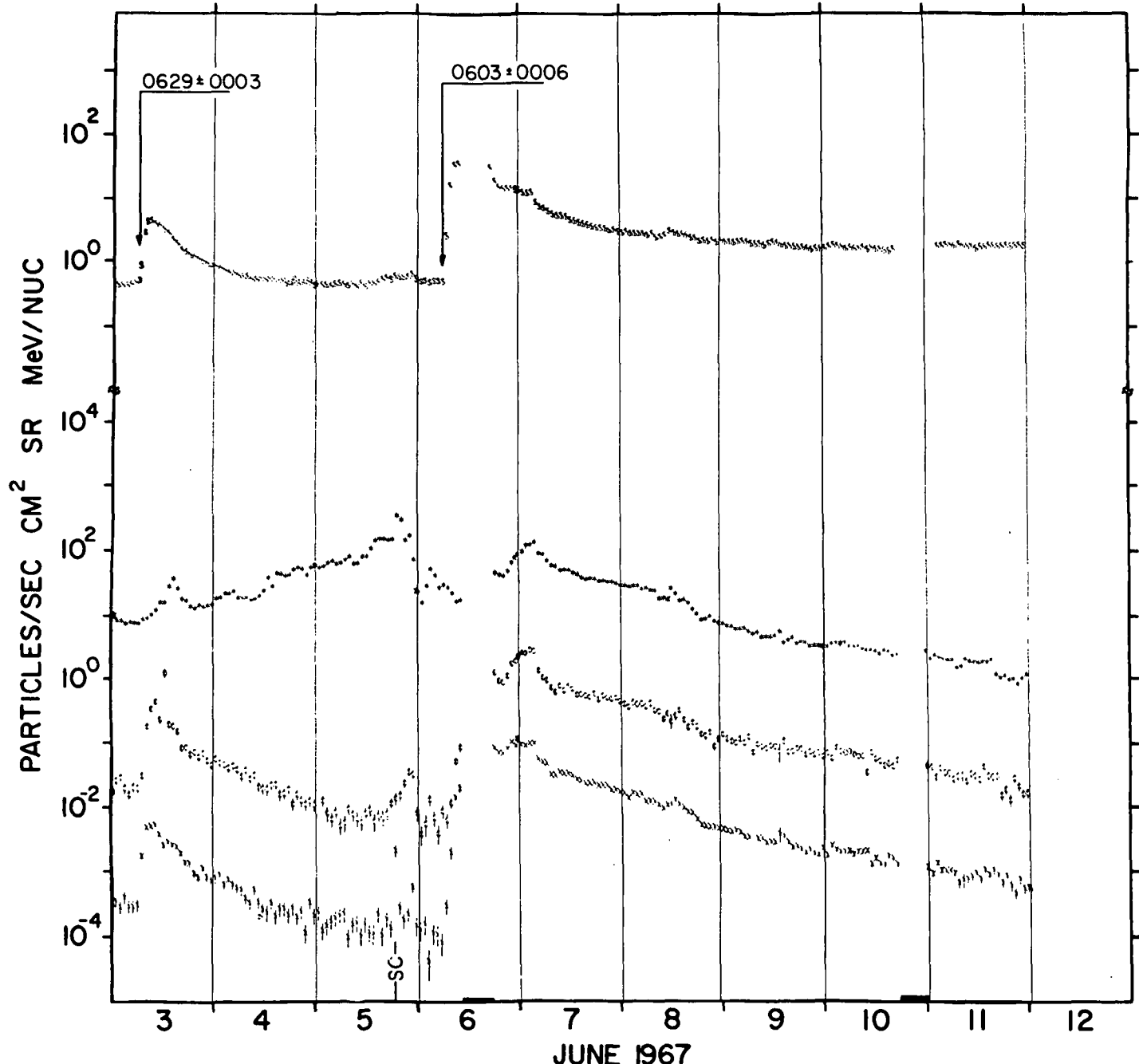
FIG. 7 BLOCK DIAGRAM OF IMP-IV COSMIC RAY EXPERIMENT ELECTRONICS

FRAME NUMBER		INCLUDING DATES	FRAME NUMBER		INCLUDING DATES	FRAME NUMBER		INCLUDING DATES
1	1967	May 25 - June 02	36	1968	Nov. 17 - Nov. 26	71	1970	Aug. 18 - Aug. 27
2		June 03 - June 11	37		Dec. 02 - Dec. 11	72		Nov. 04 - Nov. 13
3		June 11 - June 20	38		Dec. 10 - Dec. 19	73		Nov. 14 - Nov. 22
4		July 04 - July 11	39	1968-69	Dec. 26 - Jan. 01	74		Nov. 22 - Nov. 27
5		July 29 - Aug. 06	40	1969	Jan. 23 - Jan. 28	75		Dec. 11 - Dec. 19
6		Aug. 07 - Aug. 14	41		Feb. 24 - March 05	76	1970-71	Dec. 23 - Jan. 01
7		Aug. 17 - Aug. 22	42		March 11 - March 18	77	1970-71	Dec. 28 - Jan. 05
8		Oct. 28 - Nov. 06	43		March 20 - March 29	78	1971	Jan. 24 - Feb. 02
9		Nov. 06 - Nov. 15	44		March 29 - April 07	79		Feb. 01 - Feb. 10
10		Nov. 15 - Nov. 23	45		April 08 - April 17	80		April 01 - April 10
11		Dec. 02 - Dec. 08	46		April 17 - April 26	81		April 20 - April 25
12		Dec. 11 - Dec. 15	47		April 24 - May 03	82		May 11 - May 20
13		Dec. 15 - Dec. 24	48		Sept. 09 - Sept. 18	83		June 29 - July 02
14	1967-68	Dec. 28 - Jan. 02	49		Sept. 24 - Oct. 03	84		Sept. 01 - Sept. 10
15	1968	Jan. 11 - Jan. 16	50		Oct. 13 - Oct. 17	85		Sept. 10 - Sept. 19
16		Feb. 01 - Feb. 10	51		Nov. 01 - Nov. 10	86		Sept. 24 - Sept. 27
17		Feb. 12 - Feb. 19	52		Nov. 11 - Nov. 20	87		Oct. 02 - Oct. 11
18		Feb. 21 - Feb. 28	53		Nov. 21 - Nov. 30	88	1972	Feb. 08 - Feb. 16
19		March 06 - March 11	54		Nov. 29 - Dec. 06	89		Feb. 17 - Feb. 26
20		March 21 - March 23	55		Dec. 17 - Dec. 24	90		March 05 - March 14
21		April 21 - April 30	56	1969-70	Dec. 30 - Jan. 08	91		March 27 - March 30
22		June 08 - June 16	57	1970	Jan. 28 - Feb. 06	92		April 17 - April 24
23		June 26 - June 29	58		Feb. 15-18; Feb. 25-28	93		April 25 - April 29
24		July 05 - July 14	59		March 04 - March 13	94		May 27 - June 05
25		July 11 - July 20	60		March 20 - March 29	95		June 06 - June 15
26		July 25 - Aug. 03	61		March 28 - April 06	96		June 14 - June 23
27		Aug. 02 - Aug. 11	62		April 05 - April 14	97		July 18 - July 27
28		Aug. 11 - Aug. 20	63		April 13 - April 20	98		July 25 - Aug. 03
29		Aug. 19 - Aug. 24	64		May 04 - May 13	99		Aug. 02 - Aug. 11
30		Aug. 28 - Sept. 06	65		May 29 - June 07	100		Aug. 12 - Aug. 21
31		Sept. 25 - Oct. 04	66		June 14 - June 22	101		Aug. 22 - Aug. 31
32		Oct. 02 - Oct. 10	67		June 25 - July 04	102		Sept. 01 - Sept. 10
33		Oct. 23 - Nov. 01	68		July 06 - July 11	103		Oct. 29 - Nov. 04
34		Nov. 01 - Nov. 10	69		July 22 - July 29	104		Nov. 24 - Nov. 29
35		Nov. 10 - Nov. 17	70		Aug. 09 - Aug. 18	105	1970	Oct. 31-Nov. 02; Dec. 05-07
				V		106	1971	Jan. 13-15; July 24-26

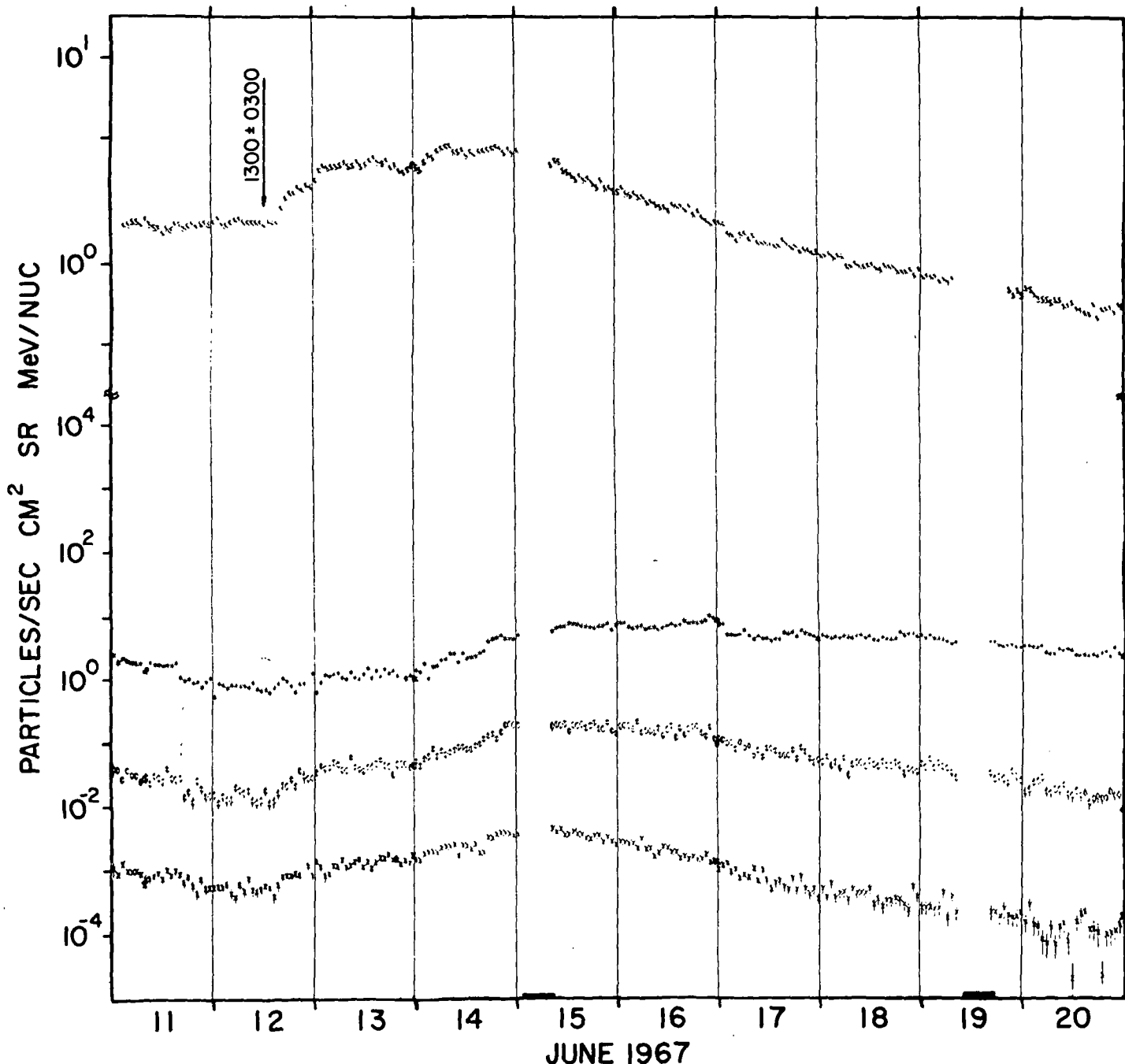
- 1 -
\$.5-.11 MeV ELECTRONS X .9-.15 MeV PROTONS ϕ 6-19 MeV PROTONS X 19-80 MeV PROTONS

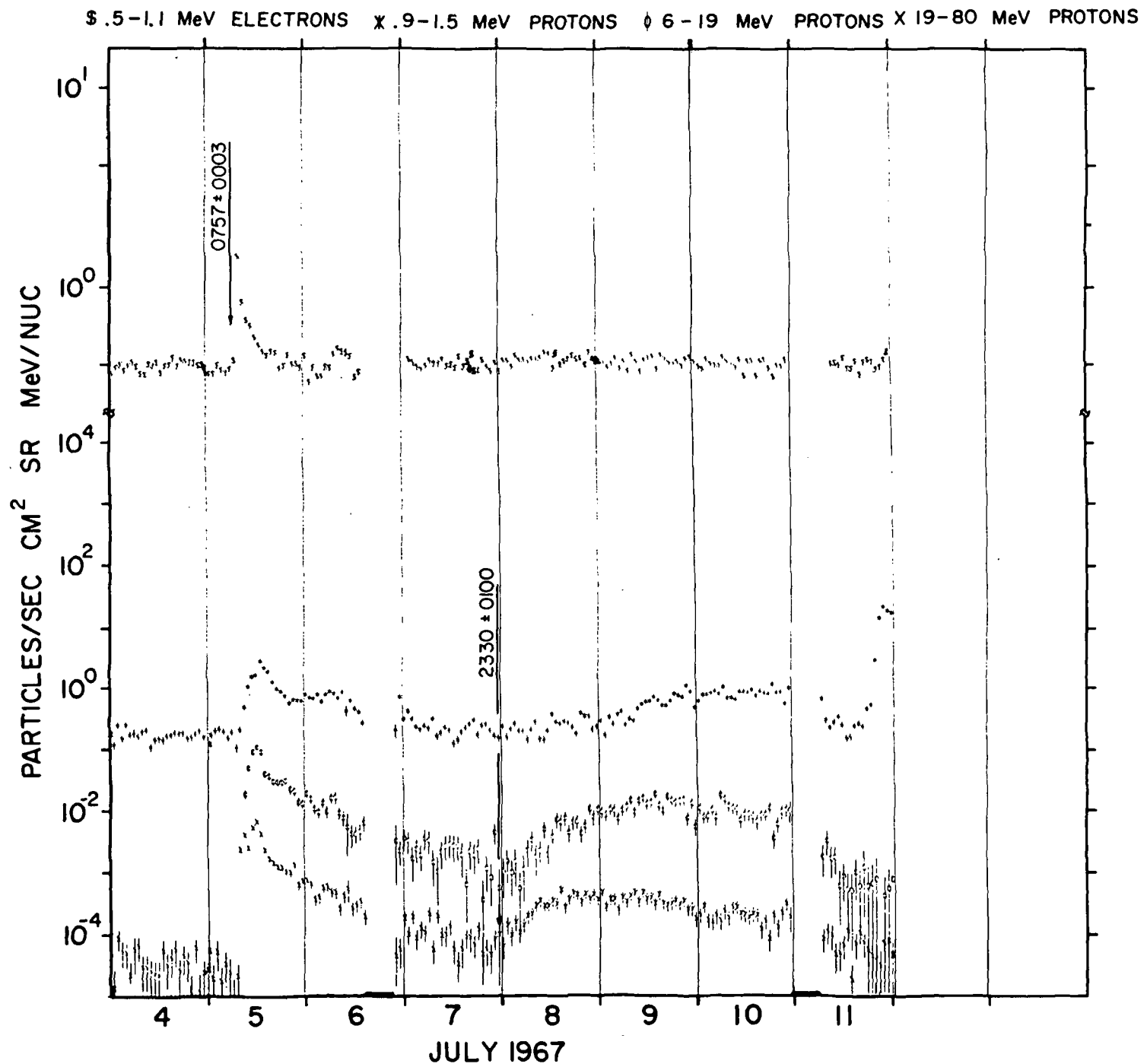


.5-1.1 MeV ELECTRONS X .9-1.5 MeV PROTONS ♦ 6-19 MeV PROTONS X 19-80 MeV PROTONS

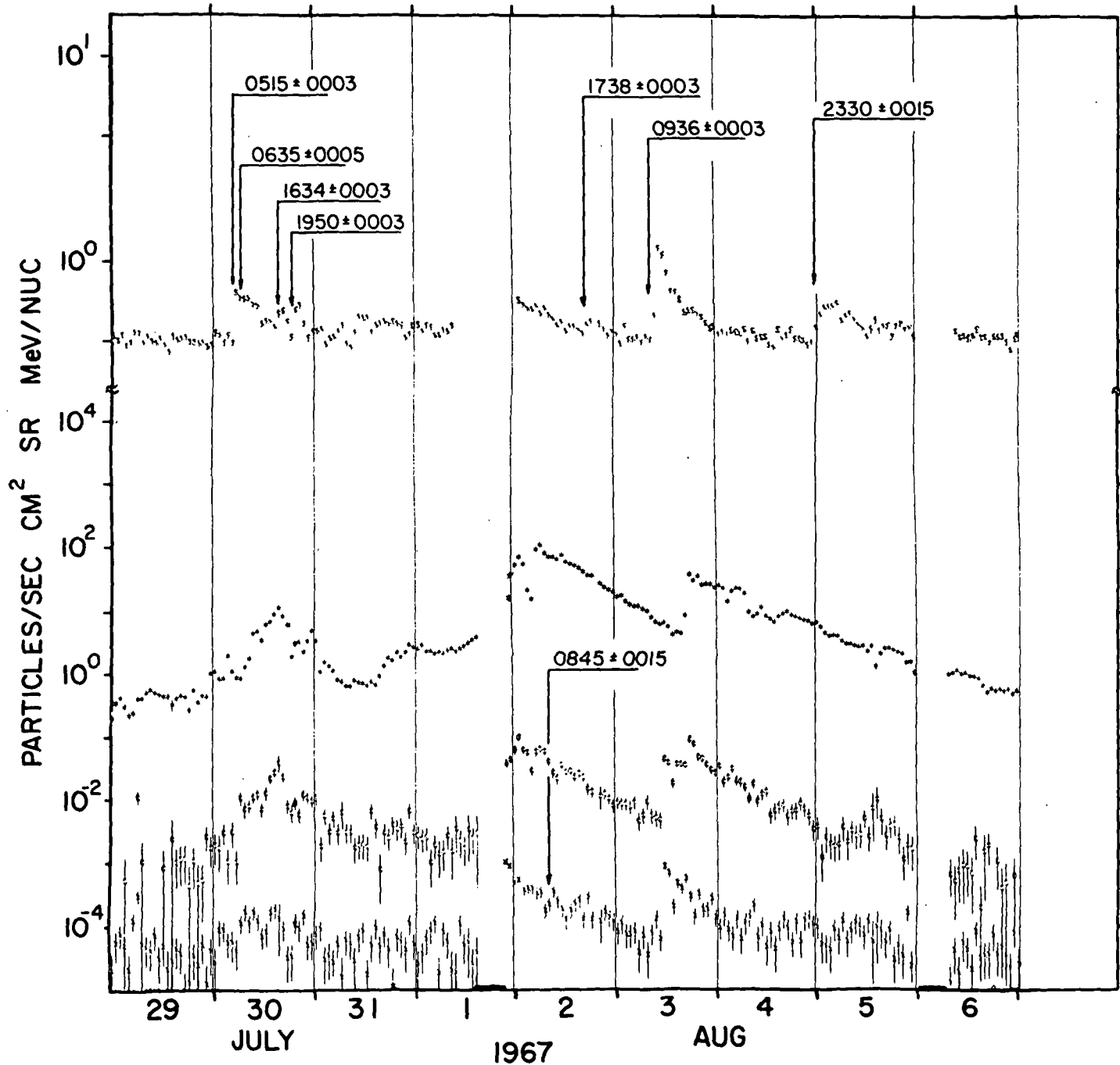


\$.5 - 1.1 MeV ELECTRONS X .9 - 1.5 MeV PROTONS ϕ 6 - 19 MeV PROTONS X 19 - 80 MeV PROTONS

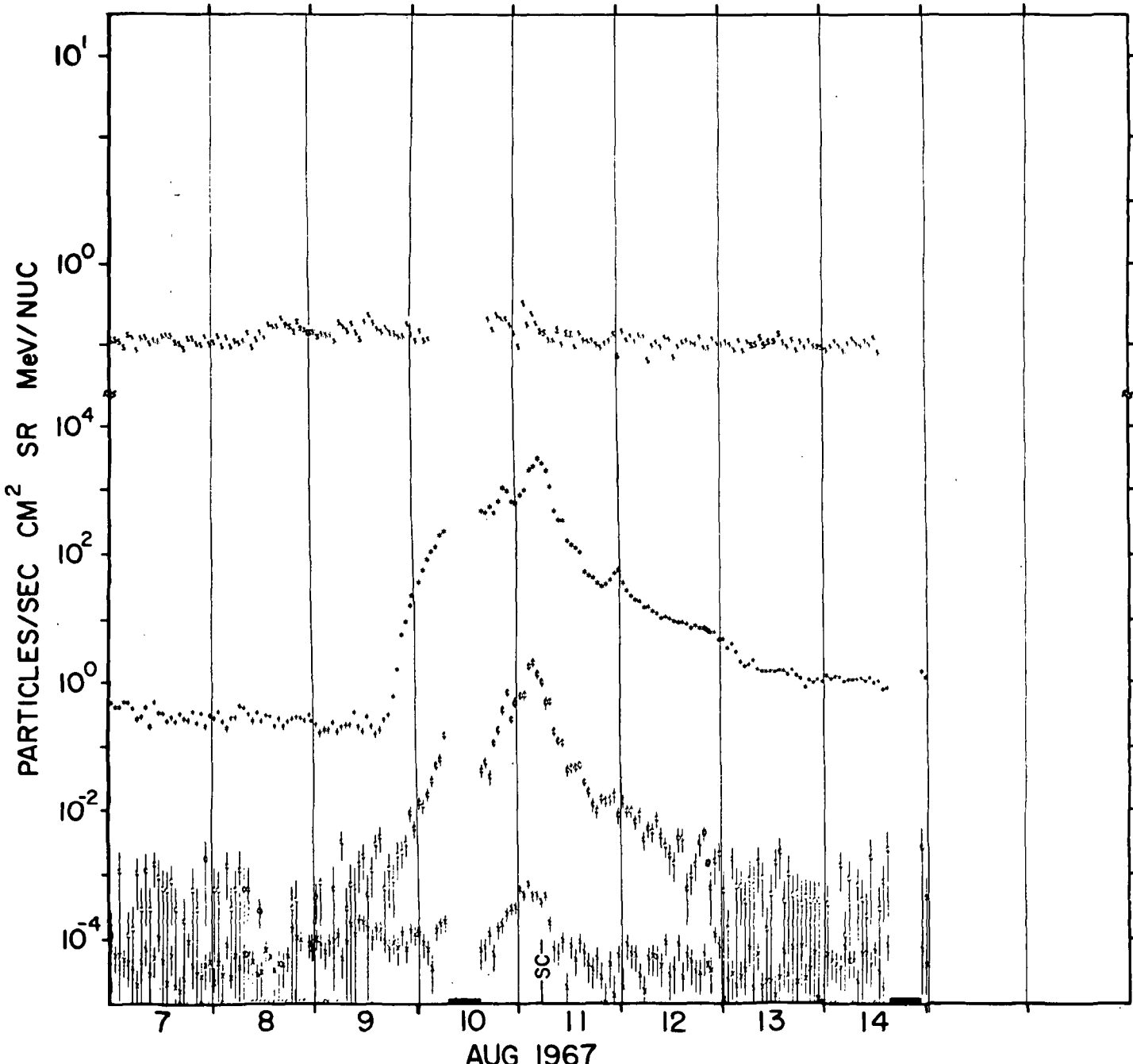




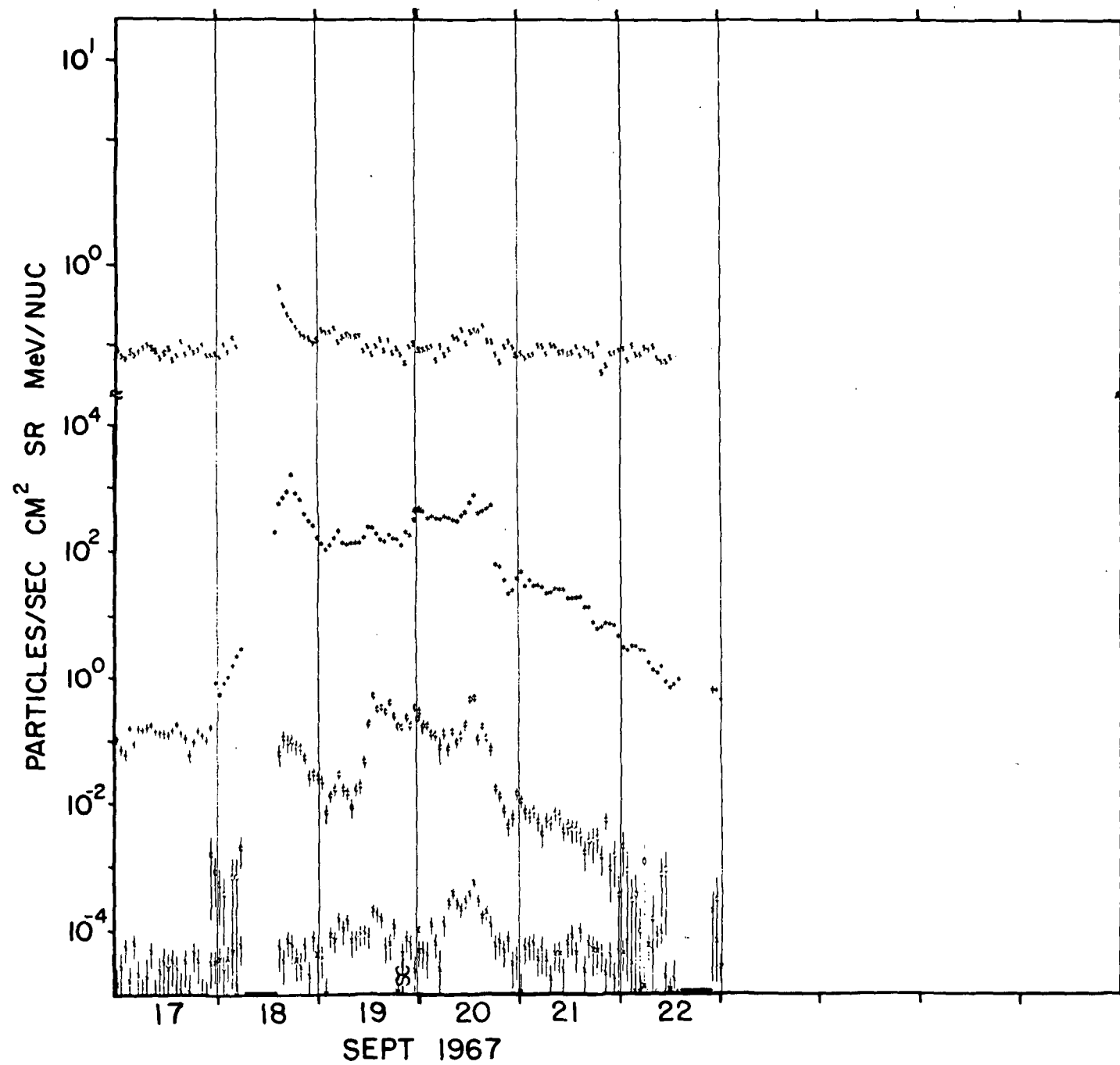
\$.5-1.1 MeV ELECTRONS X .9-1.5 MeV PROTONS ϕ 6-19 MeV PROTONS X 19-80 MeV PROTONS



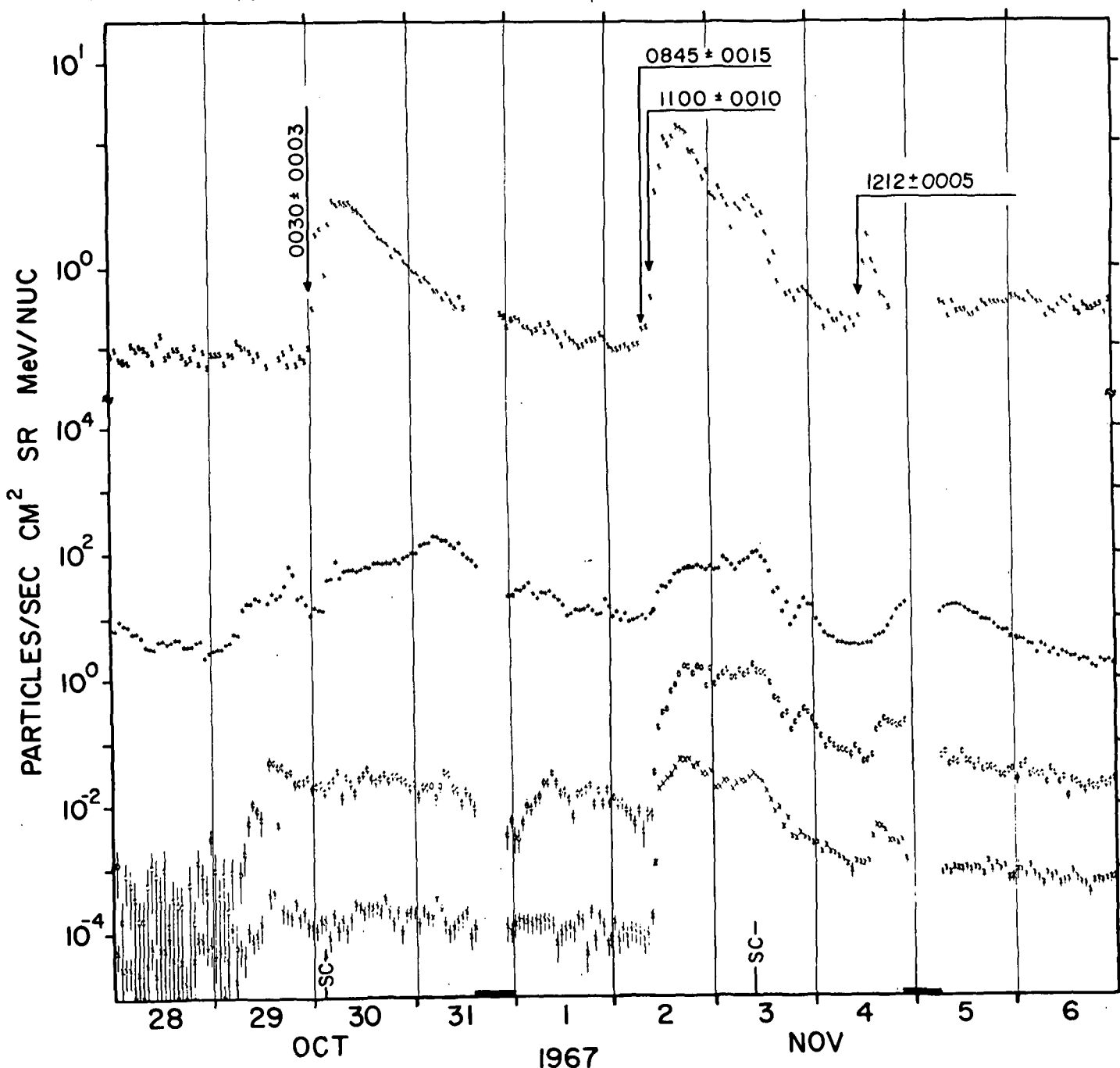
S .5-1.1 MeV ELECTRONS X 9-1.5 MeV PROTONS O 6-19 MeV PROTONS X 19-80 MeV PROTONS



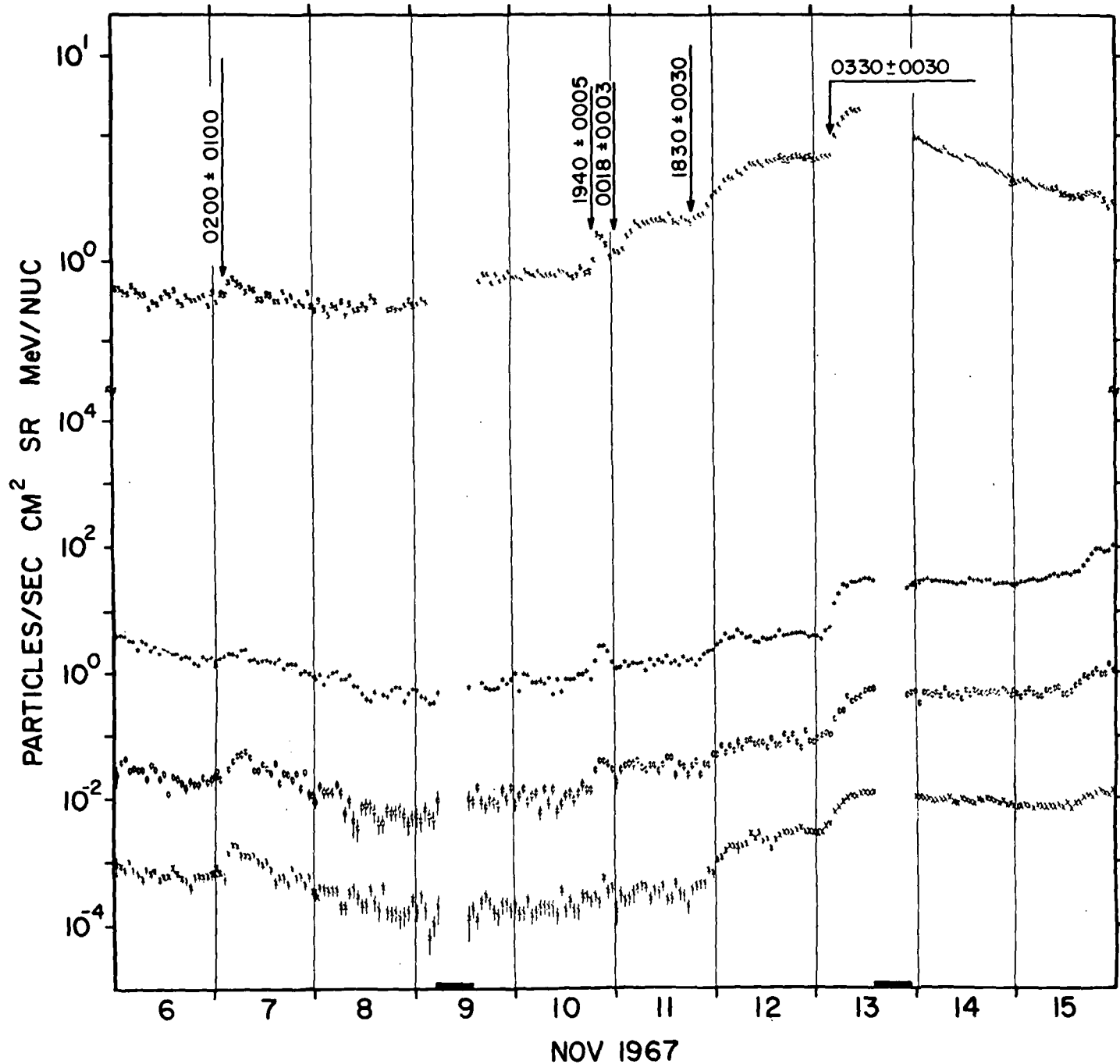
- 7 -
\$.5-1.1 MeV ELECTRONS X .9-1.5 MeV PROTONS # 6-19 MeV PROTONS X 19-80 MeV PROTONS



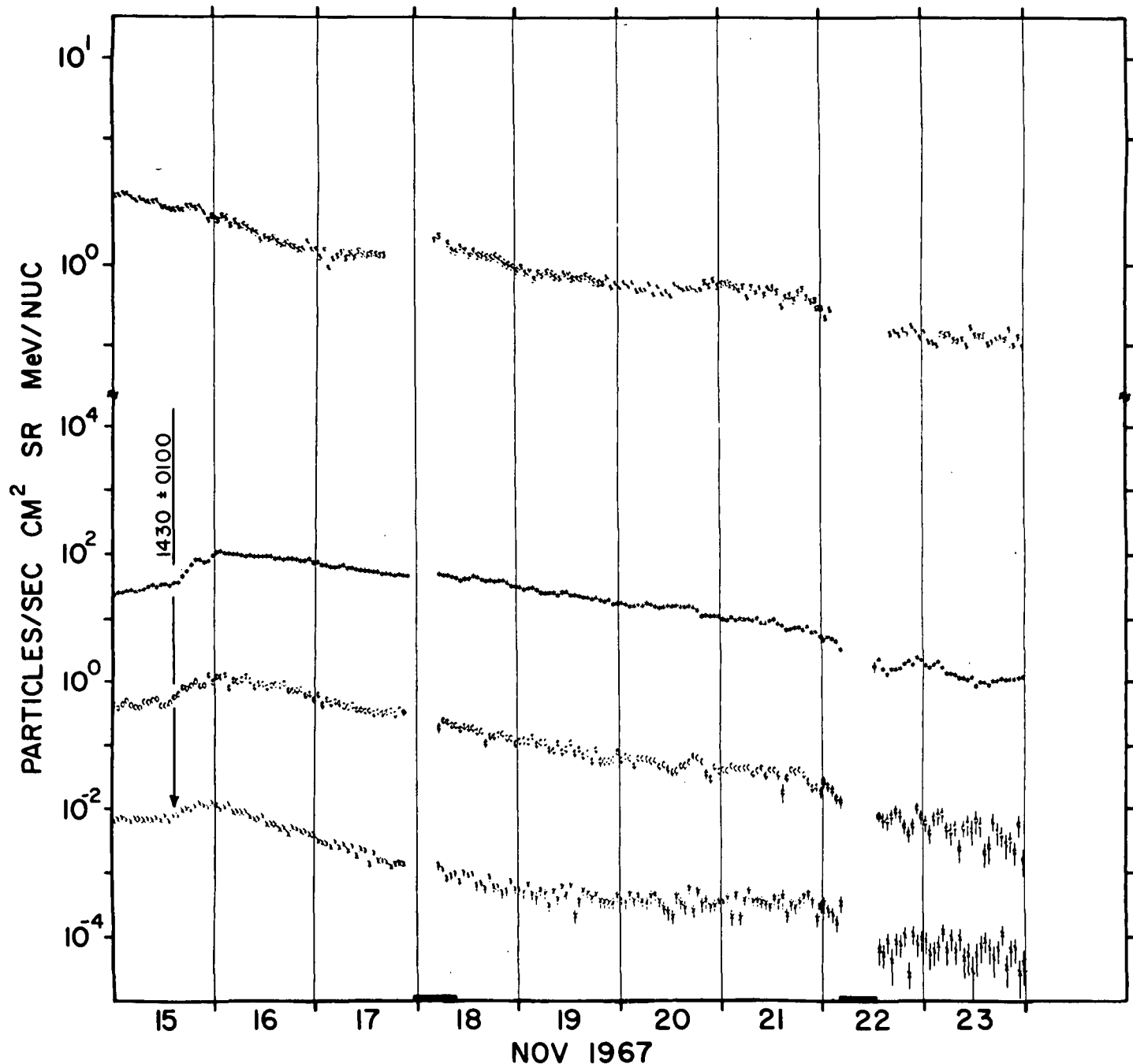
\$.5-1.1 MeV ELECTRONS X .9-1.5 MeV PROTONS O 6-19 MeV PROTONS X 19-80 MeV PROTONS

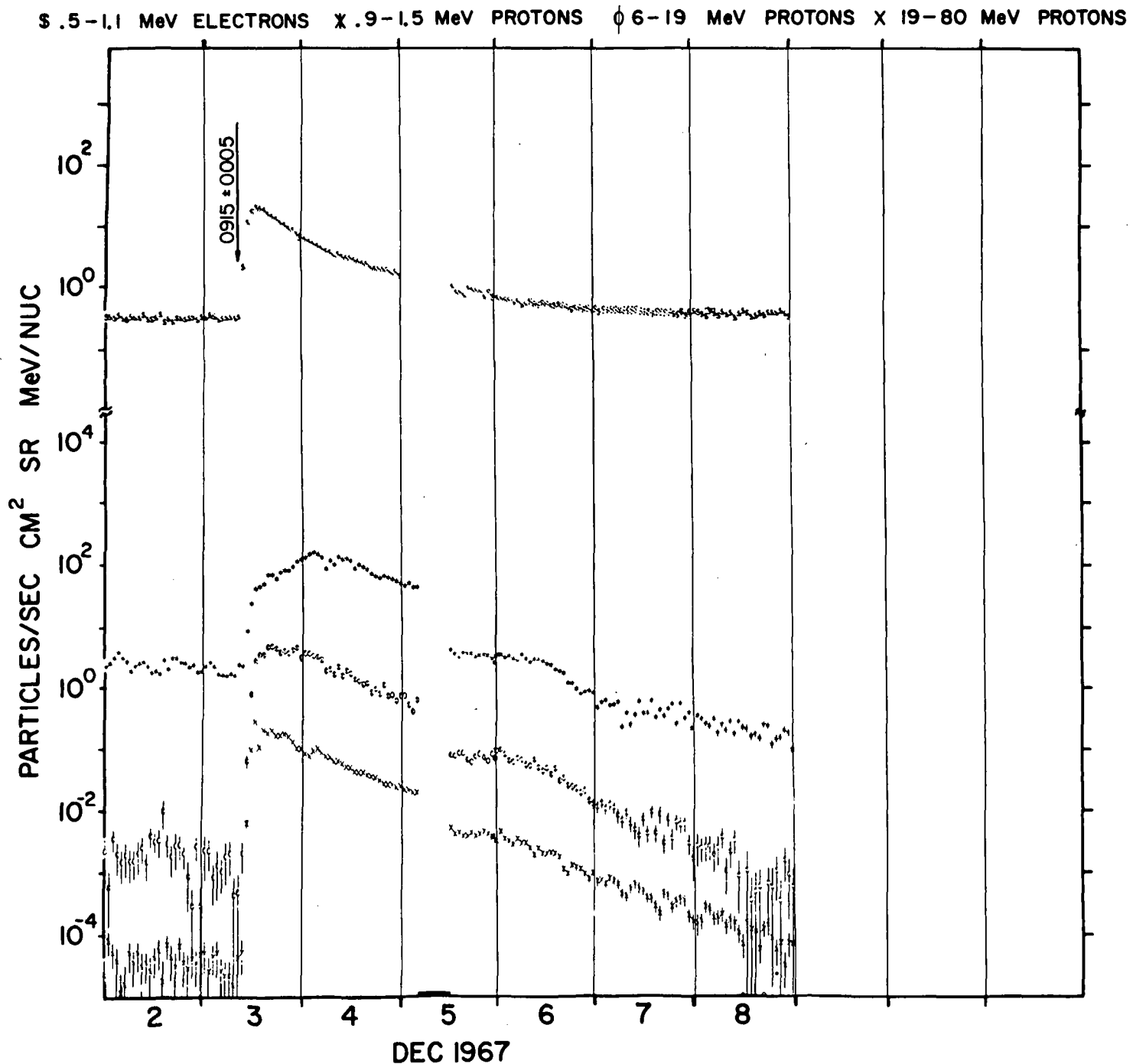


- 9 -
\$.5-1.1 MeV ELECTRONS X .9-1.5 MeV PROTONS 6-19 MeV PROTONS X 19-80 MeV PROTONS

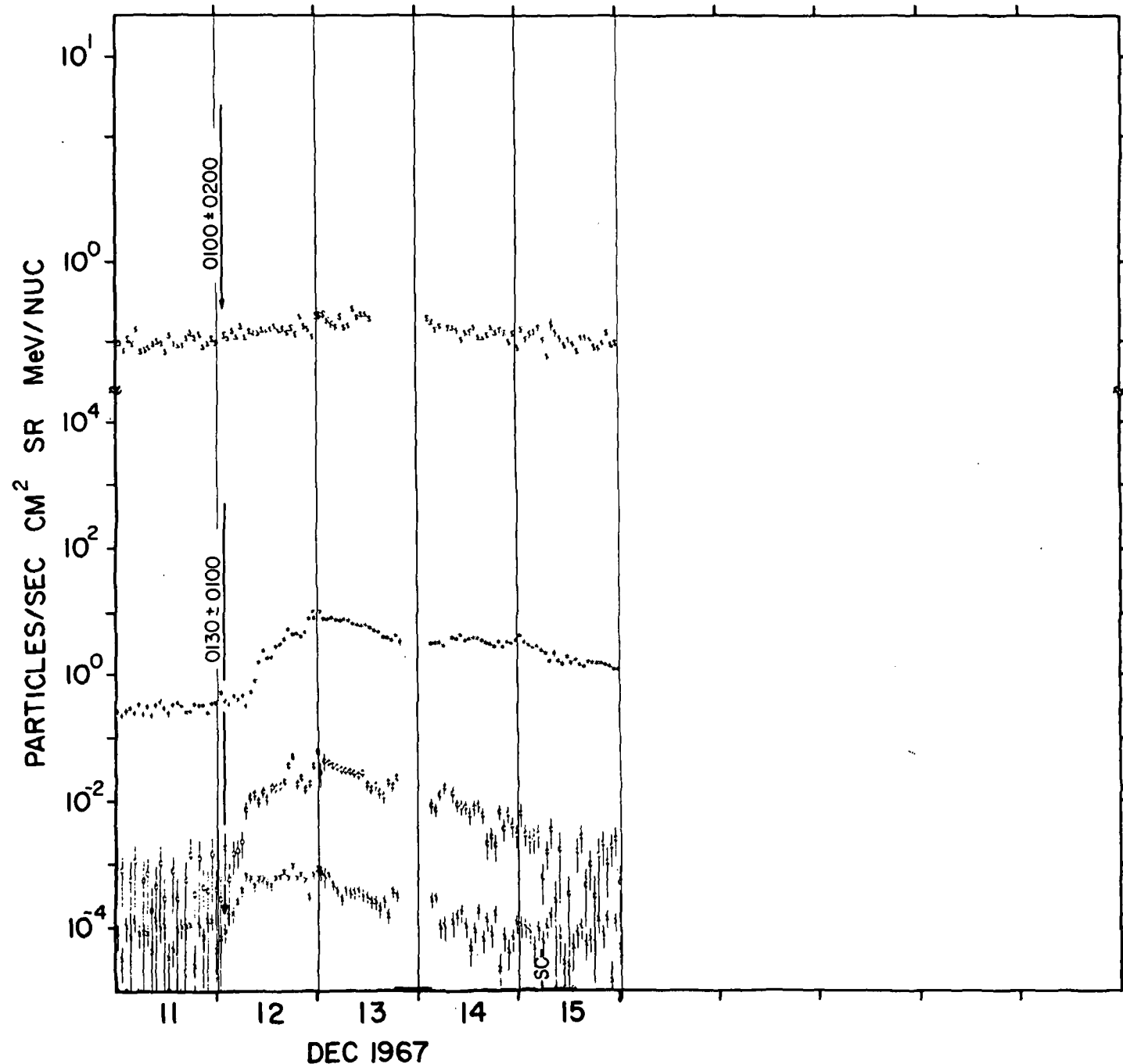


.5-1.1 MeV ELECTRONS X .9-1.5 MeV PROTONS + 6-19 MeV PROTONS X 19-80 MeV PROTONS

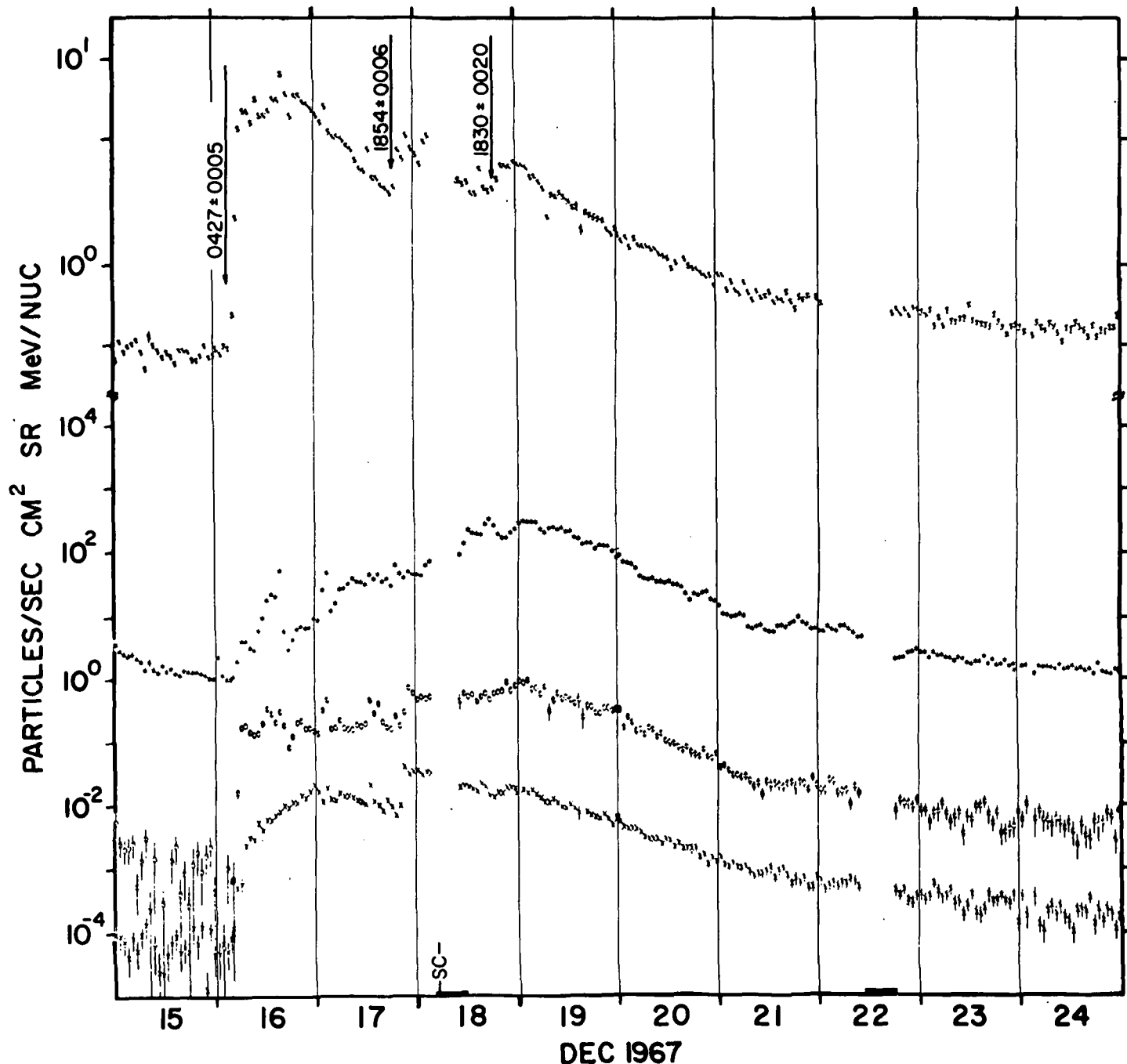




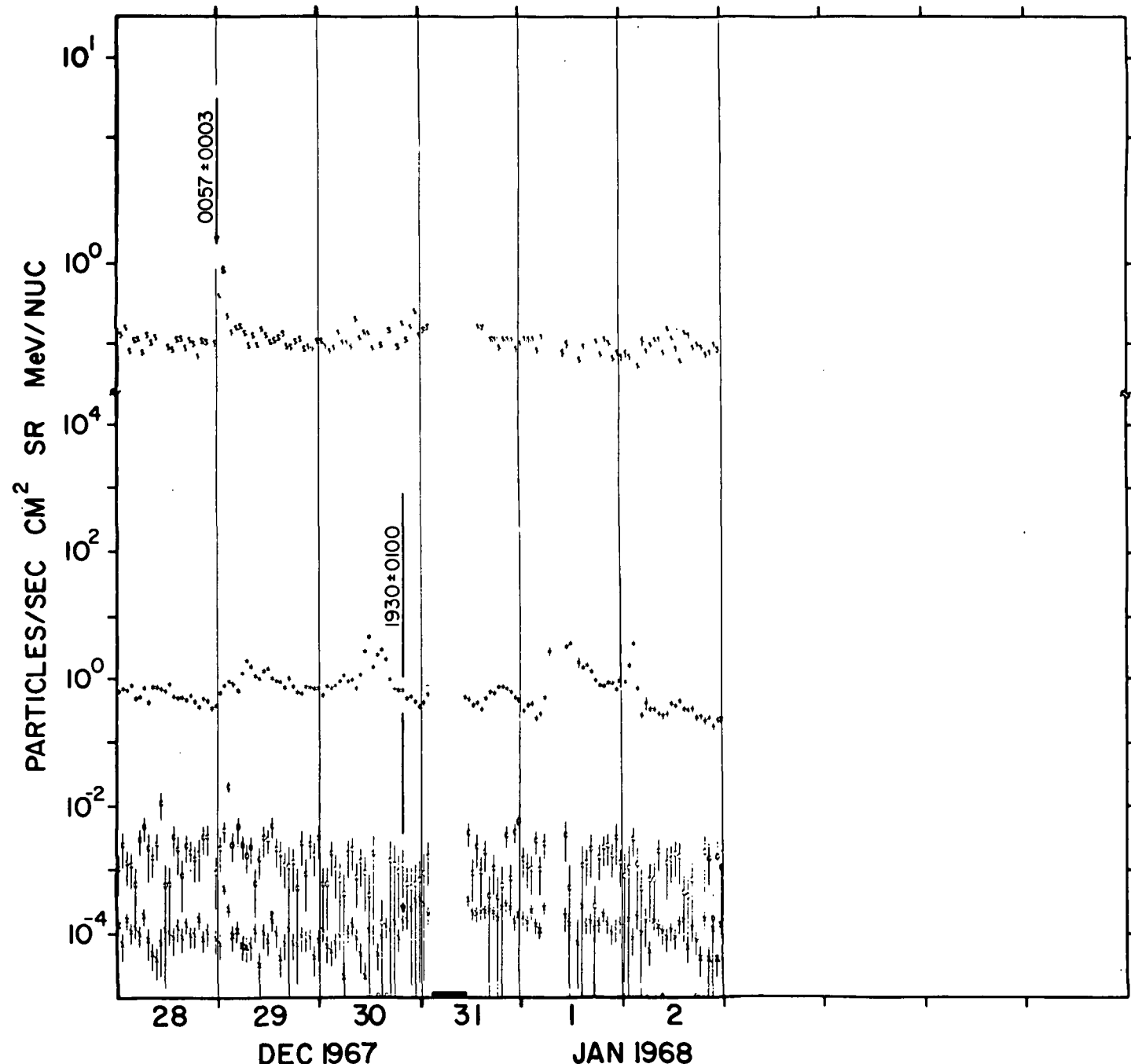
\$.5-1.1 MeV ELECTRONS X .9-1.5 MeV PROTONS ϕ 6-19 MeV PROTONS X 19-80 MeV PROTONS



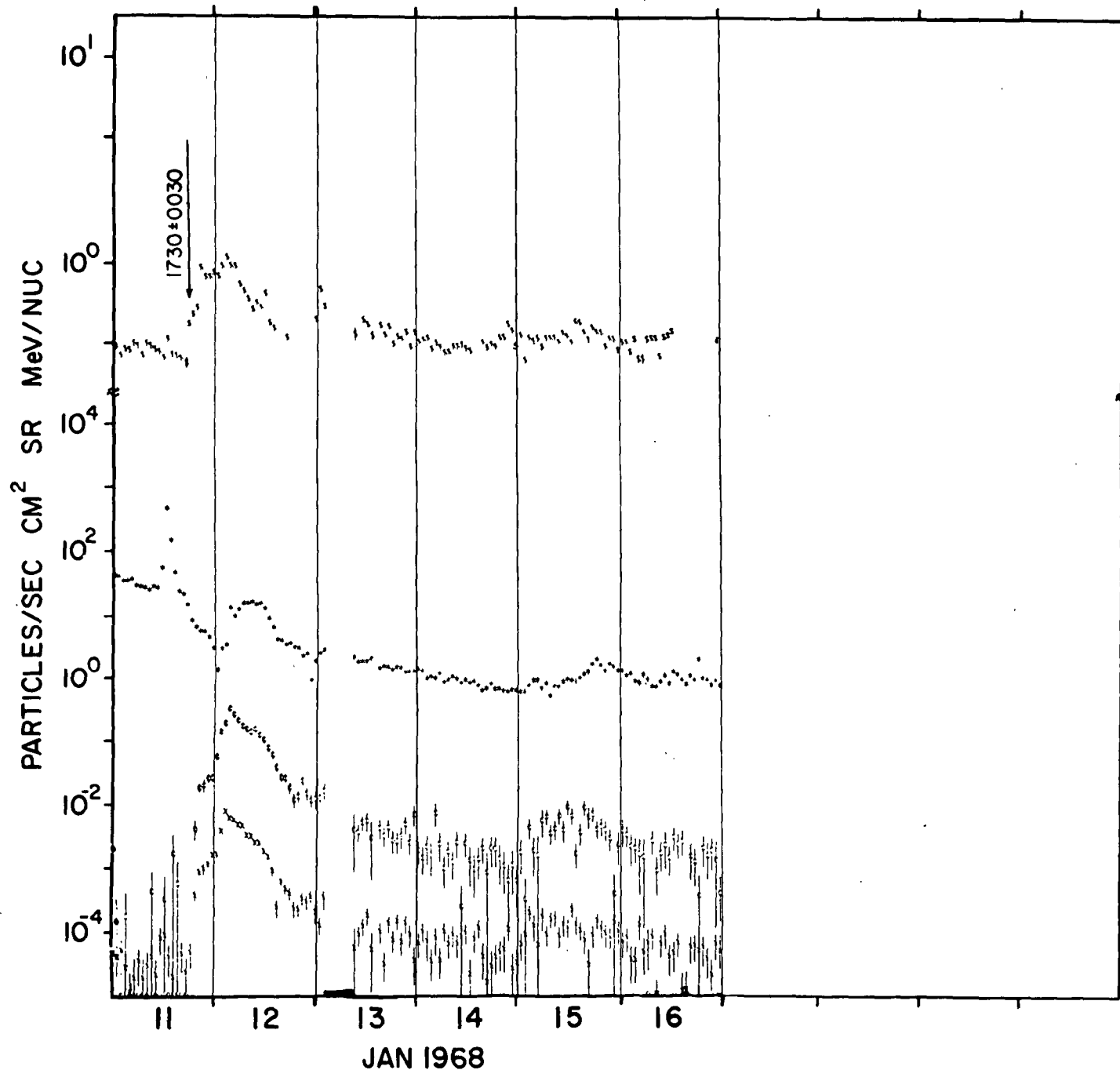
.5-1.1 MeV ELECTRONS X .9-1.5 MeV PROTONS ϕ 6-19 MeV PROTONS X 19-80 MeV PROTONS



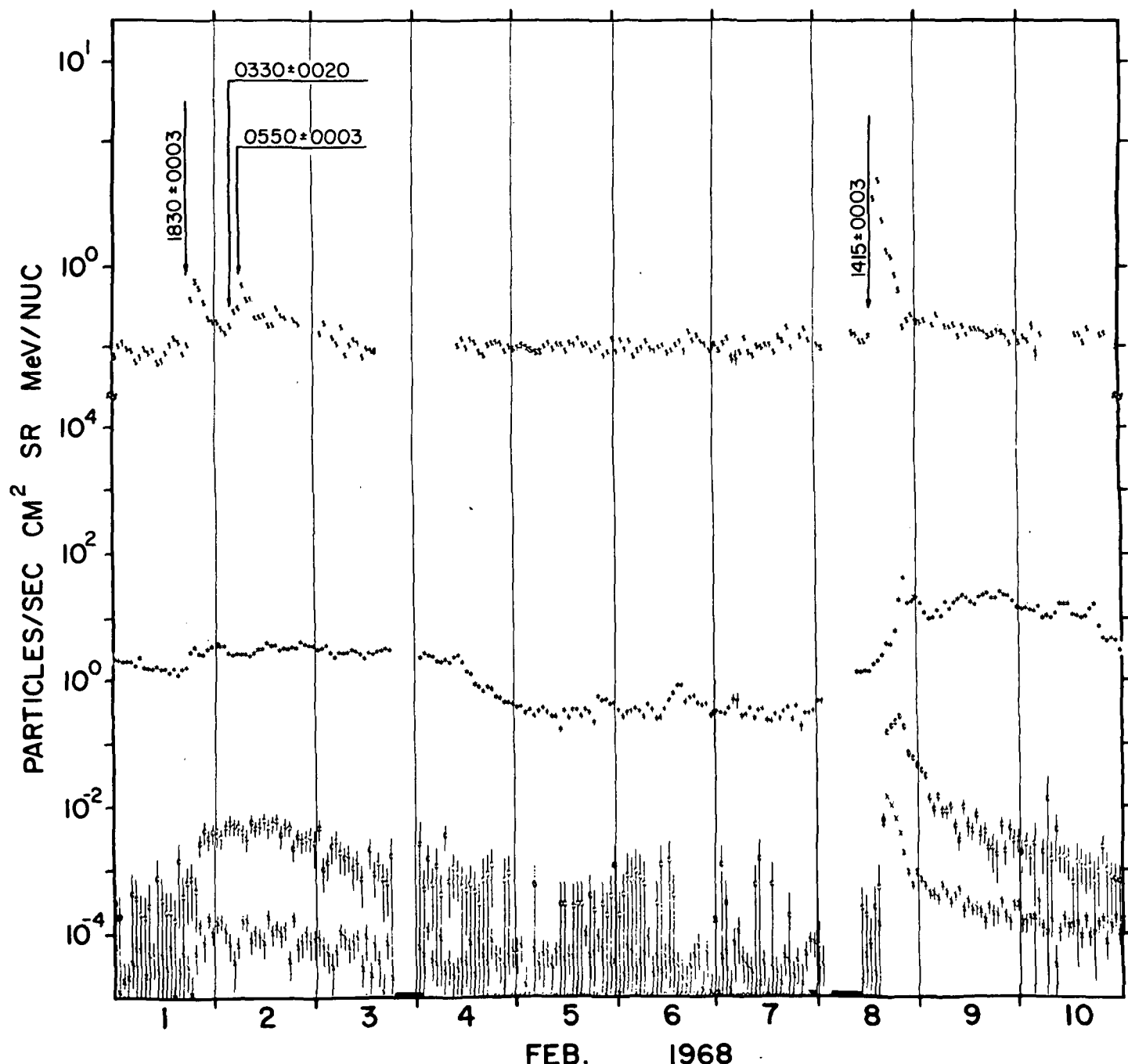
.5-.11 MeV ELECTRONS X .9-.15 MeV PROTONS \diamond 6-19 MeV PROTONS X 19-80 MeV PROTONS



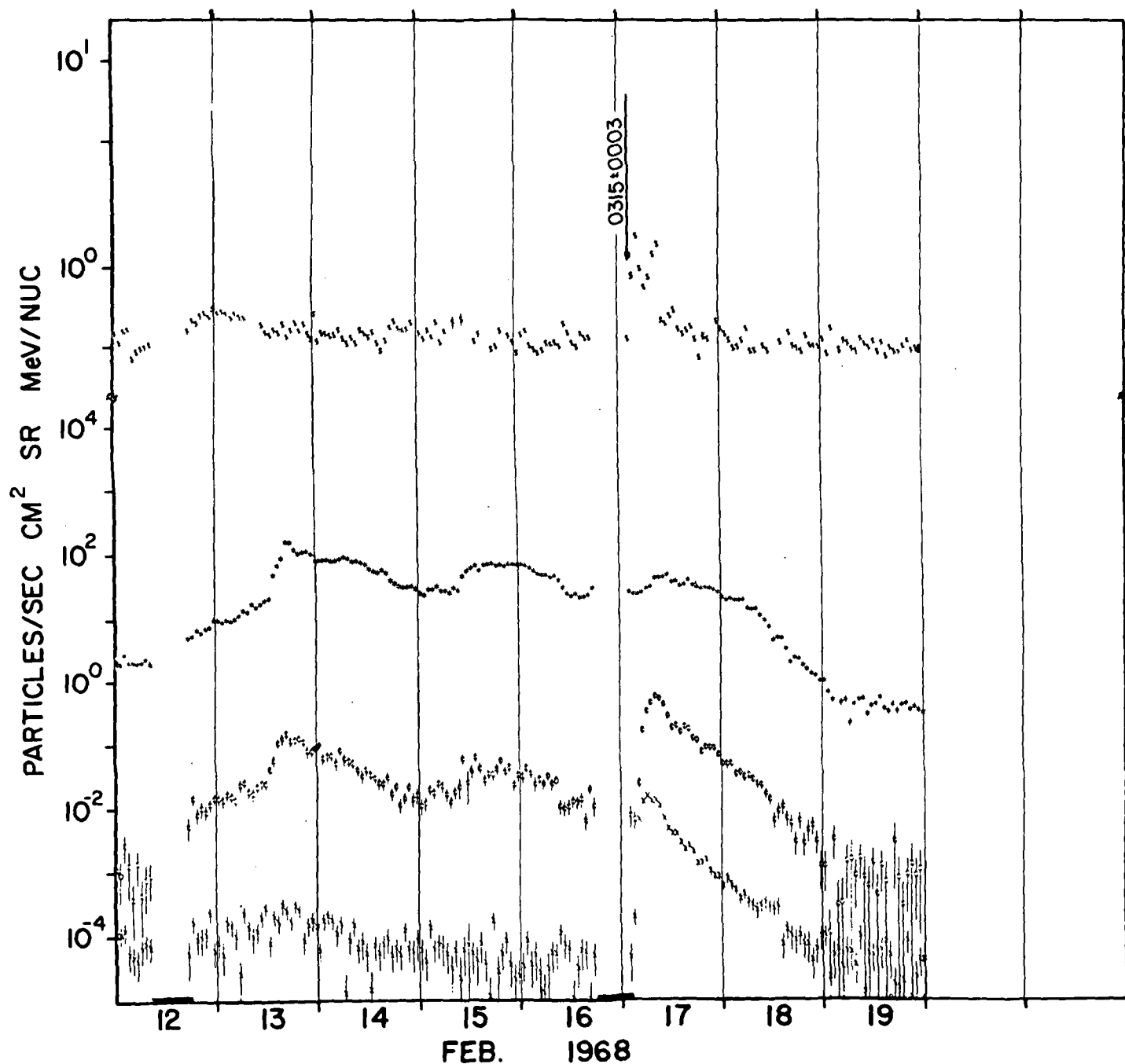
S .5-1.1 MeV ELECTRONS X .9-1.5 MeV PROTONS + 6-19 MeV PROTONS X 19-80 MeV PROTONS



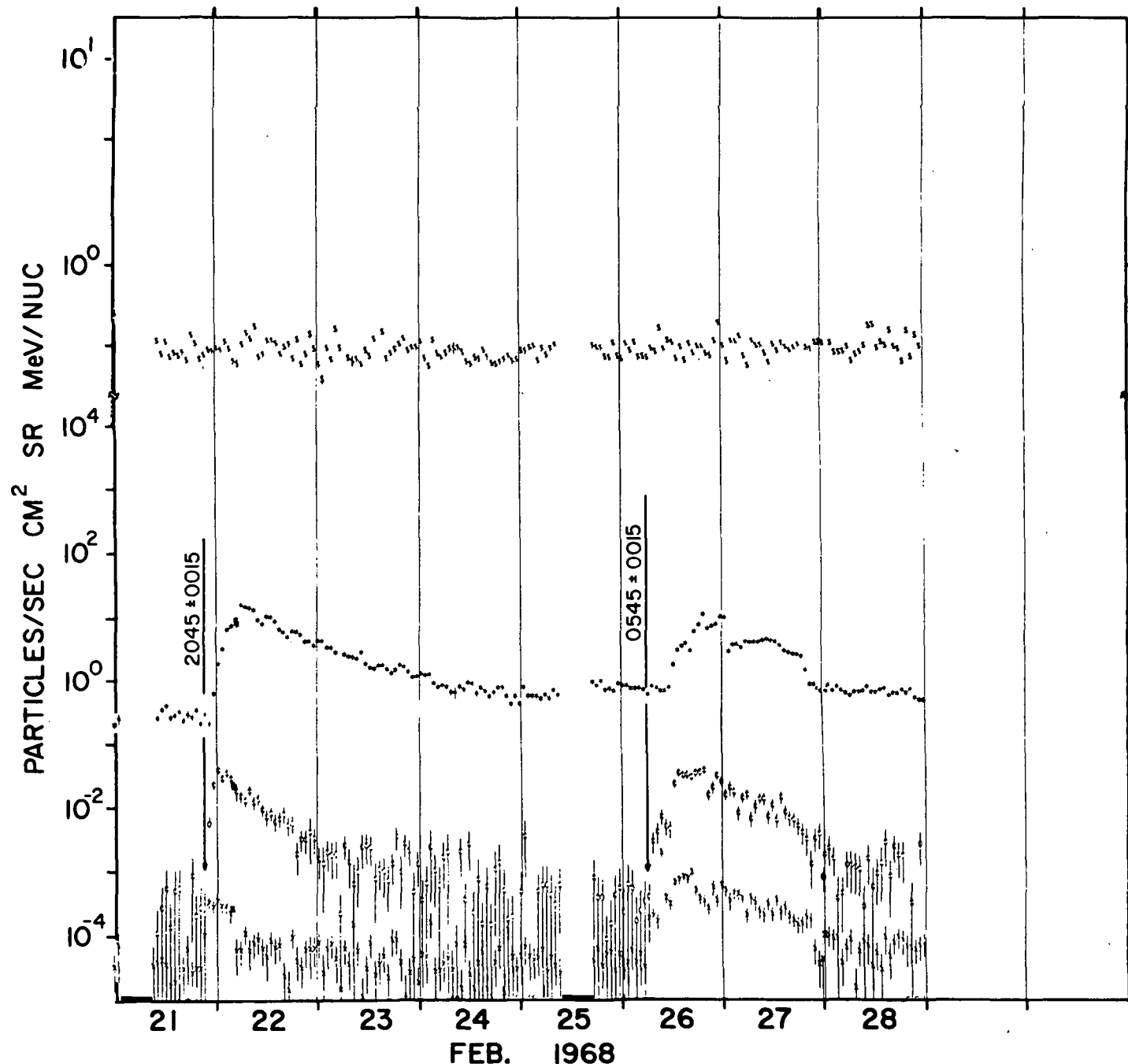
\$.5-1.1 MeV ELECTRONS X .9-1.5 MeV PROTONS ϕ 6-19 MeV PROTONS X 19-80 MeV PROTONS



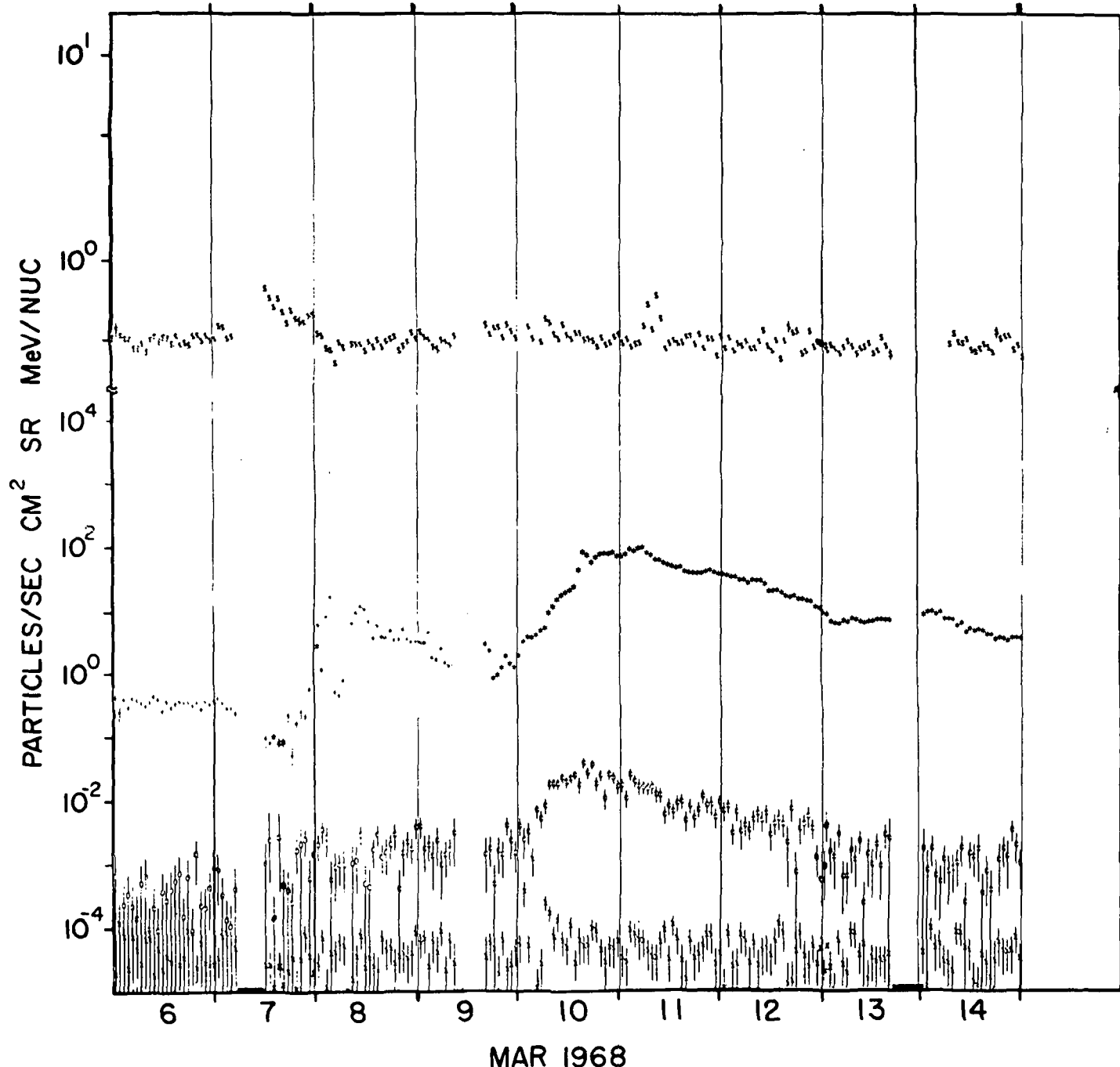
\$.5-1.1 MeV ELECTRONS X .9- 1.5 MeV PROTONS \oplus 6-19 MeV PROTONS X 19-80 MeV PROTON



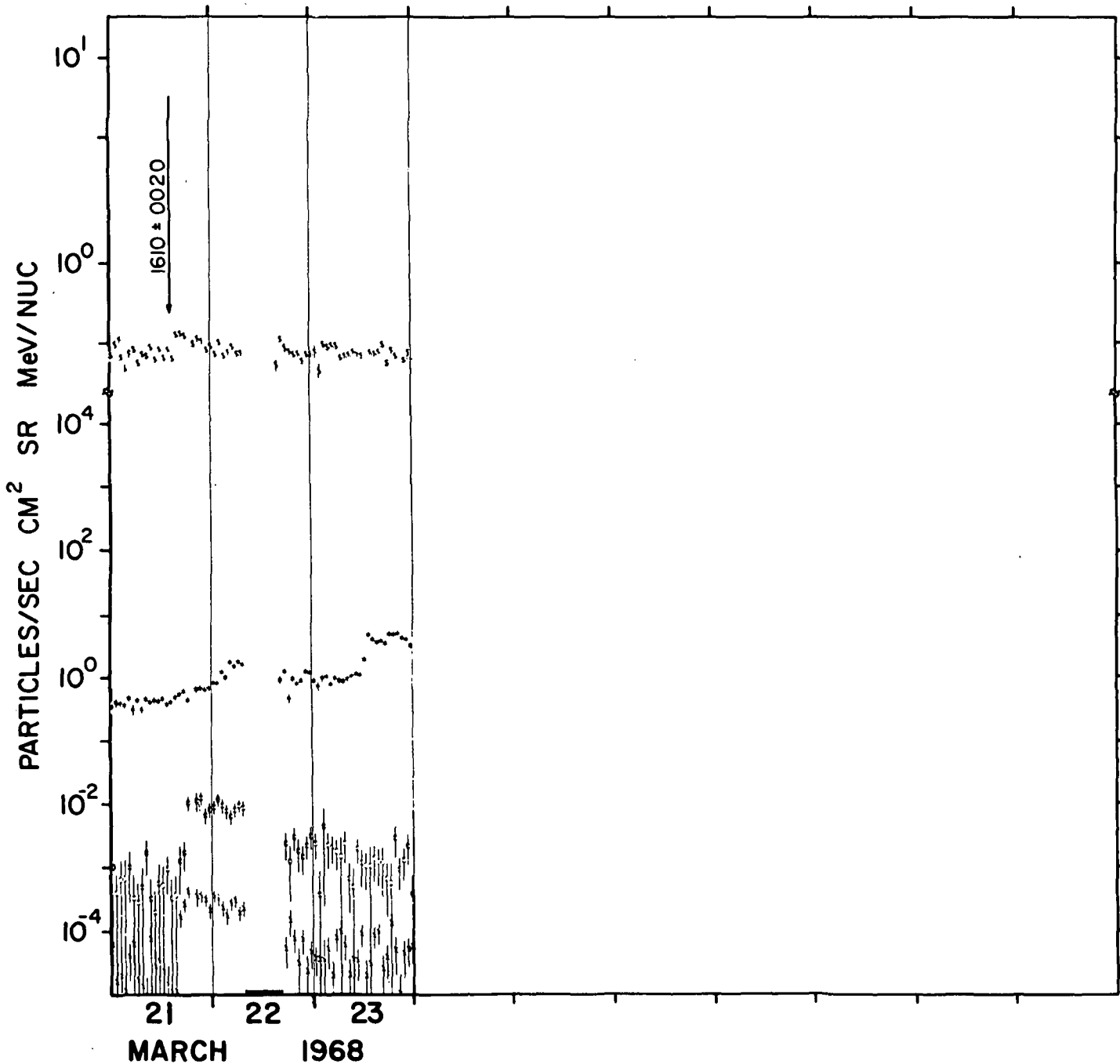
8 .5-1.1 MeV ELECTRONS X .9-1.5 MeV PROTONS O 6-19 MeV PROTONS X 19-80 MeV PROTONS



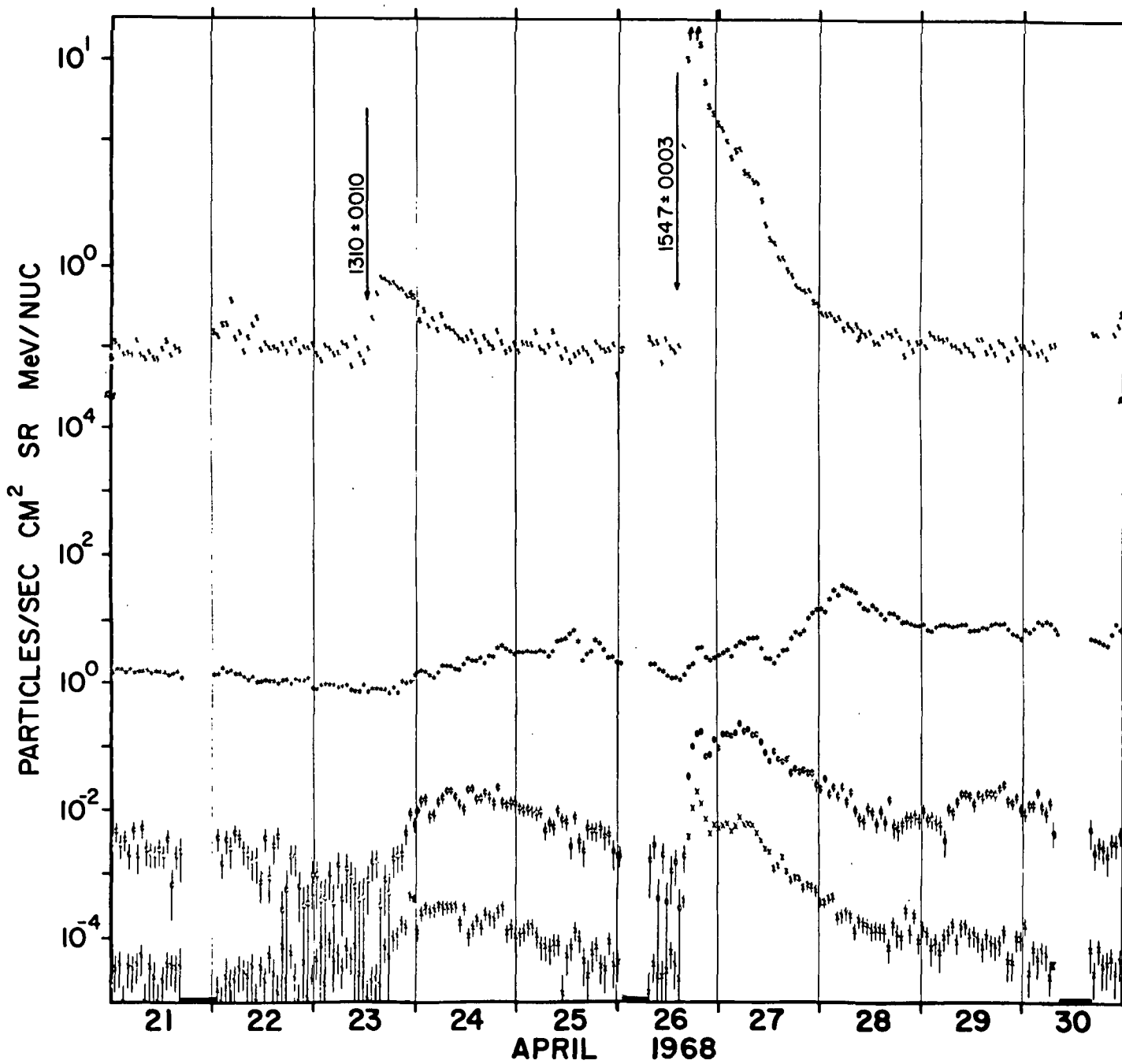
\$. 5 - 1.1 MeV ELECTRONS X . 9 - 1.5 MeV PROTONS + 6 - 19 MeV PROTONS X 19 - 80 MeV PROTONS



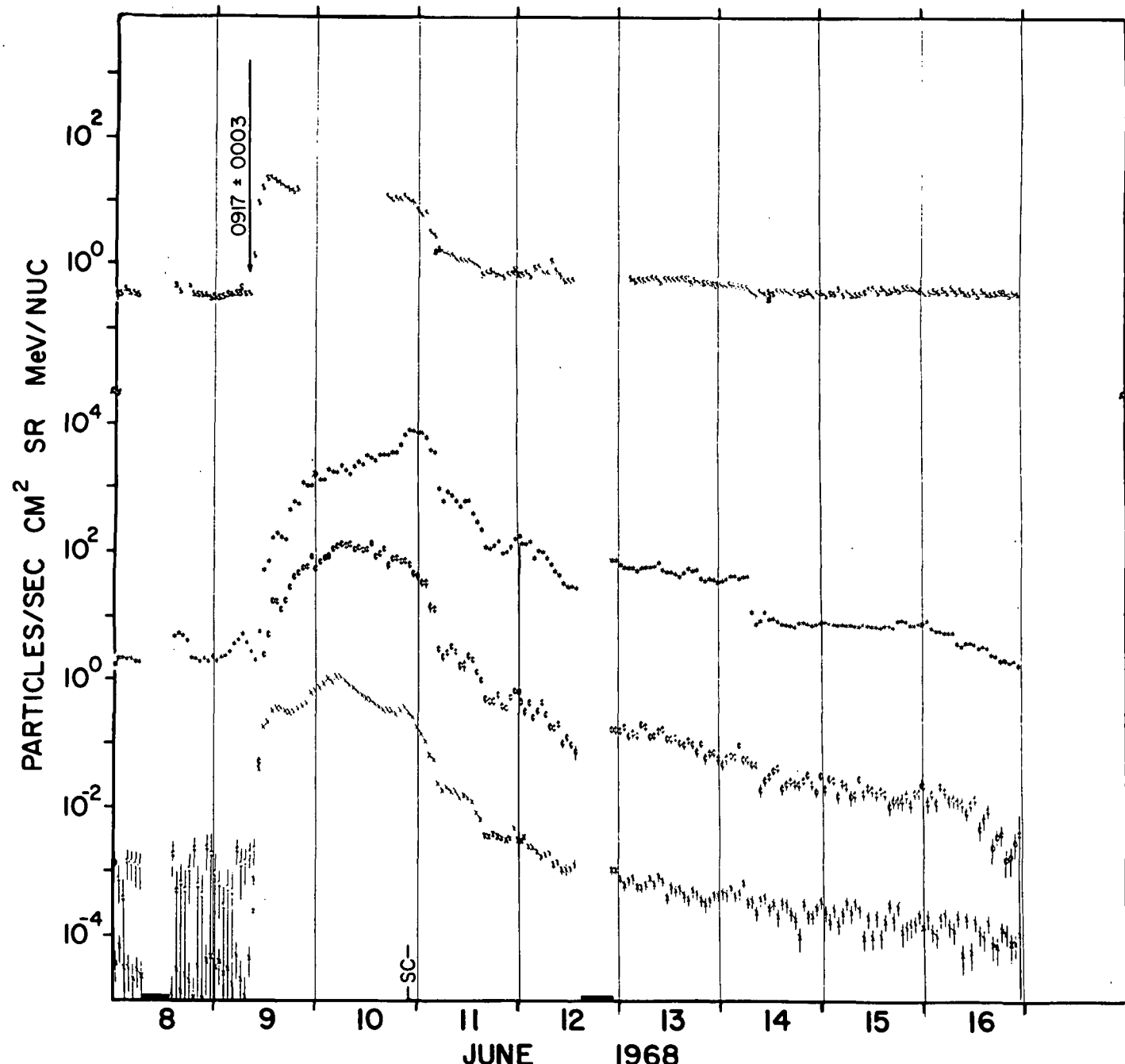
.5-1.1 MeV ELECTRONS X .9-1.5 MeV PROTONS ϕ 6-19 MeV PROTONS X 19-80 MeV PROTONS



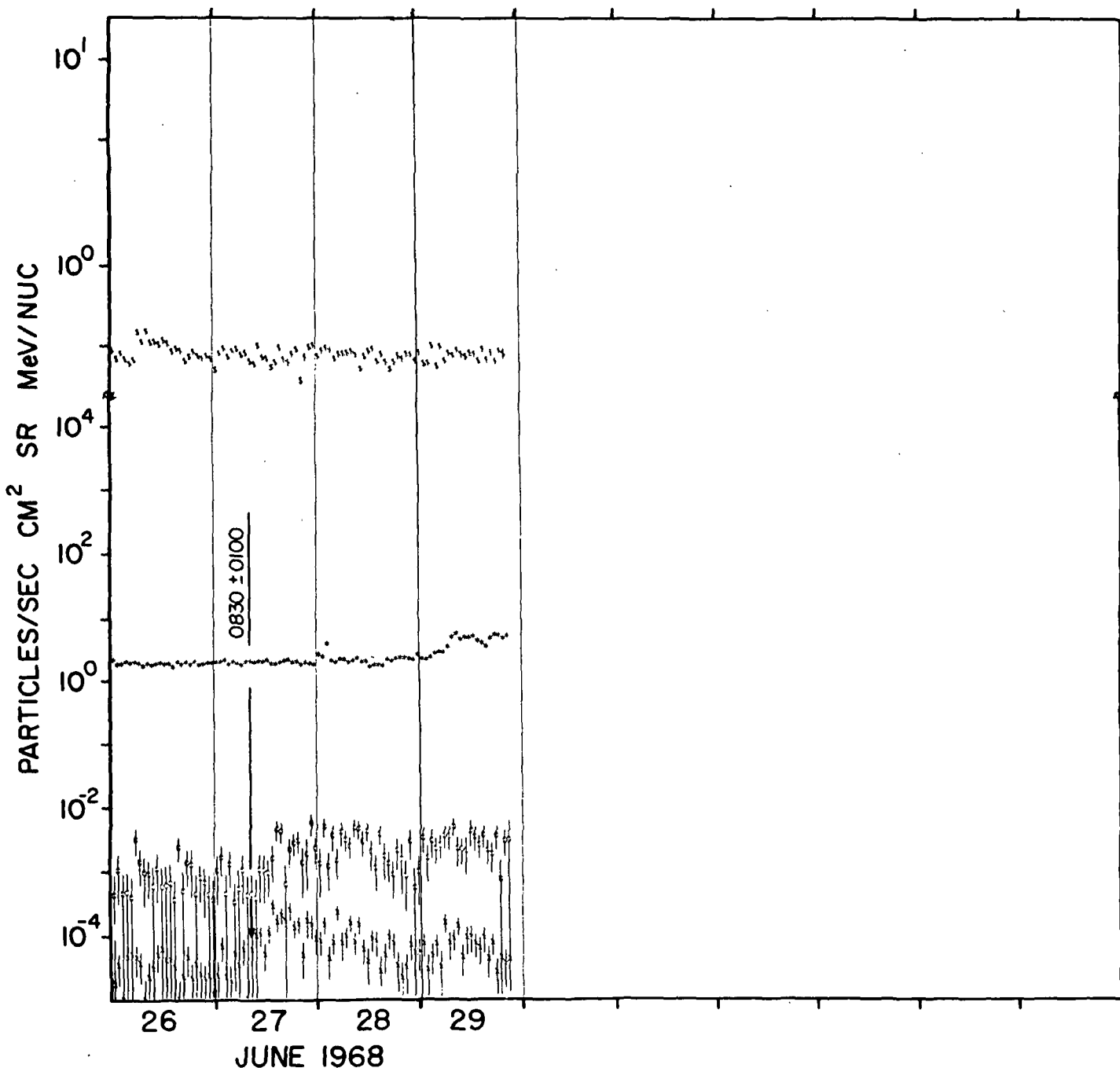
\$.5-1.1 MeV ELECTRONS X .9-1.5 MeV PROTONS 0 6-19 MeV PROTONS X 19-80 MeV PROTONS



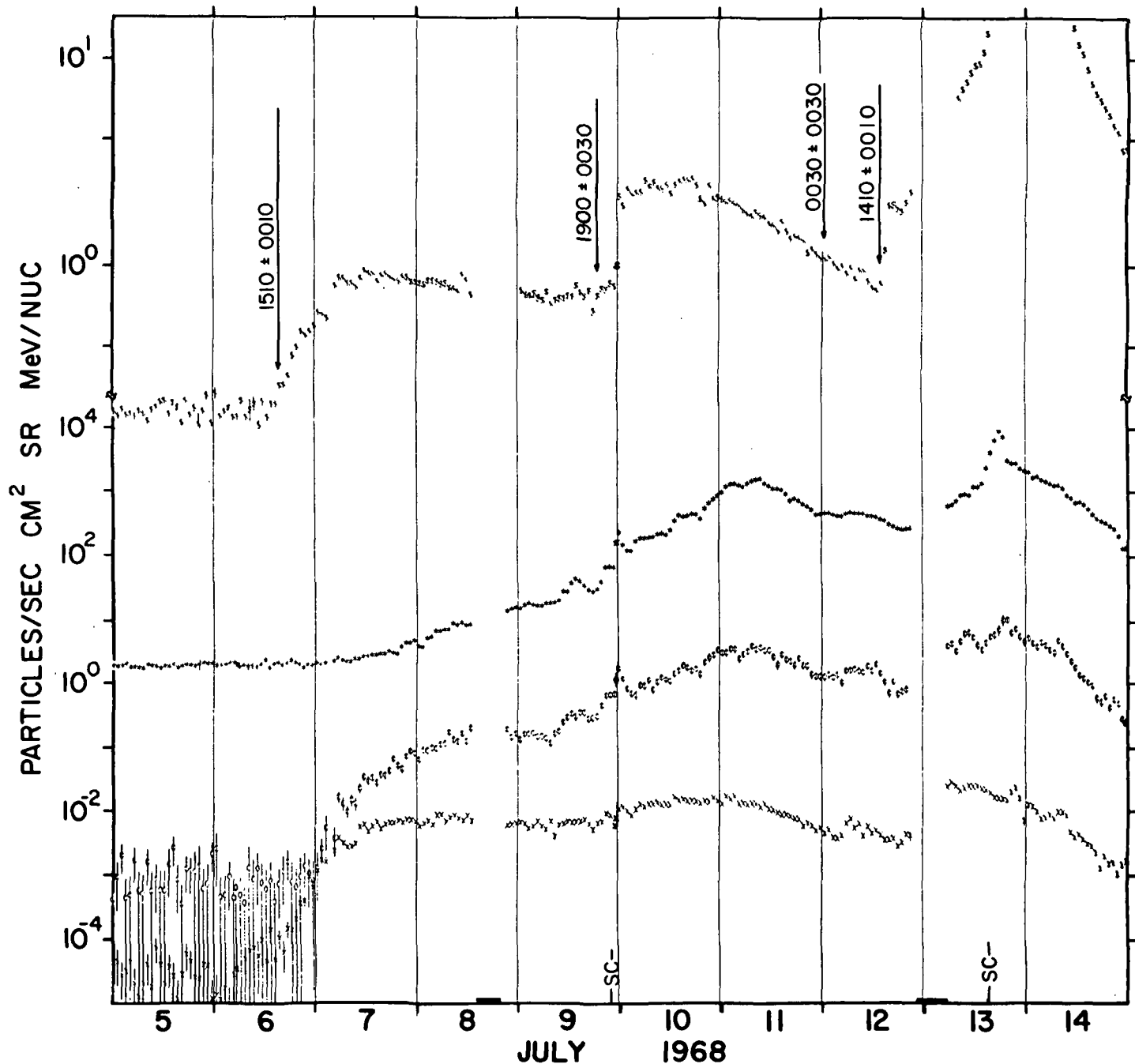
\$.5-1.1 MeV ELECTRONS X .9-1.5 MeV PROTONS 0 6-19 MeV PROTONS X 19-80 MeV PROTONS



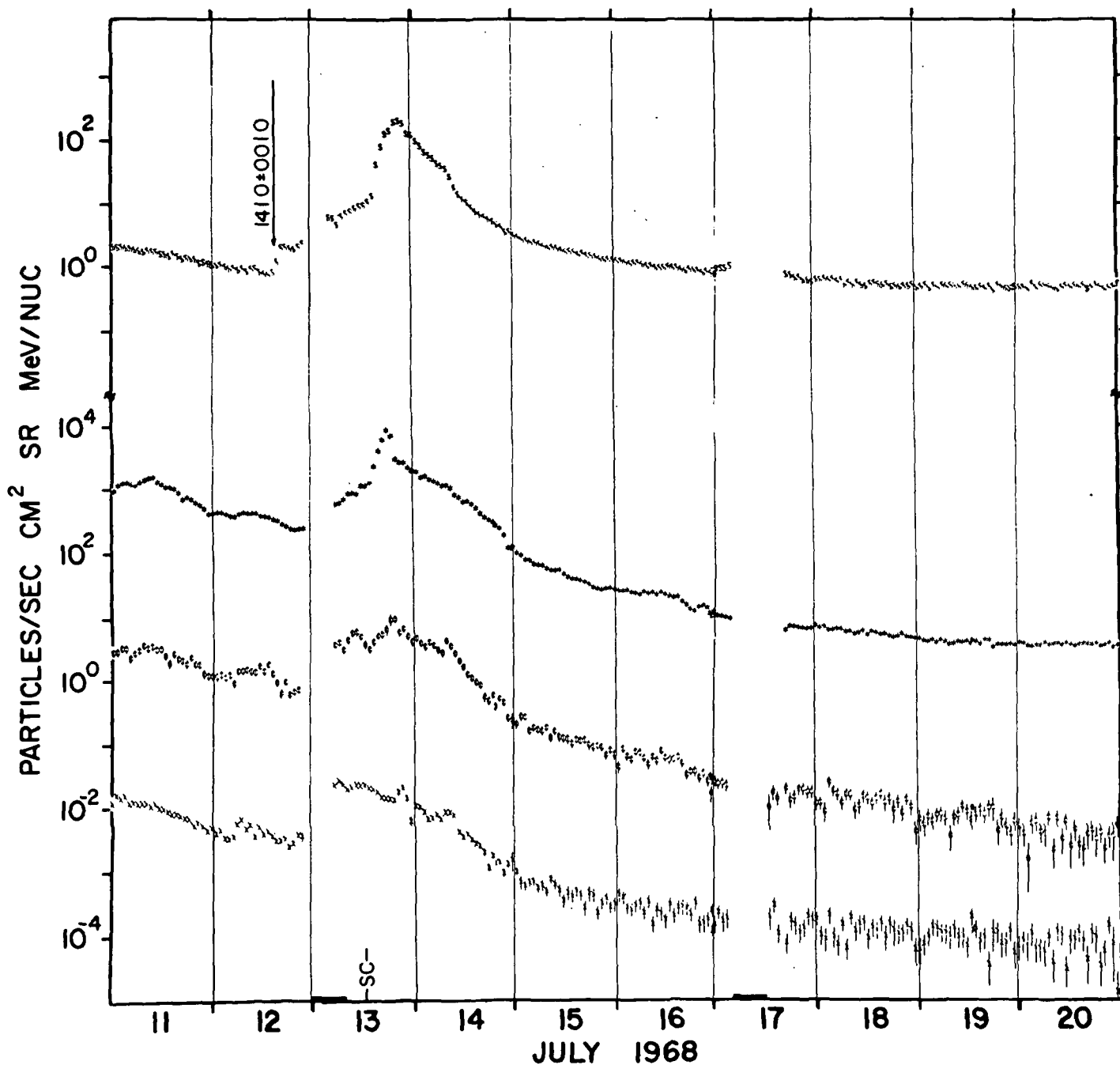
\$.5-1.1 MeV ELECTRONS X .9-1.5 MeV PROTONS @ 6-19 MeV PROTONS X 19-80 MeV PROTONS



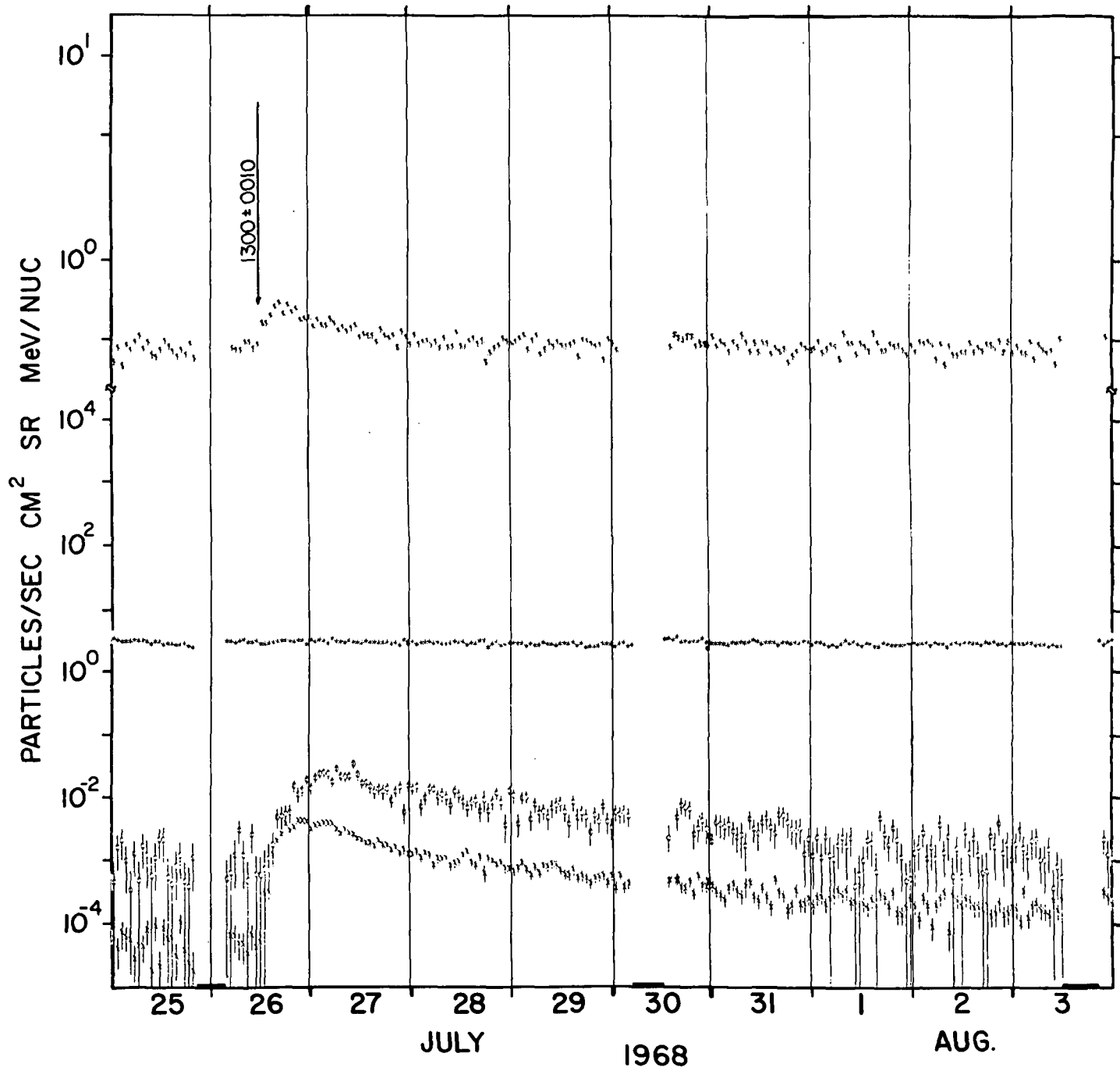
\$.5-1.1 MeV ELECTRONS X .9-1.5 MeV PROTONS ϕ 6-19 MeV PROTONS X 19-80 MeV PROTON



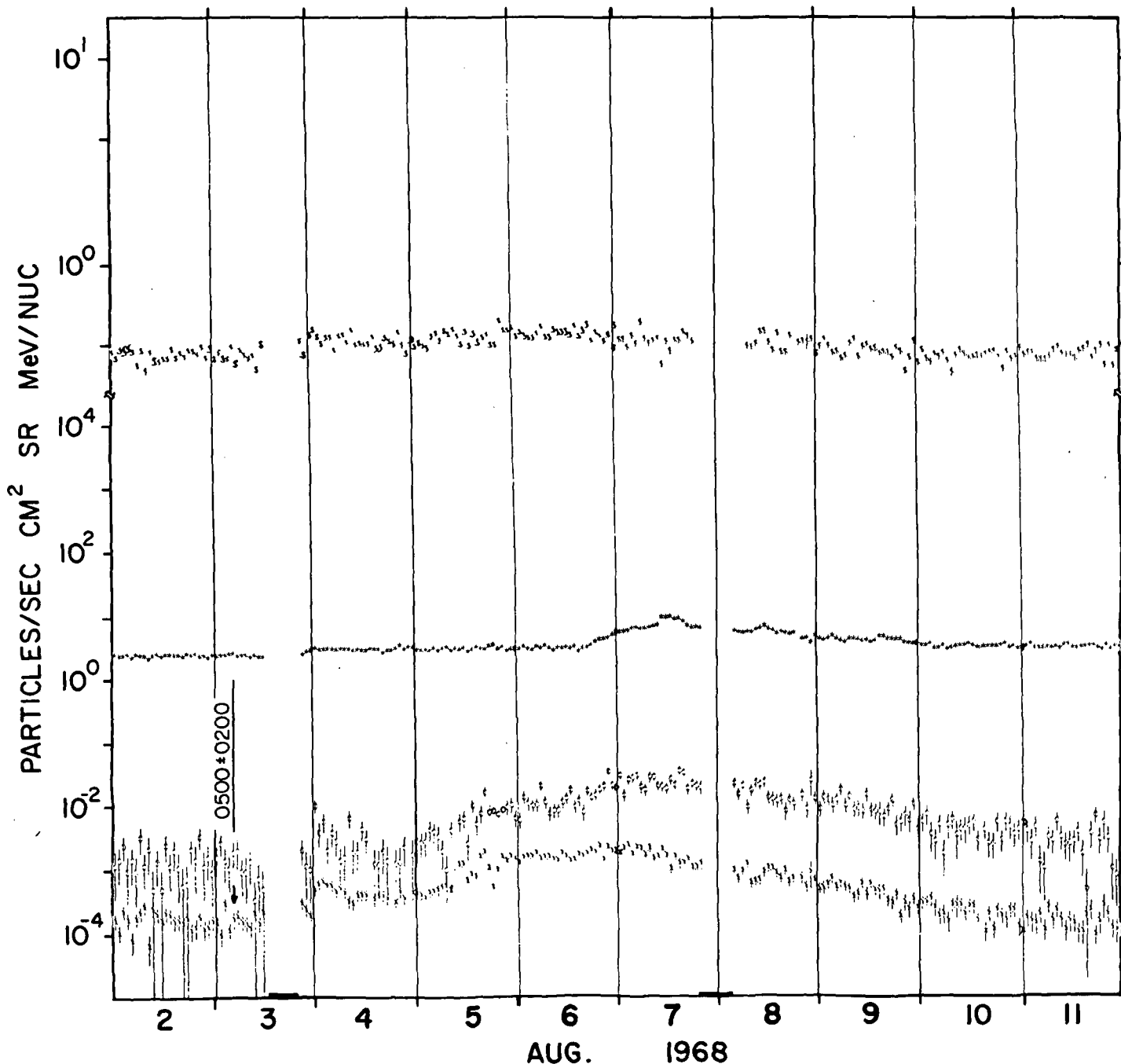
.5-1.1 MeV ELECTRONS X .9-1.5 MeV PROTONS + 6-19 MeV PROTONS X 19-80 MeV PROTONS

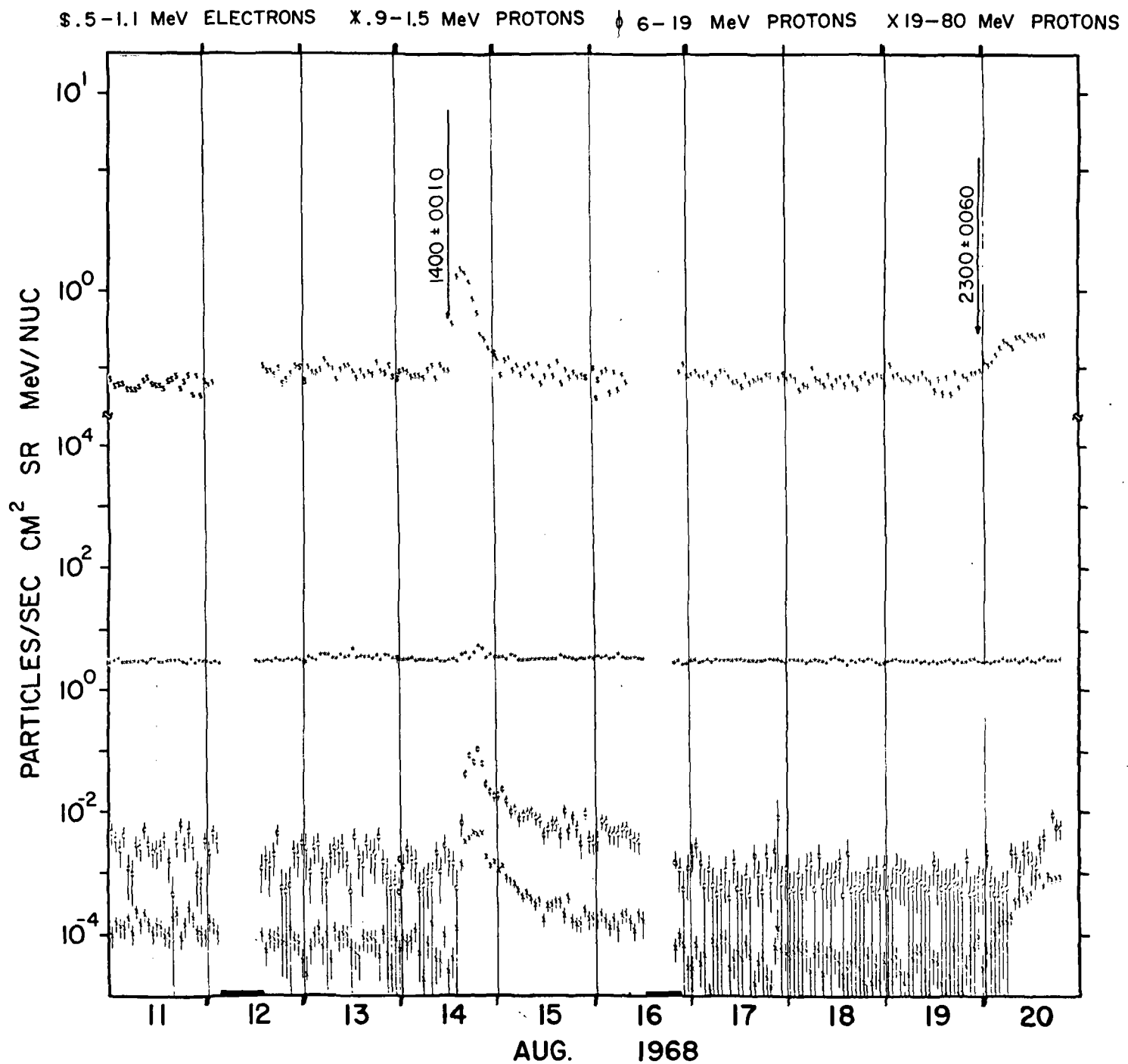


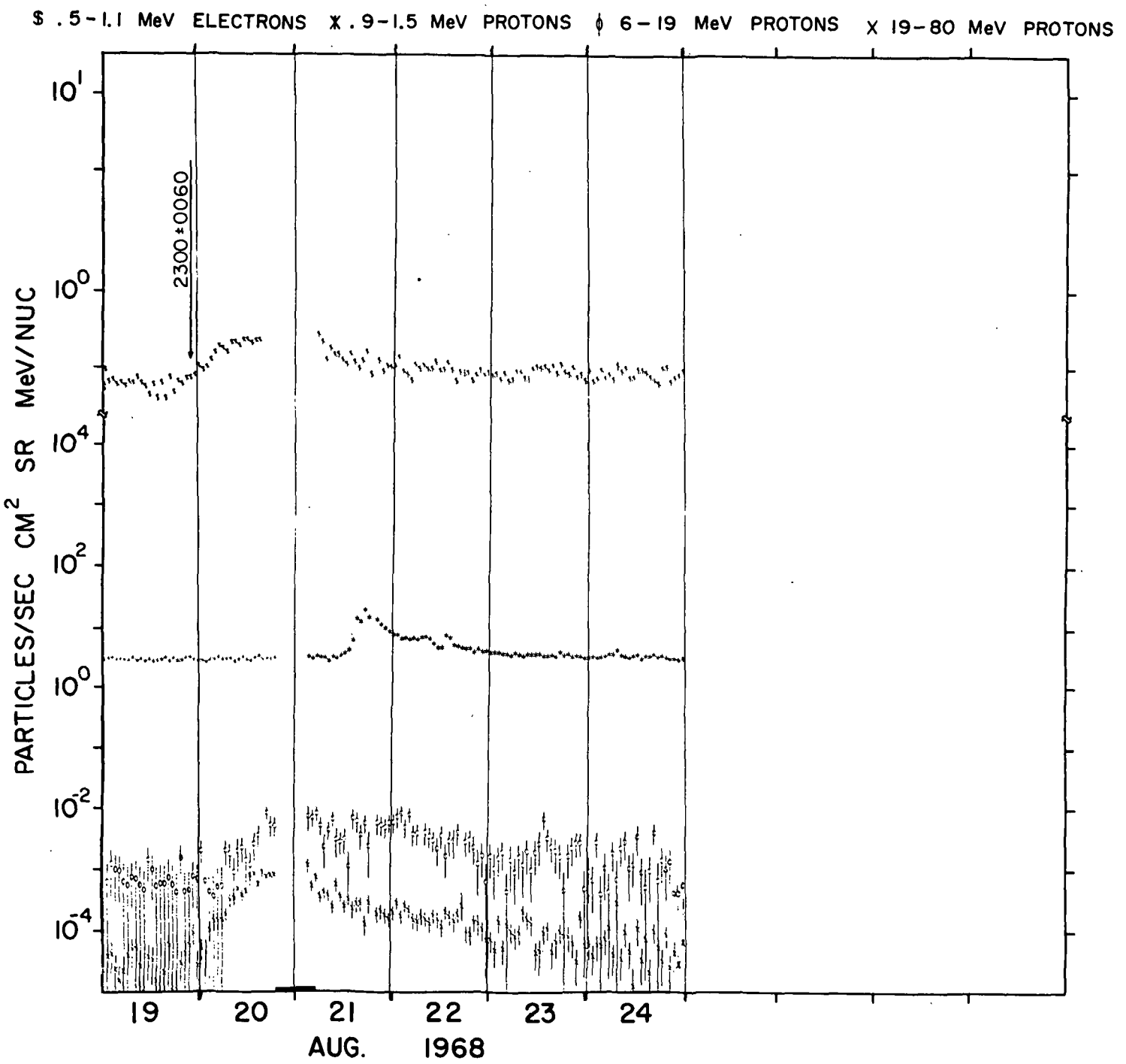
.5-1.1 MeV ELECTRONS X .9-1.5 MeV PROTONS ϕ 6-19 MeV PROTONS X 19-80 MeV PROTONS



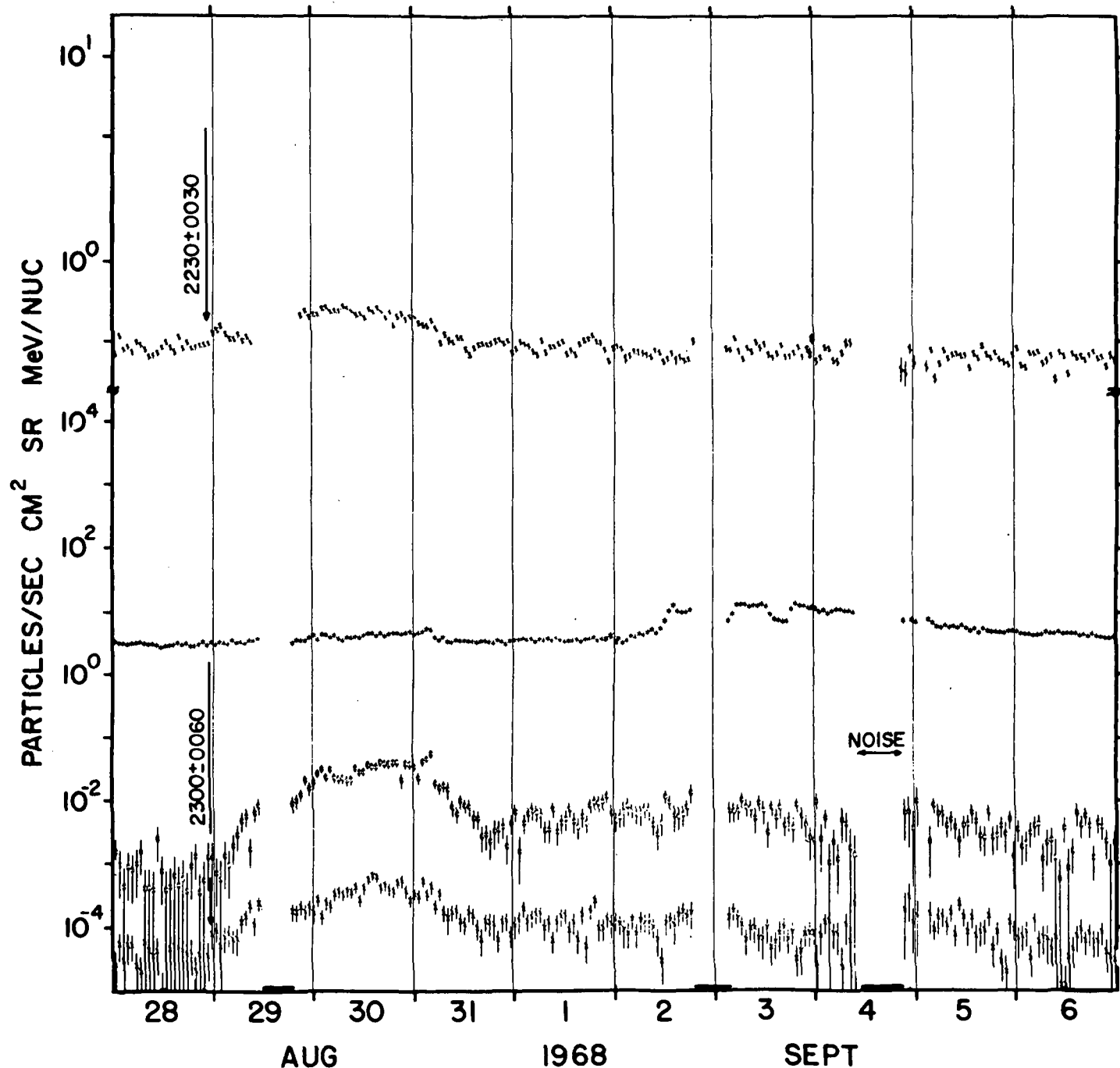
\$.5 - 1.1 MeV ELECTRONS X .9 - 1.5 MeV PROTONS + 6 - 19 MeV PROTONS X 19 - 80 MeV PROTONS



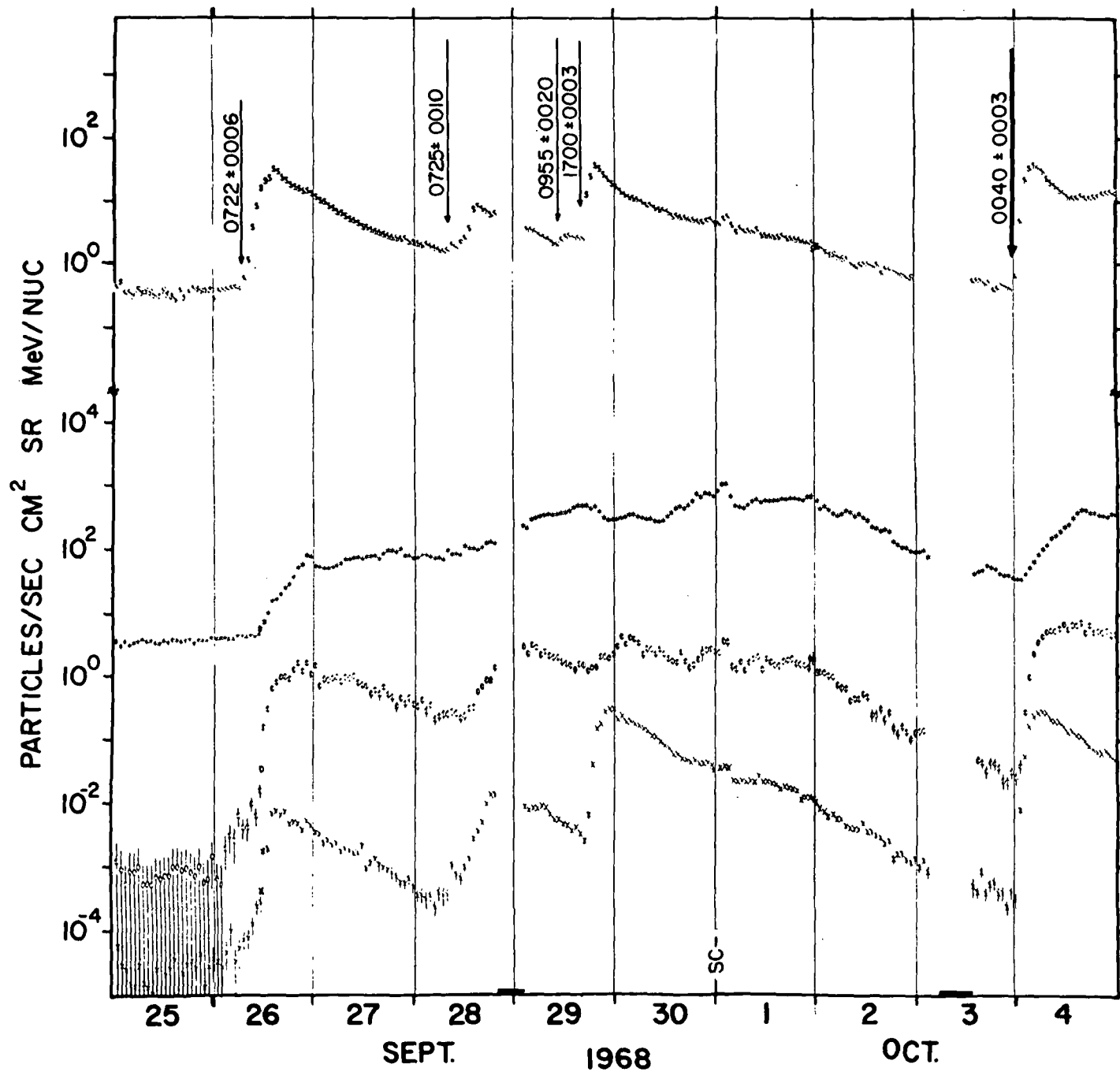




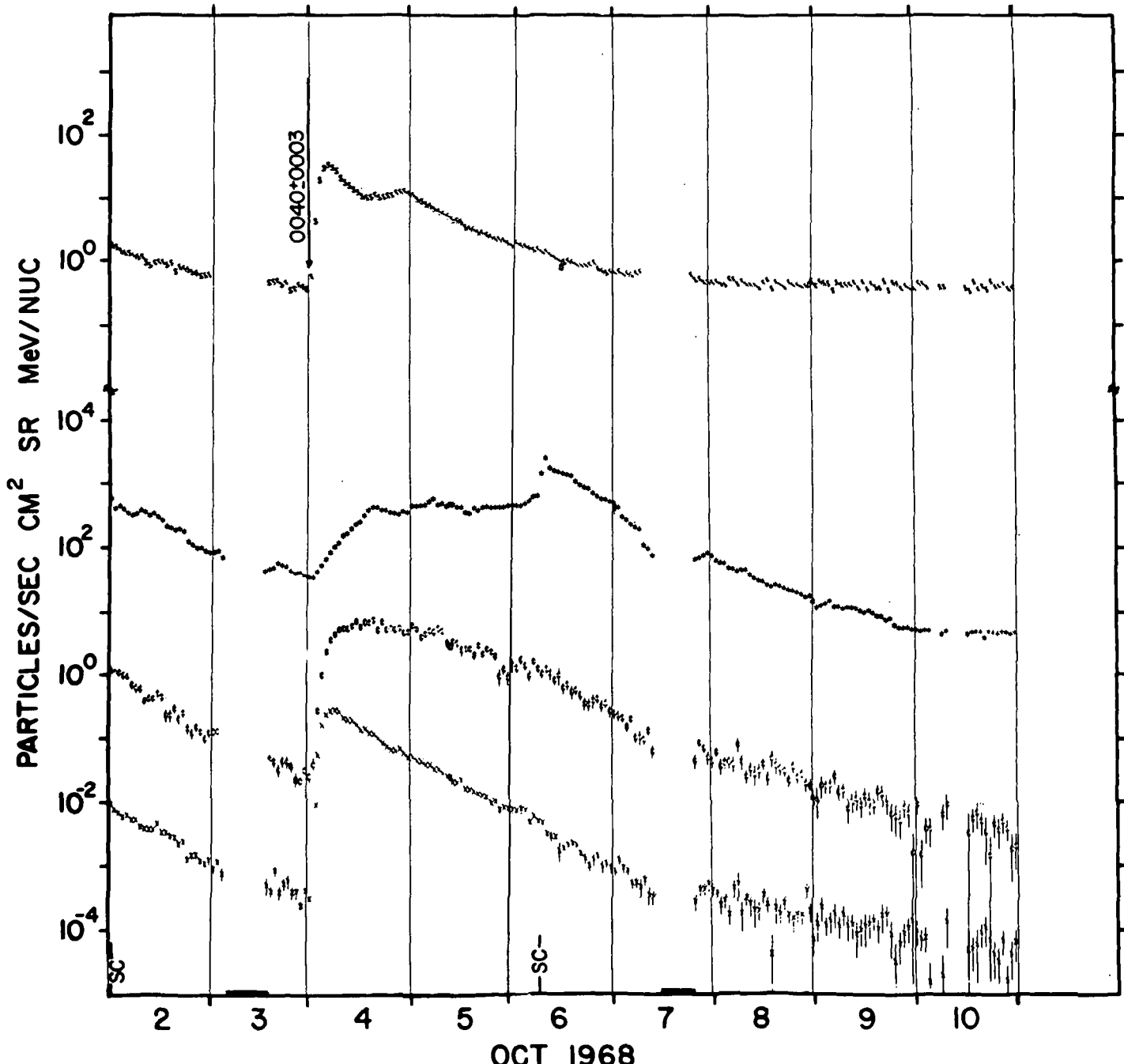
S.5-1.1 MeV ELECTRONS X .9-1.5 MeV PROTONS + 6-19 MeV PROTONS X 19-80 MeV PROTONS



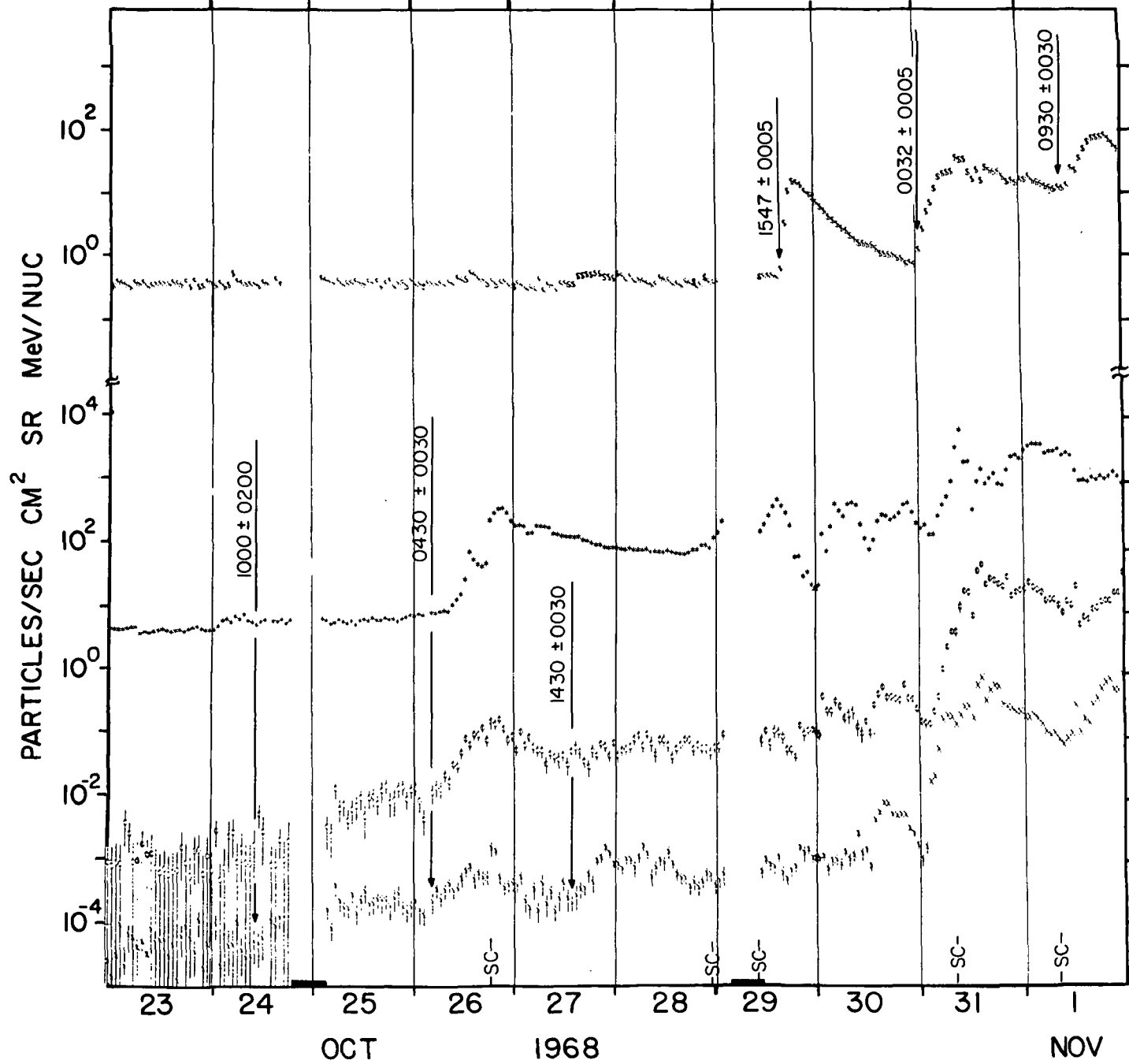
\$.5-1.1 MeV ELECTRONS X .9-1.5 MeV PROTONS @ 6-19 MeV PROTONS X 19-80 MeV PROTONS

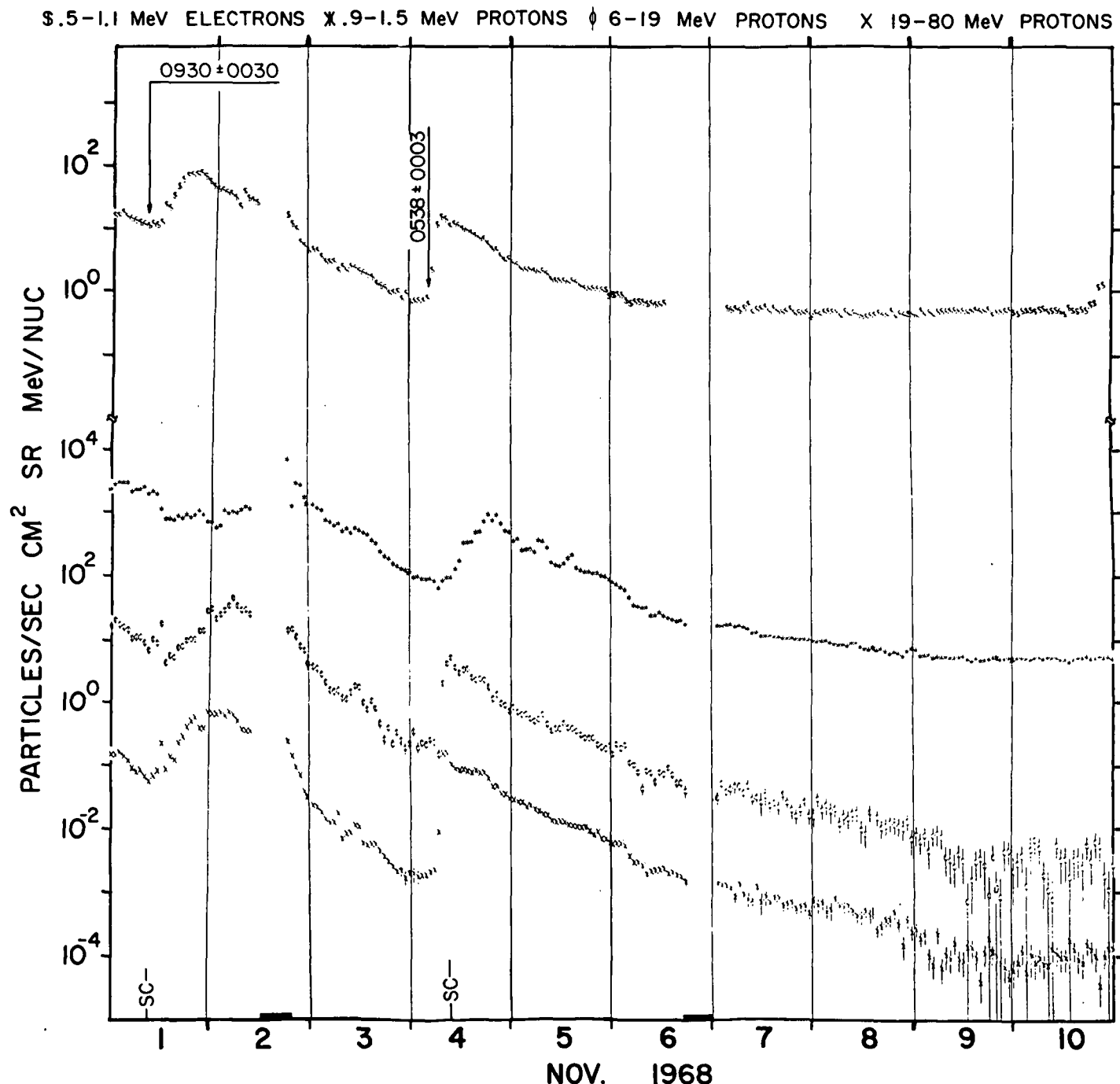


S .5-1.1 MeV ELECTRONS X 9-1.5 MeV PROTONS 6-19 MeV PROTONS X 19-80 MeV PROTONS

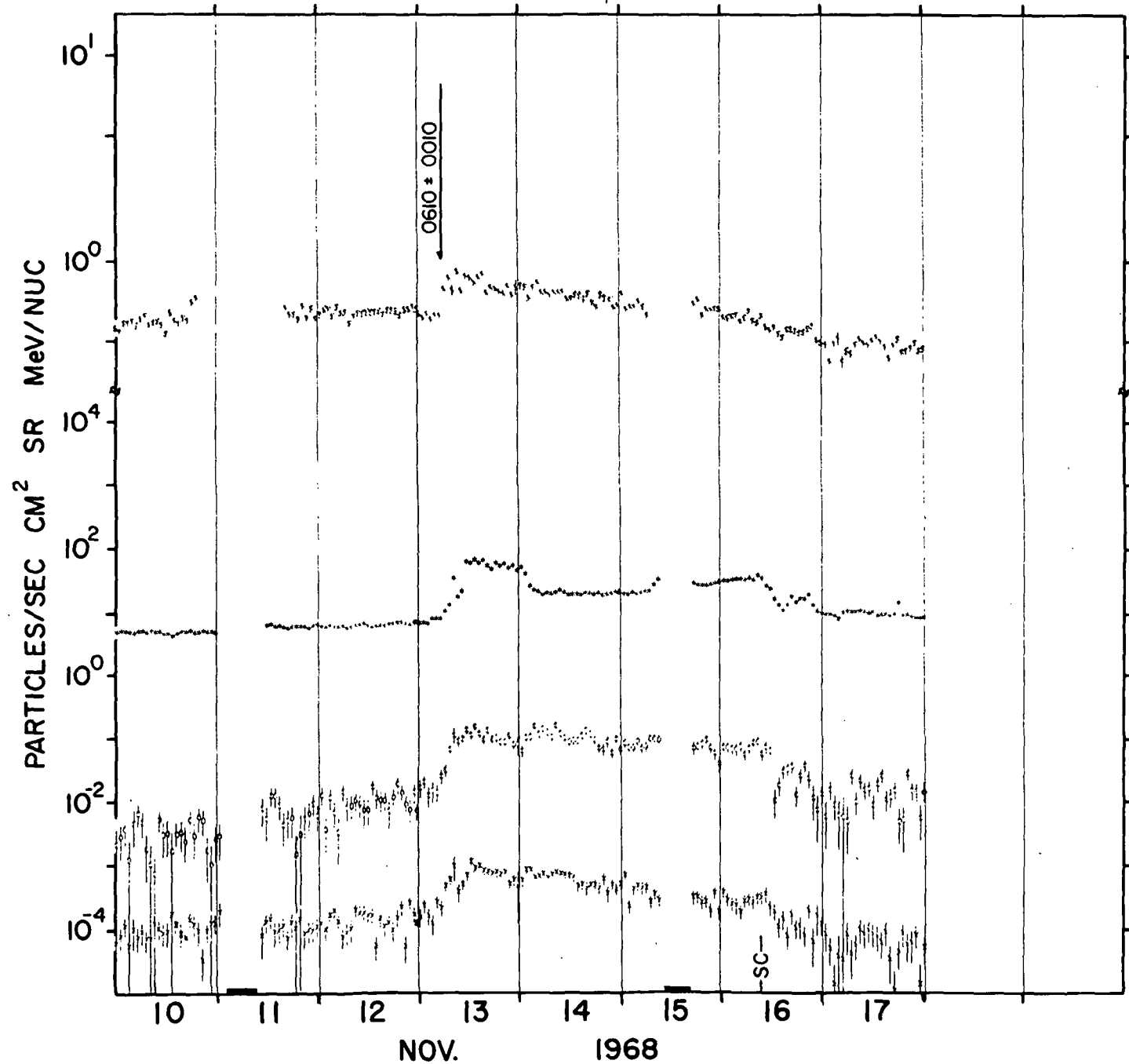


$\$.5 - 1.1$ MeV ELECTRONS $\times .9 - 1.5$ MeV PROTONS \oplus $6 - 19$ MeV PROTONS $\times 19 - 80$ MeV PROTONS

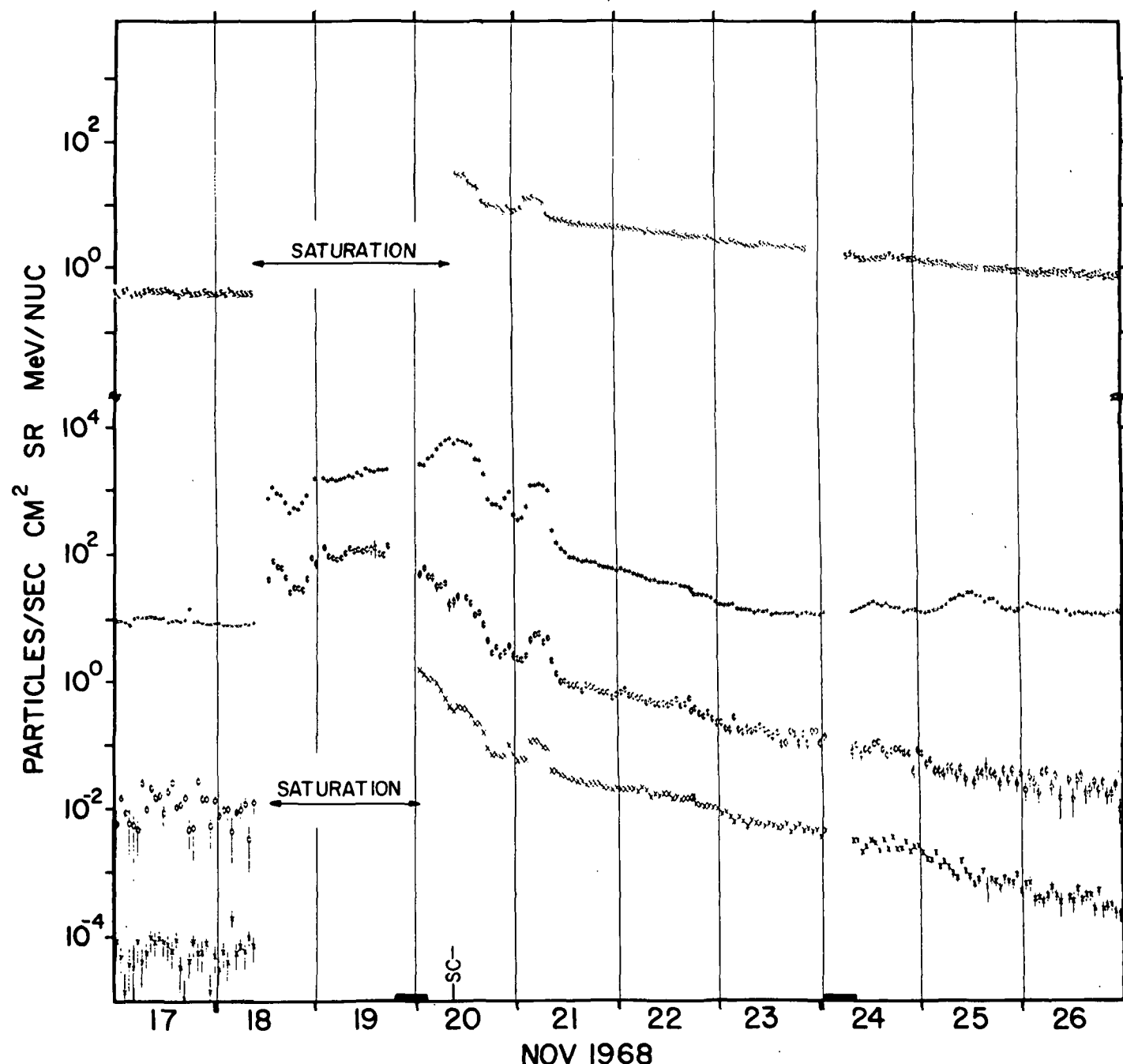




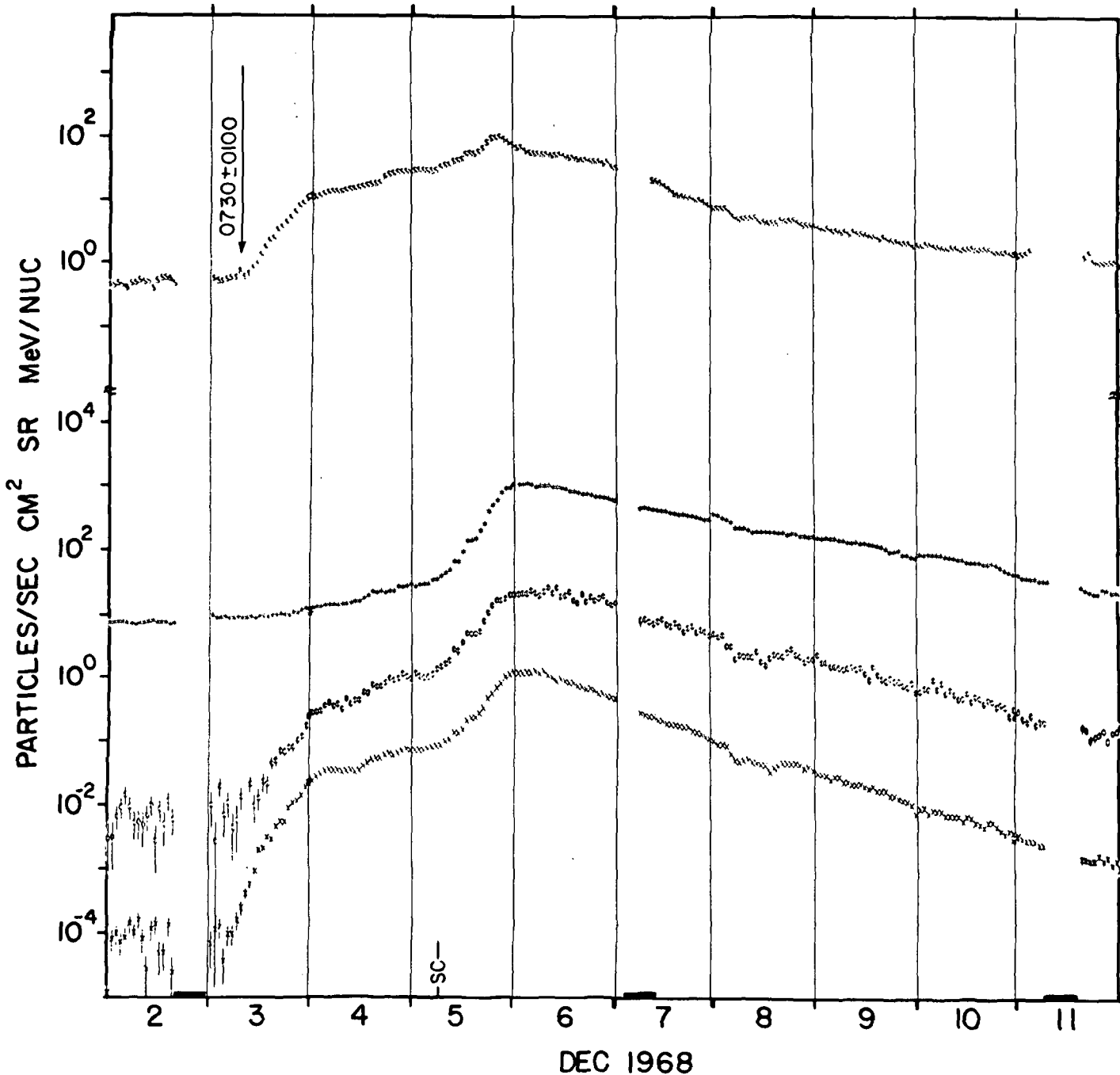
\$.5-1.1 MeV ELECTRONS X .9-1.5 MeV PROTONS 0 6-19 MeV PROTONS X 19-80 MeV PROTONS



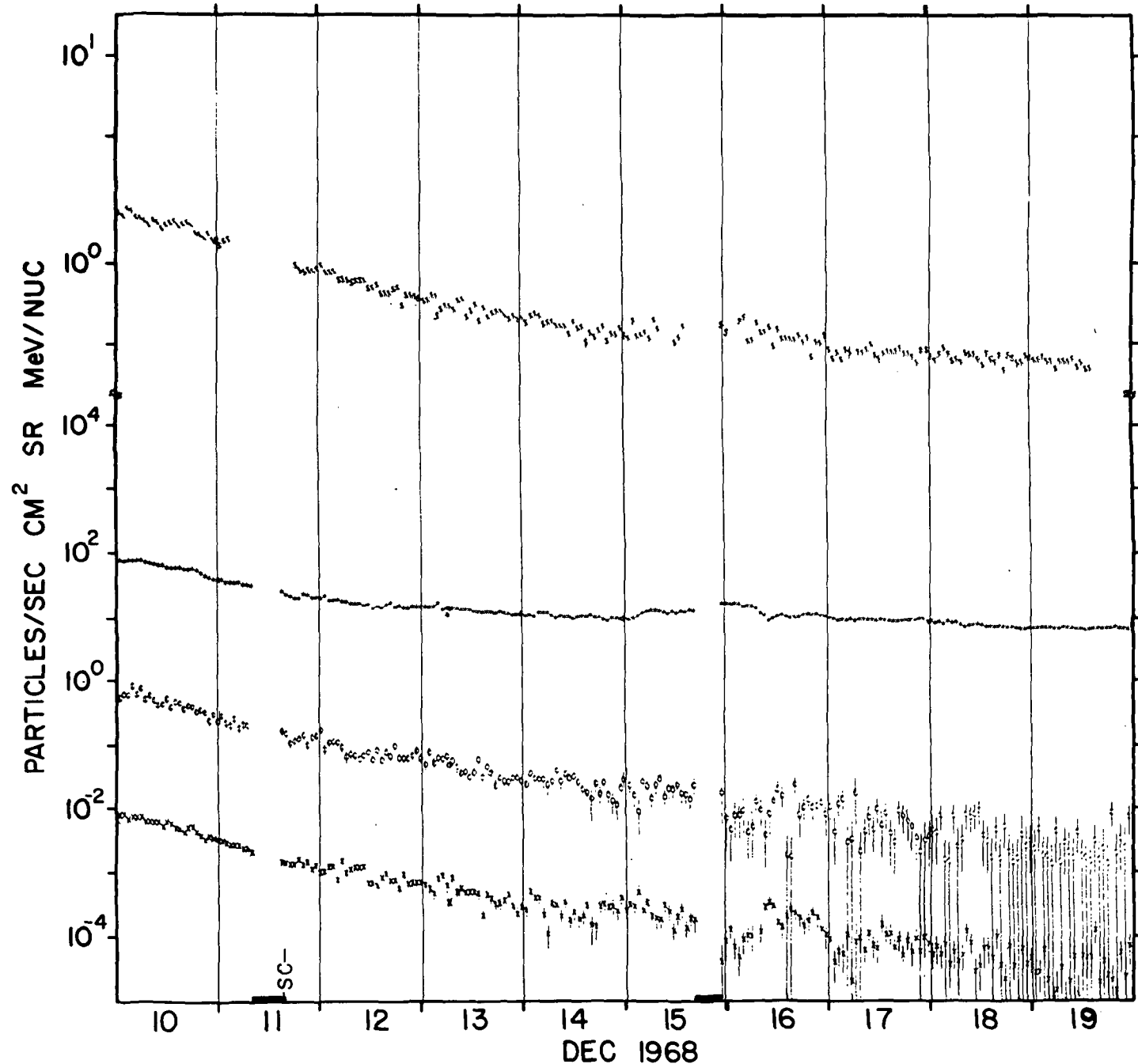
.5-1.1 MeV ELECTRONS X .9-1.5 MeV PROTONS Ø 6-19 MeV PROTONS X 19-80 MeV PROTONS



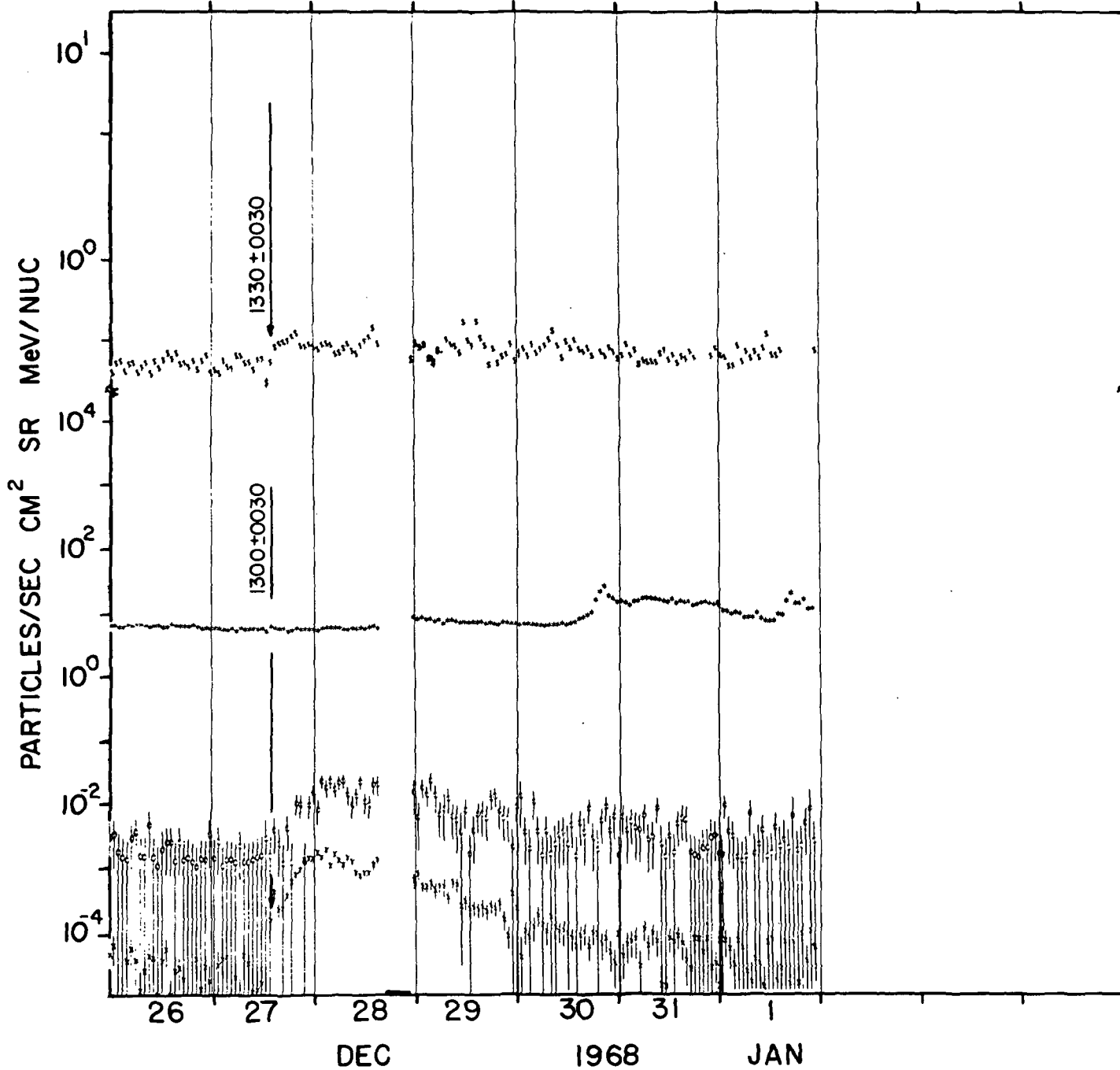
§ .5-1.1 MeV ELECTRONS X 9-1.5 MeV PROTONS O 6-19 MeV PROTONS X 19-80 MeV PROTONS



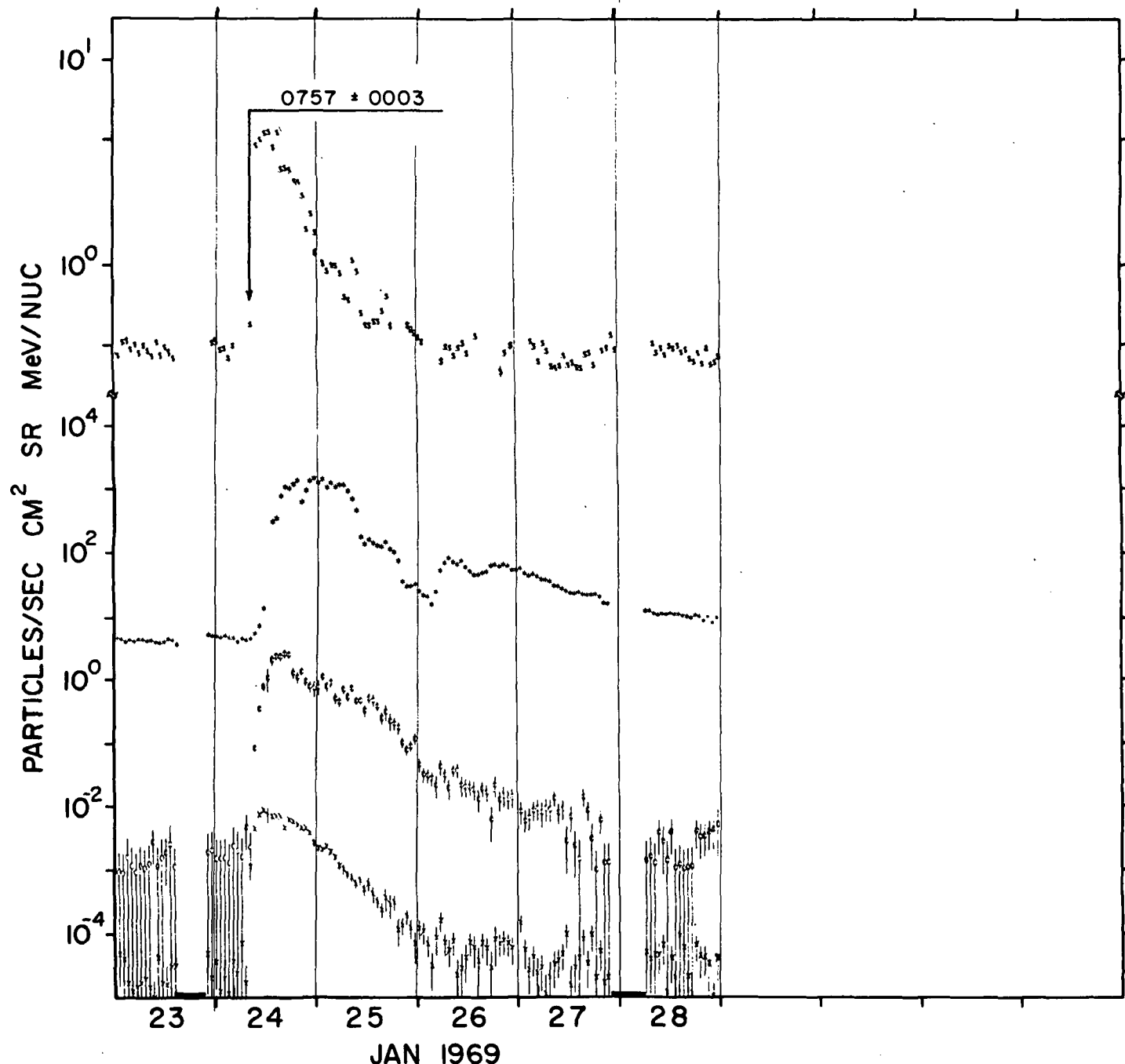
.5-1.1 MeV ELECTRONS X .9-1.5 MeV PROTONS ϕ 6-19 MeV PROTONS X 19-80 MeV PROTONS



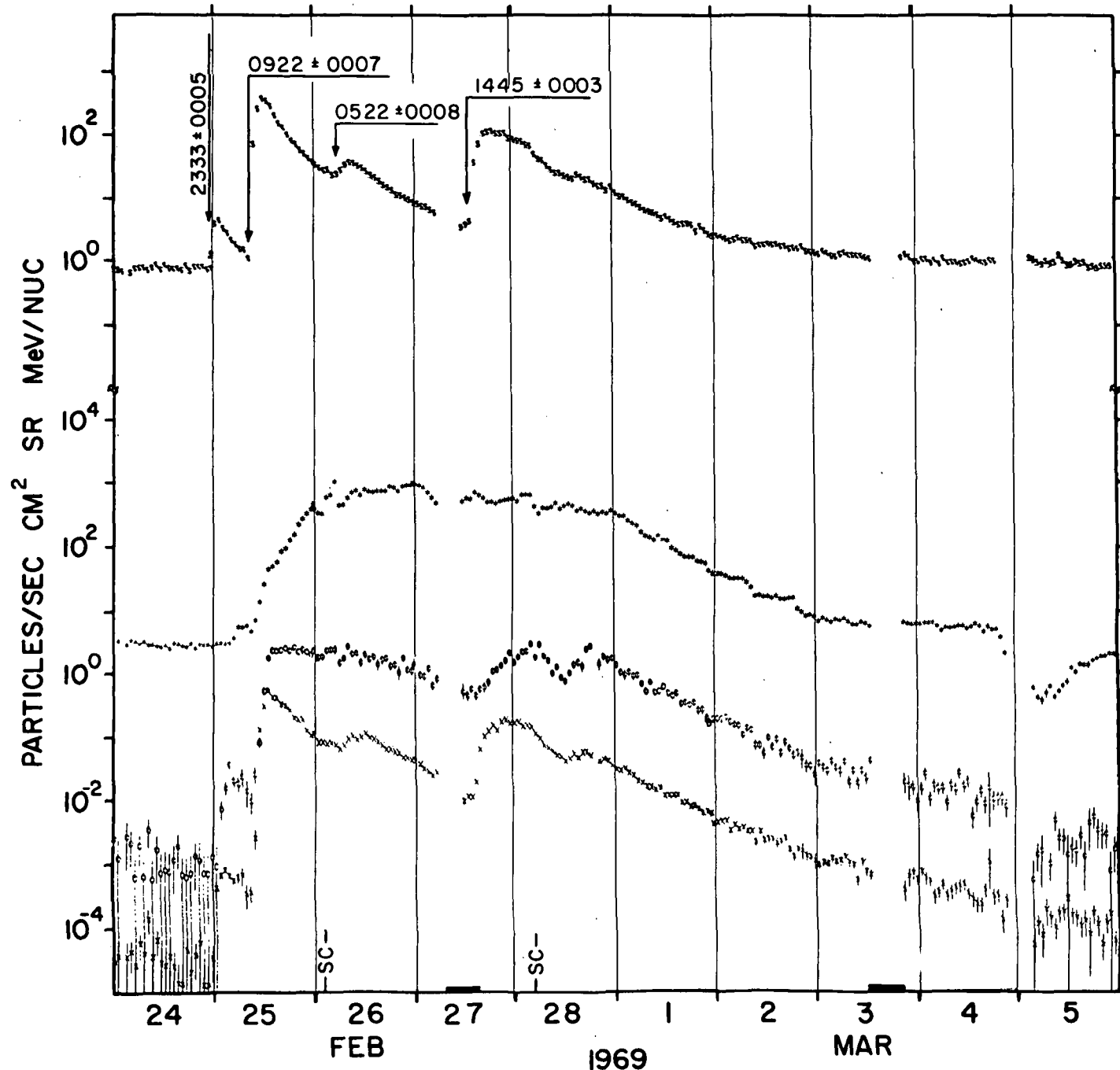
\$.5-1.1 MeV ELECTRONS X .9-1.5 MeV PROTONS O 6-19 MeV PROTONS X 19-80 MeV PROTONS



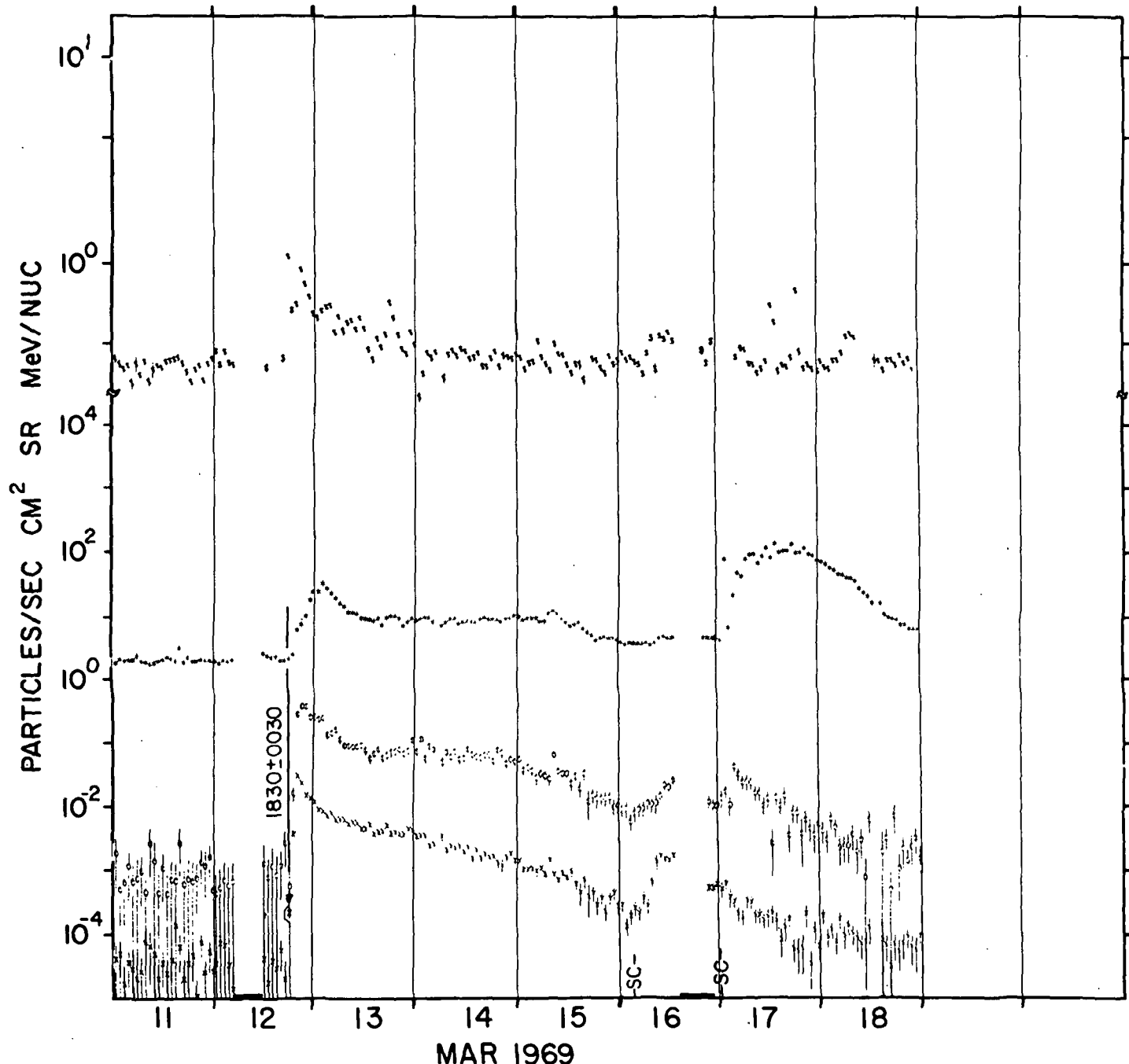
\$.5-1.1 MeV ELECTRONS X .9-1.5 MeV PROTONS O 6-19 MeV PROTONS X 19-80 MeV PROTONS



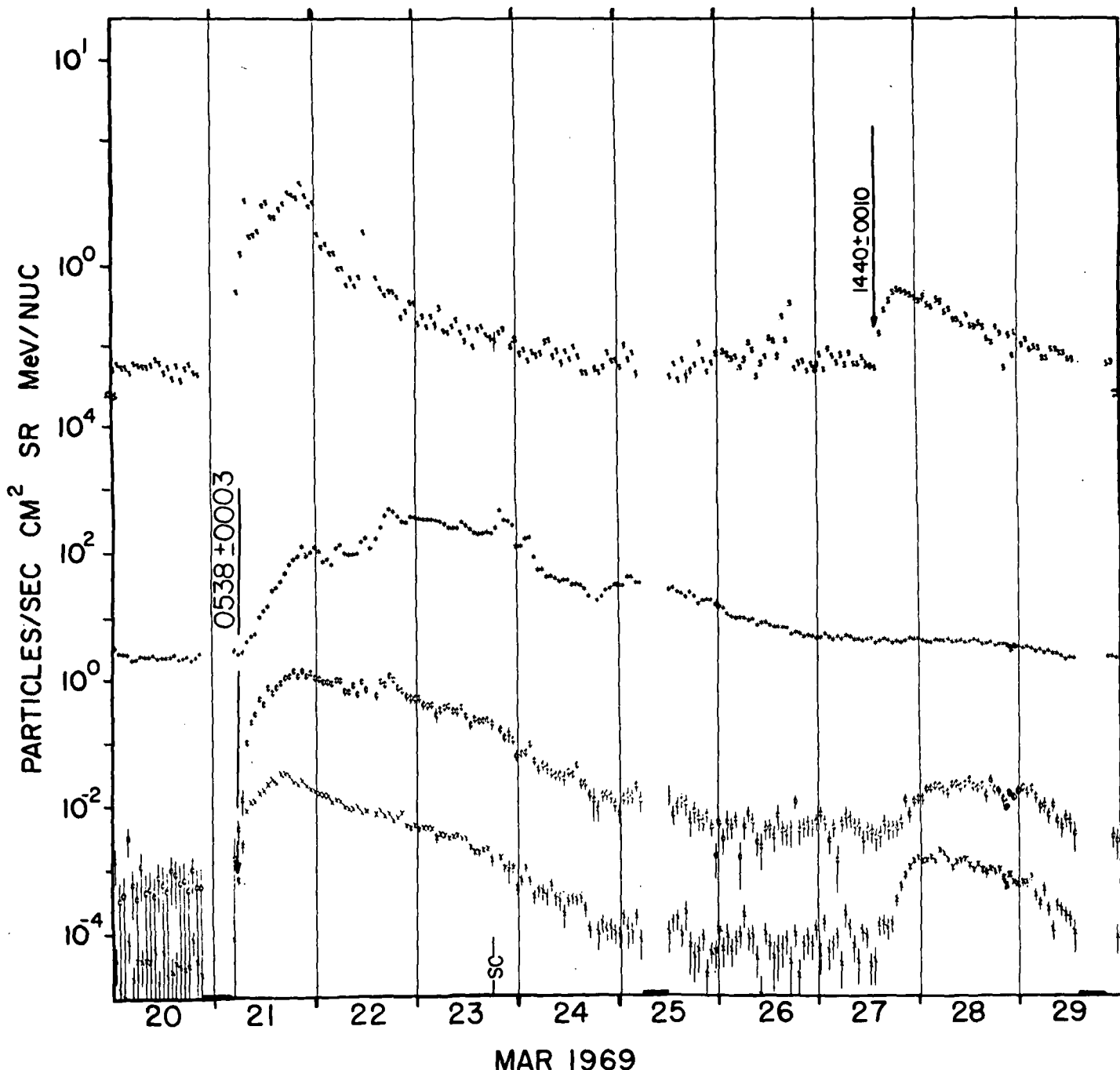
\$.5-1.1 MeV ELECTRONS X .9-1.5 MeV PROTONS ϕ 6-19 MeV PROTONS X 19-80 MeV PROTONS



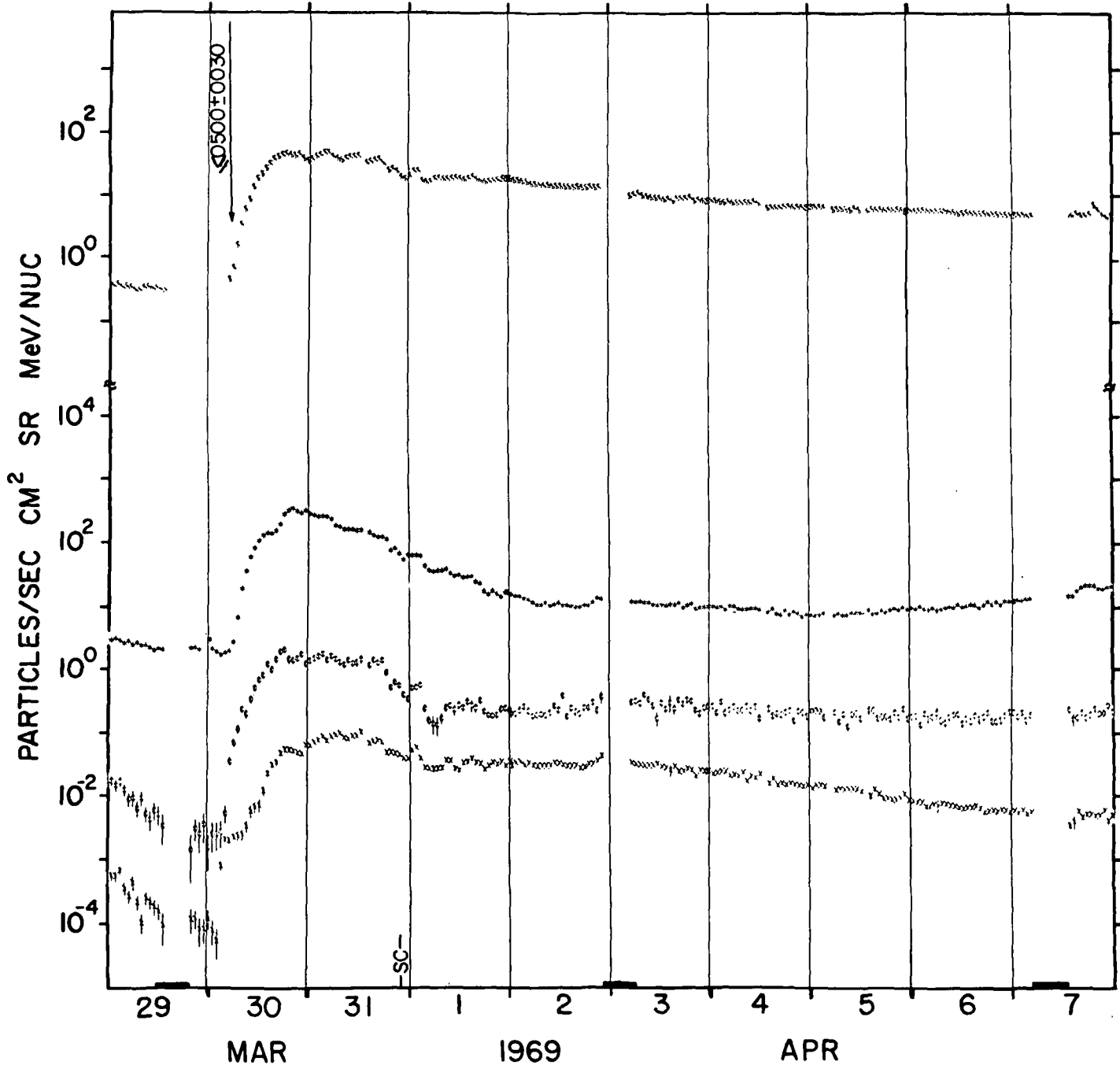
S . 5-1.1 MeV ELECTRONS X 9-1.5 MeV PROTONS Ø 6-19 MeV PROTONS X 19-80 MeV PROTONS



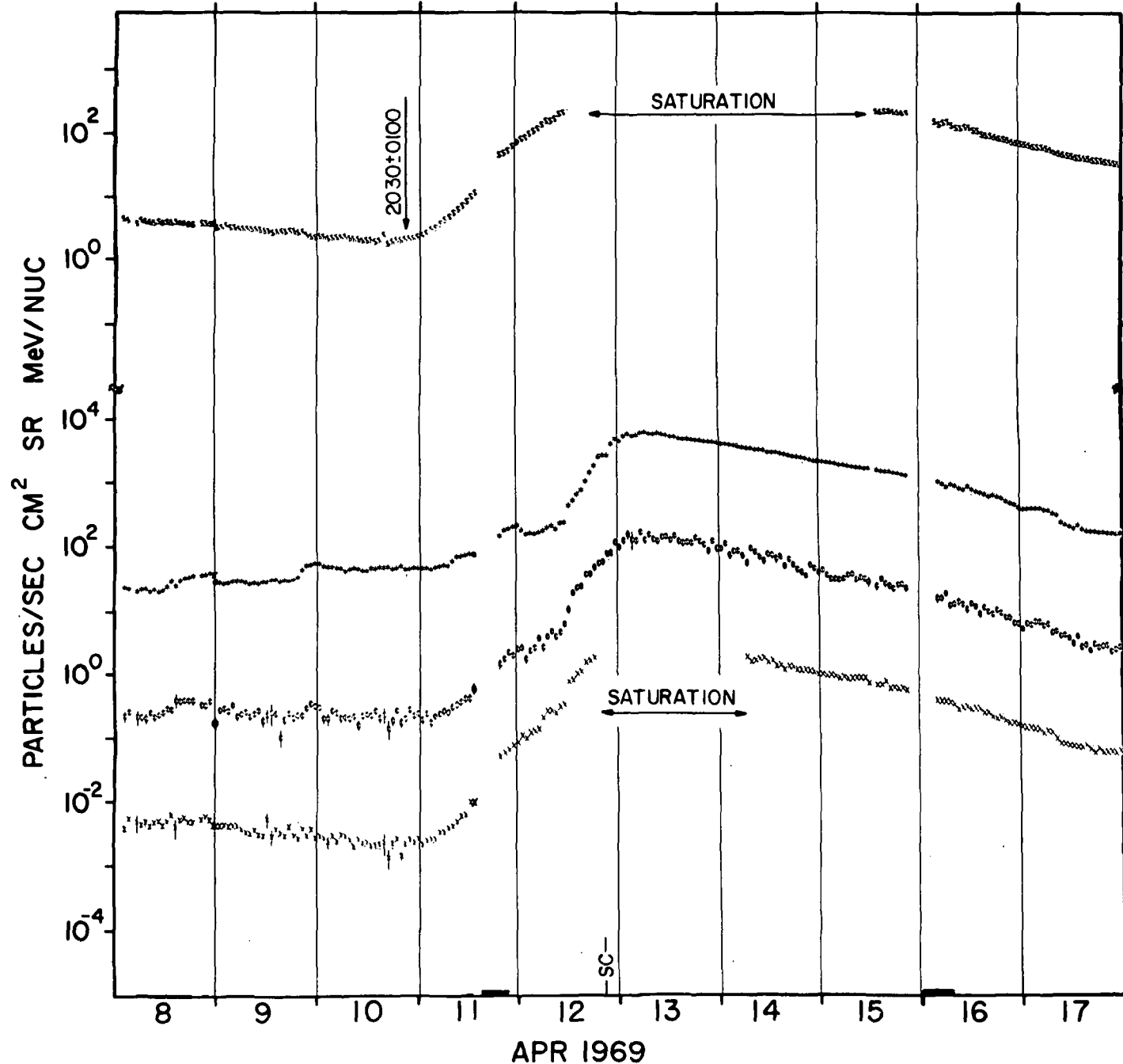
5.5-1.1 MeV ELECTRONS X 9-1.5 MeV PROTONS 16-19 MeV PROTONS X 19-80 MeV PROTONS



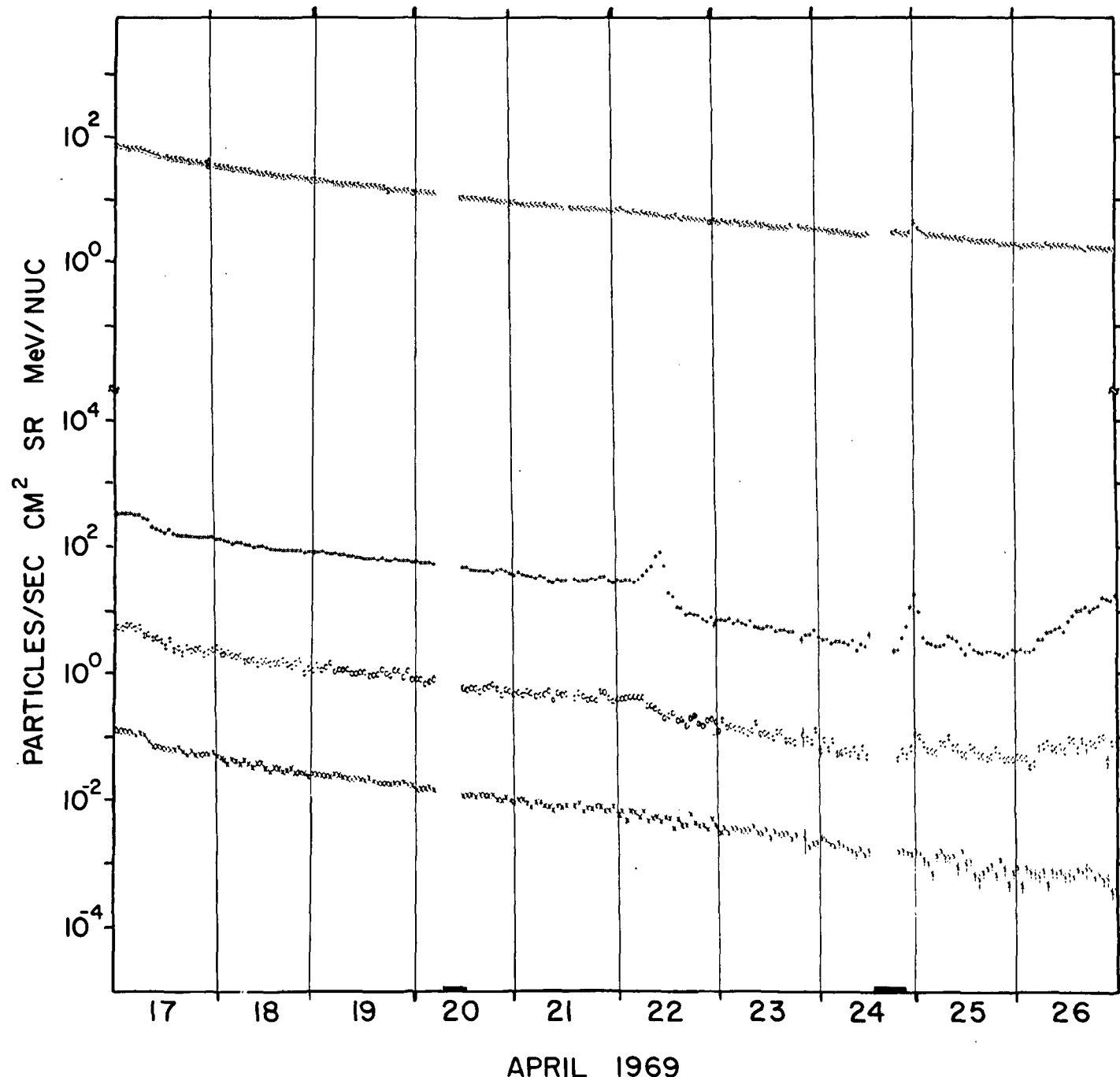
\$.5-1.1 MeV ELECTRONS X .9-1.5 MeV PROTONS \oplus 6-19 MeV PROTONS X 19-80 MeV PROTONS



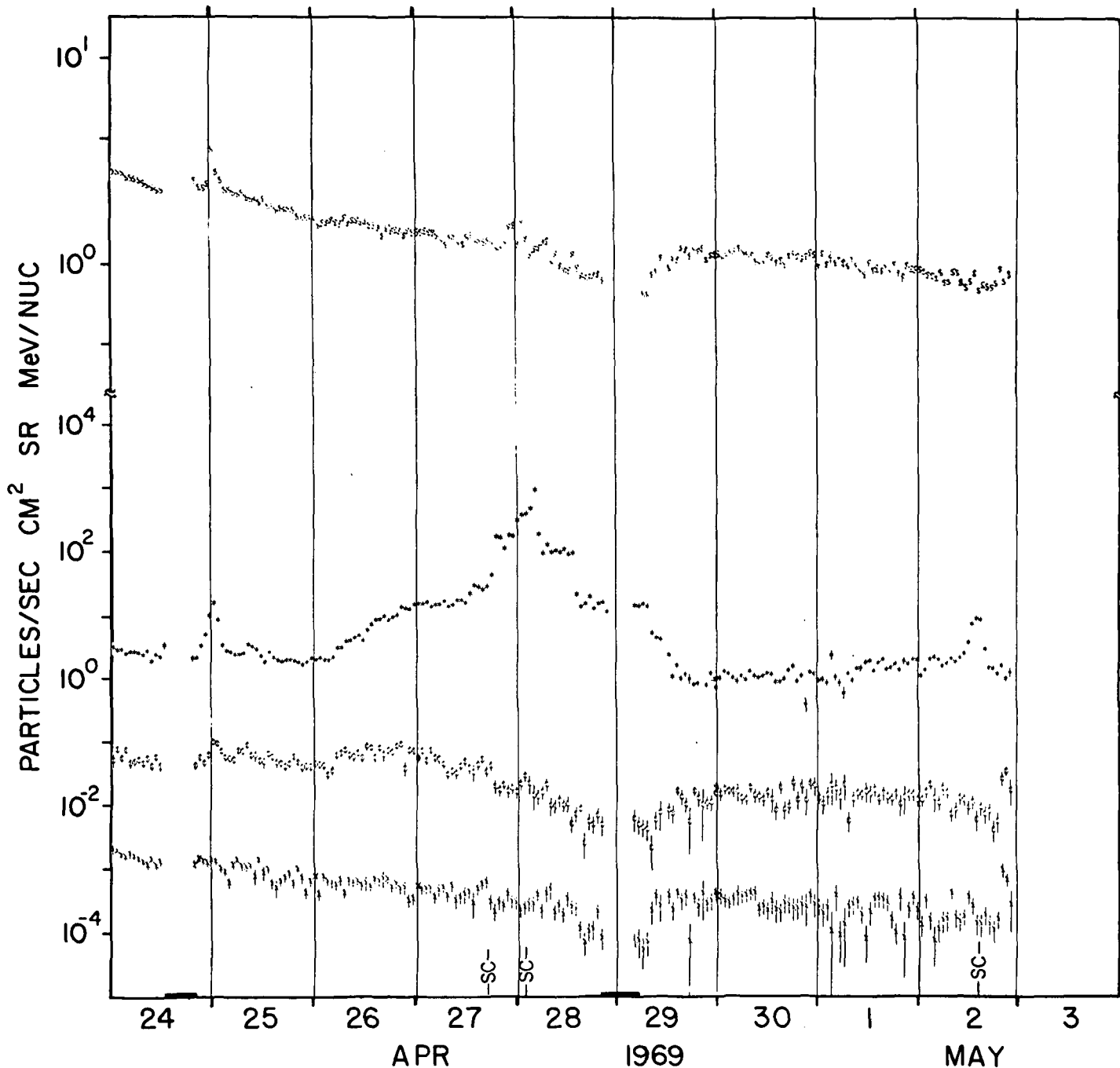
.5-1.1 MeV ELECTRONS X .9-1.5 MeV PROTONS ϕ 6-19 MeV PROTONS X 19-80 MeV PROTONS



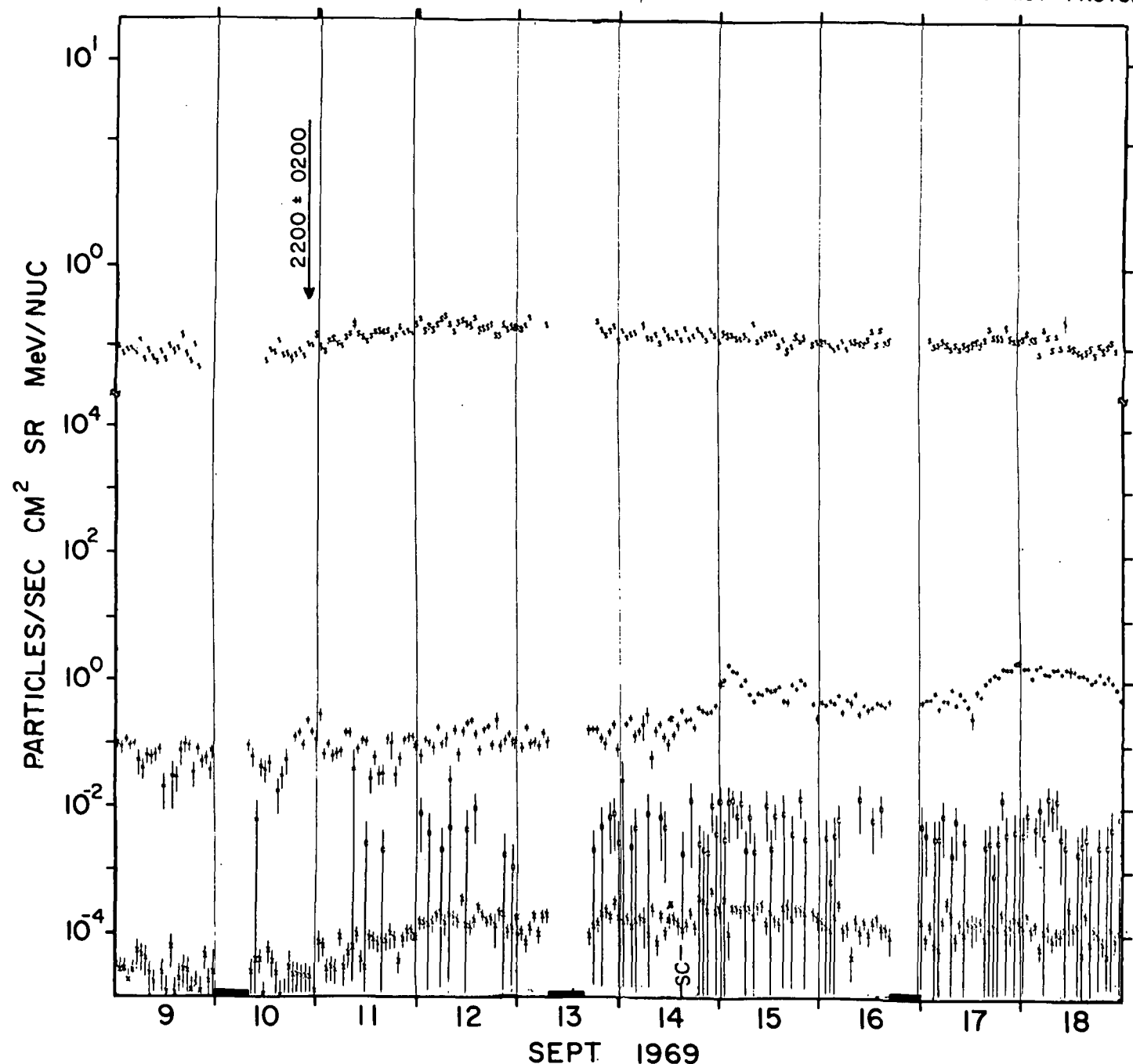
.5-1.1 MeV ELECTRONS X .9-1.5 MeV PROTONS ϕ 6-19 MeV PROTONS X 19-80 MeV PROTONS



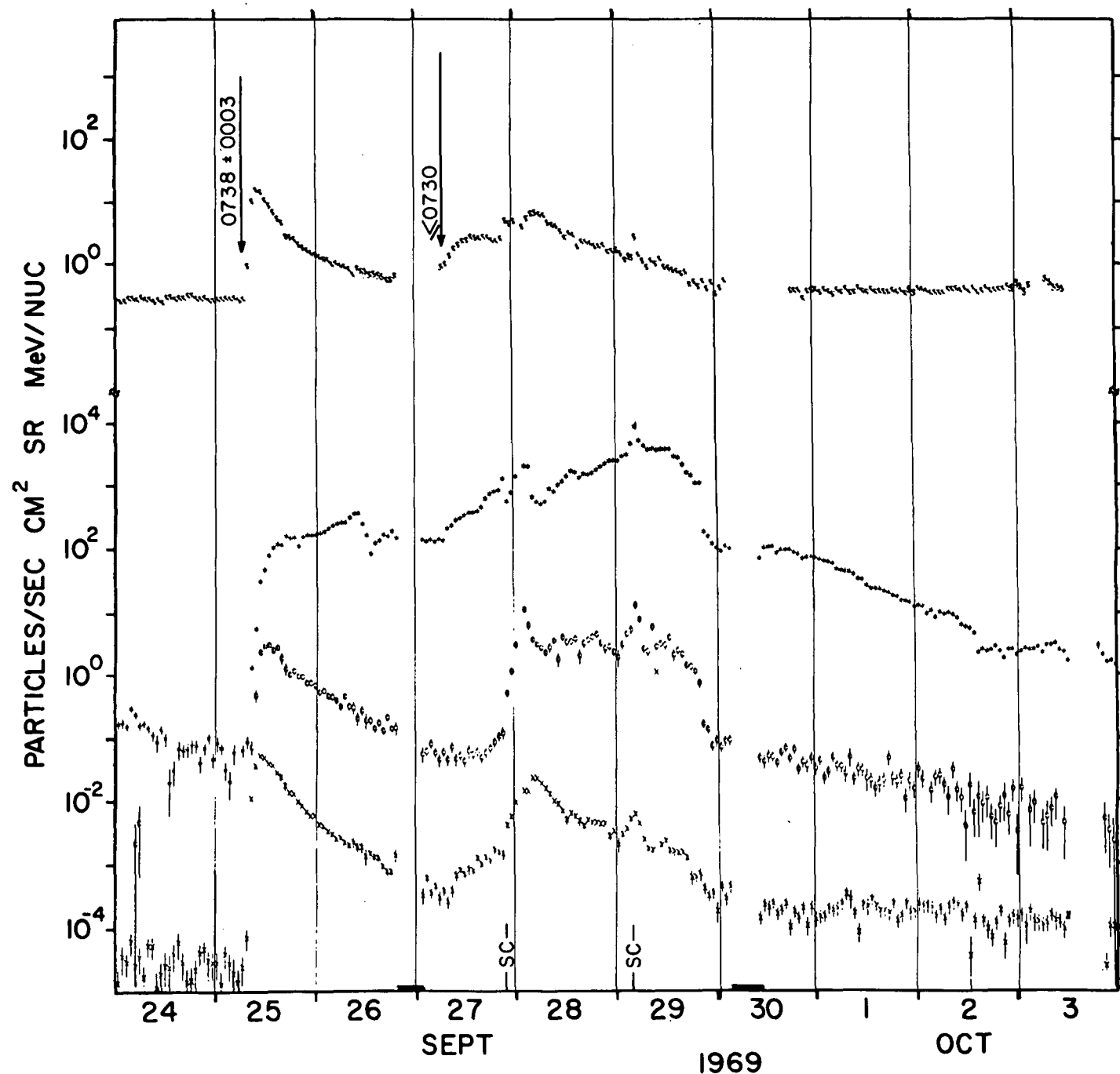
\$.5-1.1 MeV ELECTRONS X .9-1.5 MeV PROTONS Ø 6-19 MeV PROTONS X 19-80 MeV PROTONS



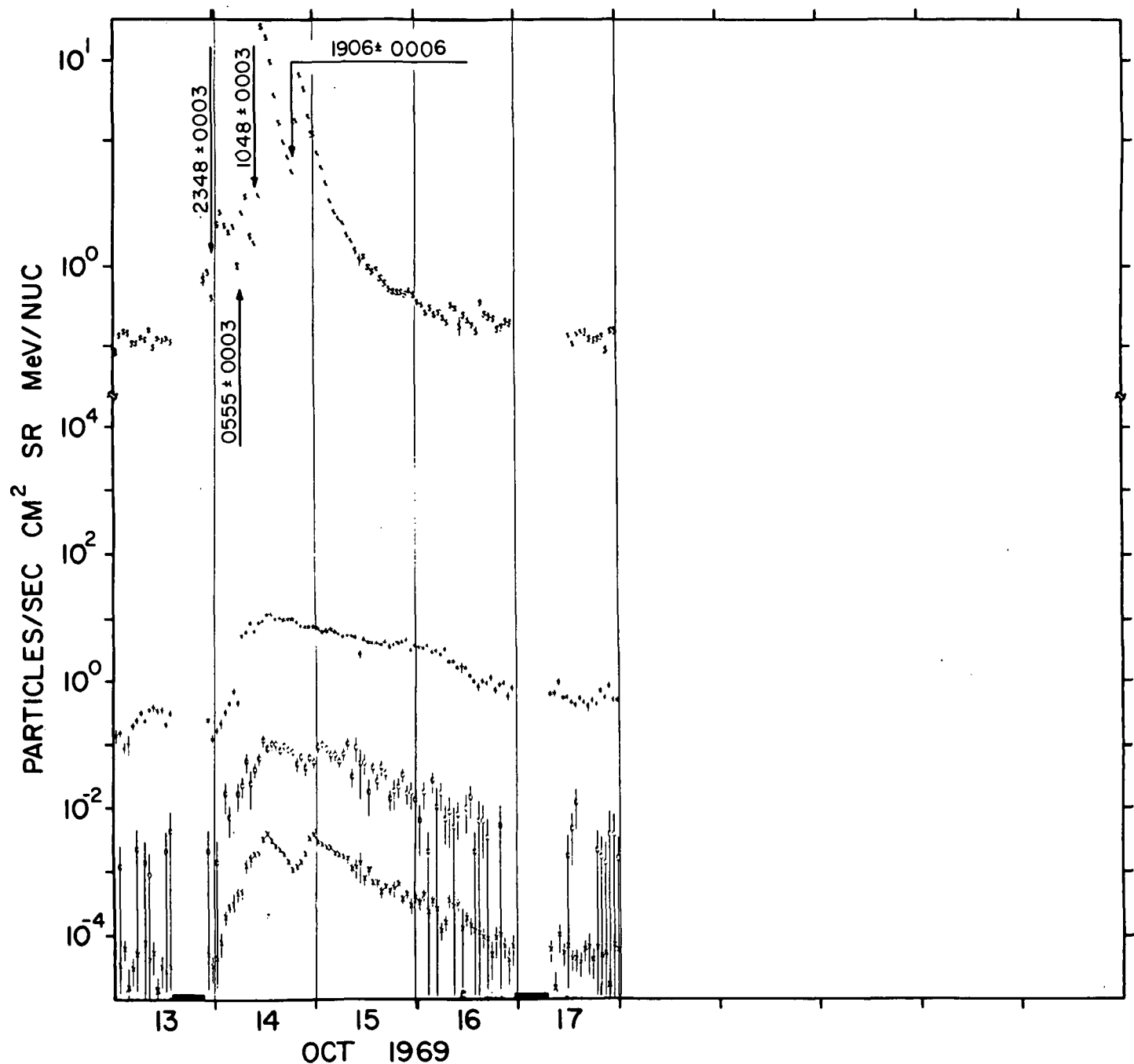
.5 - 1.1 MeV ELECTRONS \times .9 - 1.5 MeV PROTONS \circ 6 - 19 MeV PROTONS \times 19 - 80 MeV PROTONS



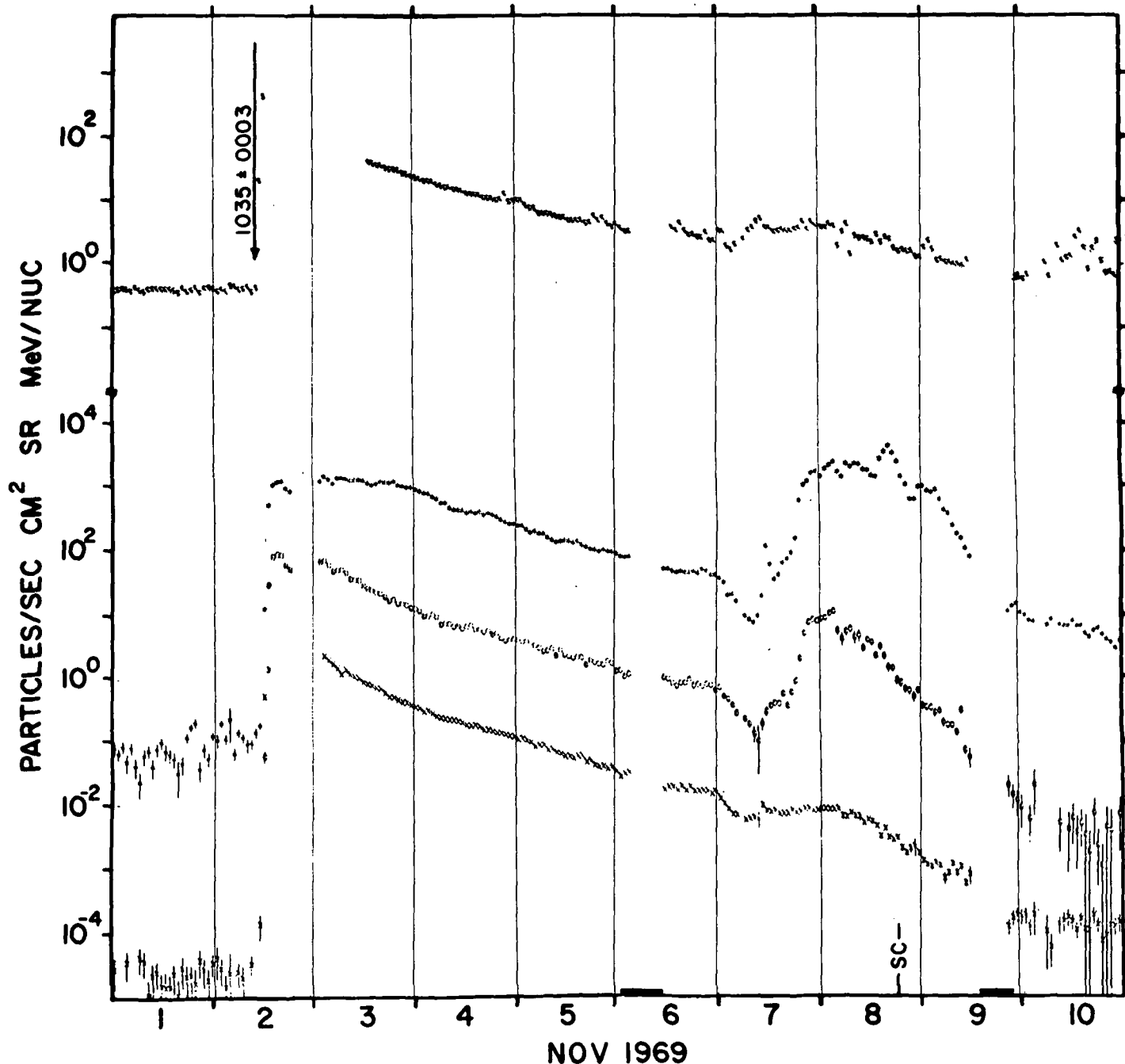
\$.5-1.1 MeV ELECTRONS X .9-1.5 MeV PROTONS O 6-19 MeV PROTONS X 19-80 MeV PROTONS



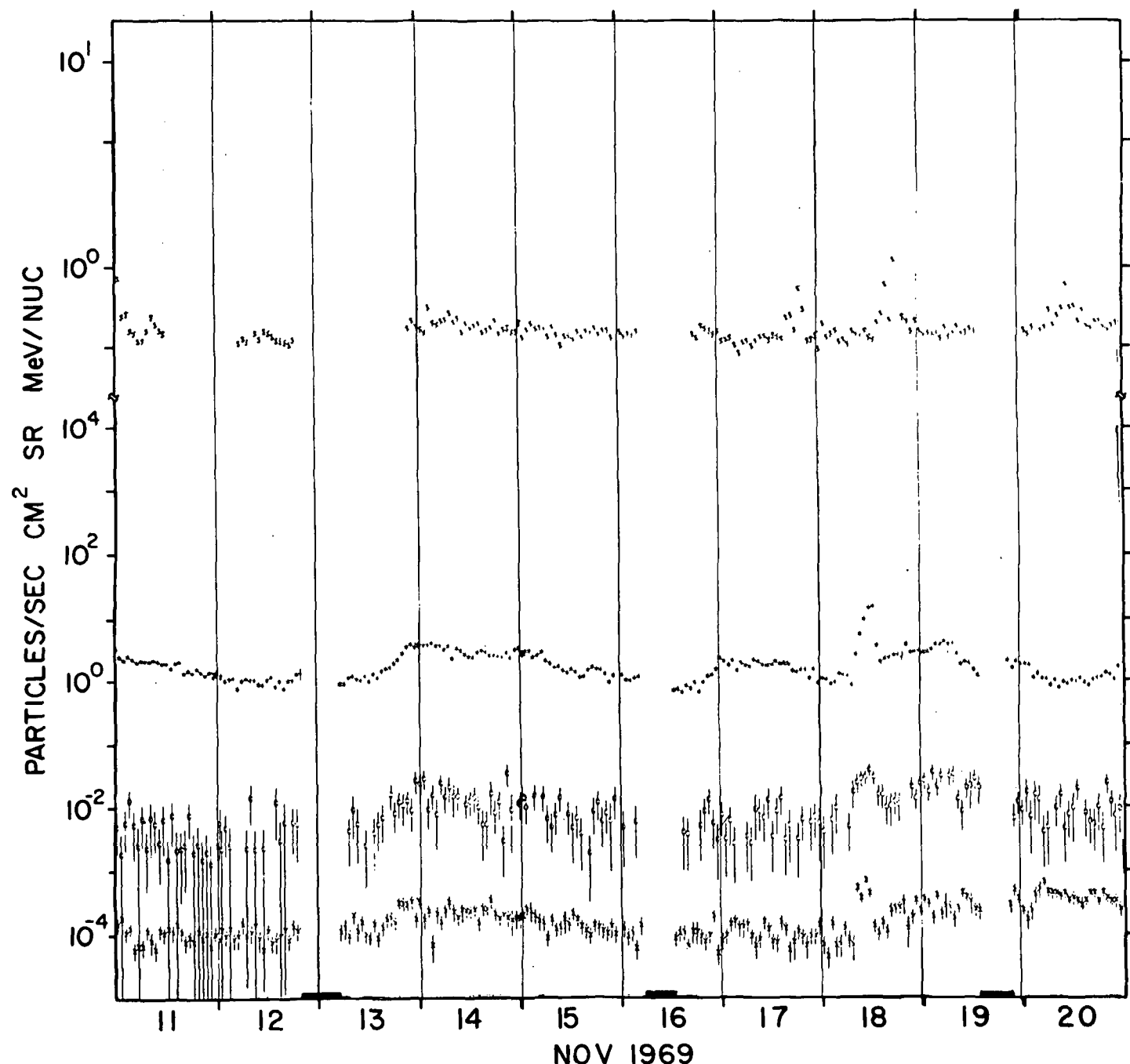
\$.5-1.1 MeV ELECTRONS X .9-1.5 MeV PROTONS \emptyset 6-19 MeV PROTONS X 19-80 MeV PROTONS



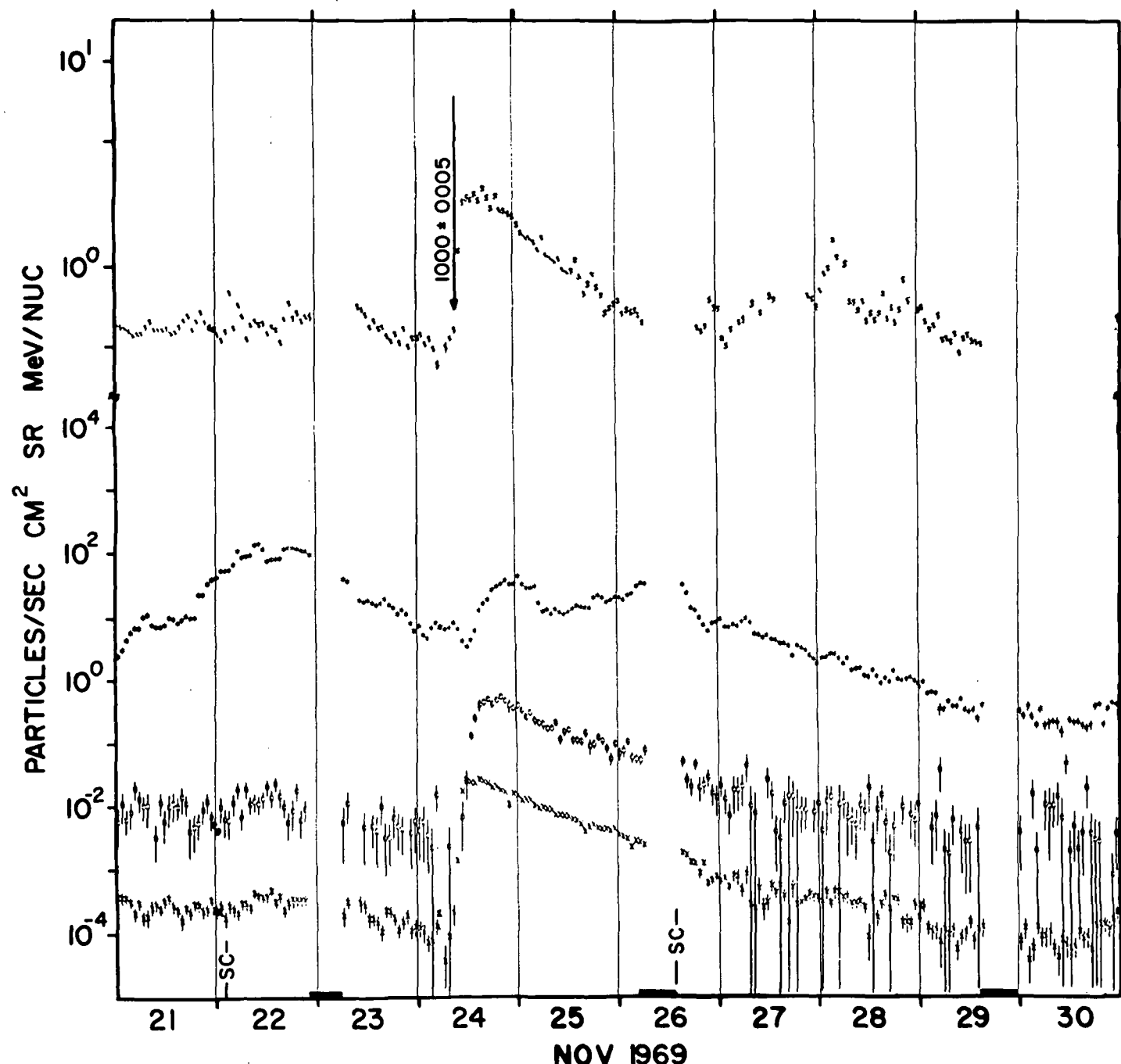
\$.5-1.1 MeV ELECTRONS X .9-1.5 MeV PROTONS 0 6-19 MeV PROTONS X 19-80 MeV PROTONS



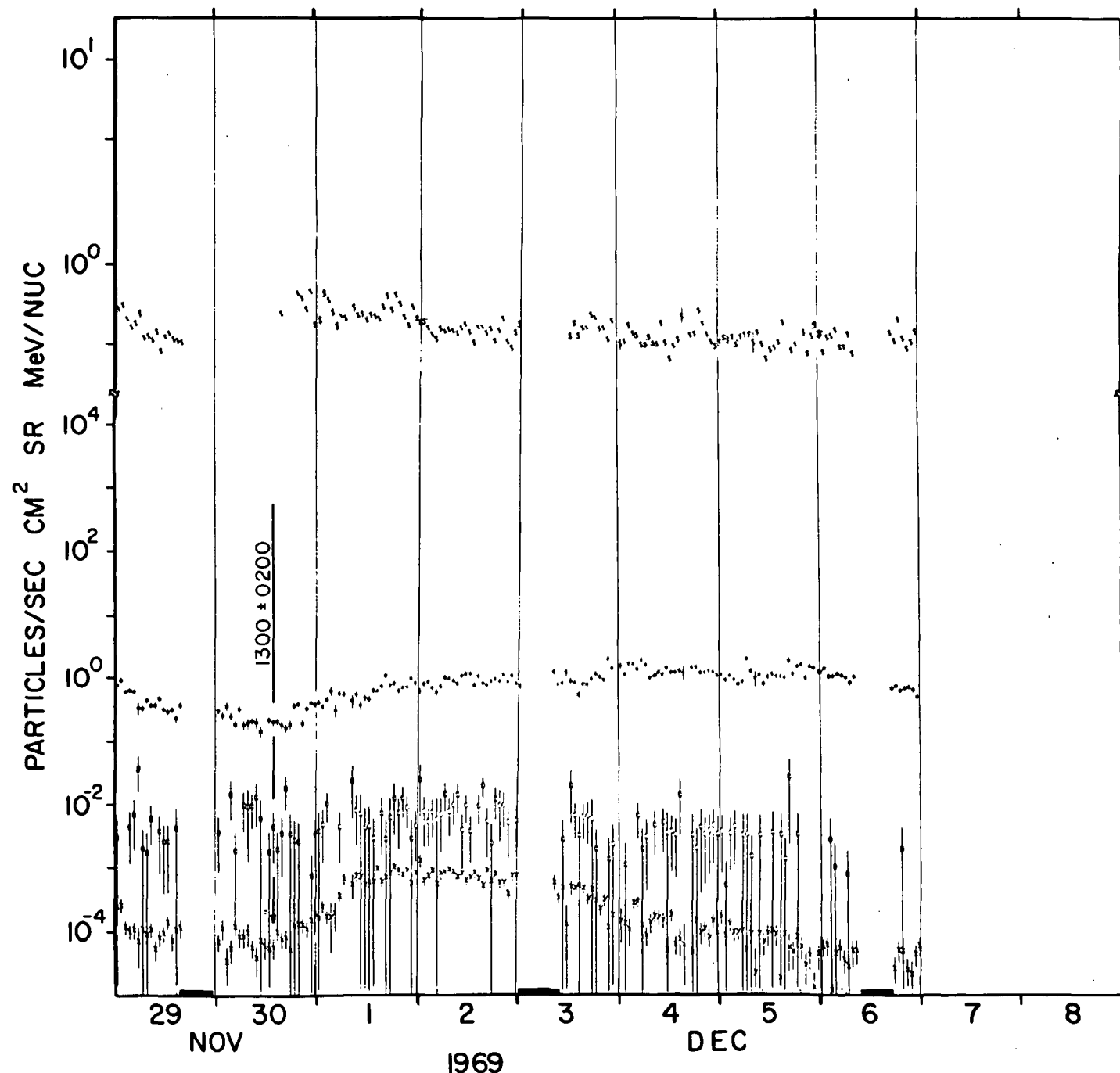
\$.5-1.1 MeV ELECTRONS x .9-1.5 MeV PROTONS o 6-19 MeV PROTONS x 19-80 MeV PROTONS



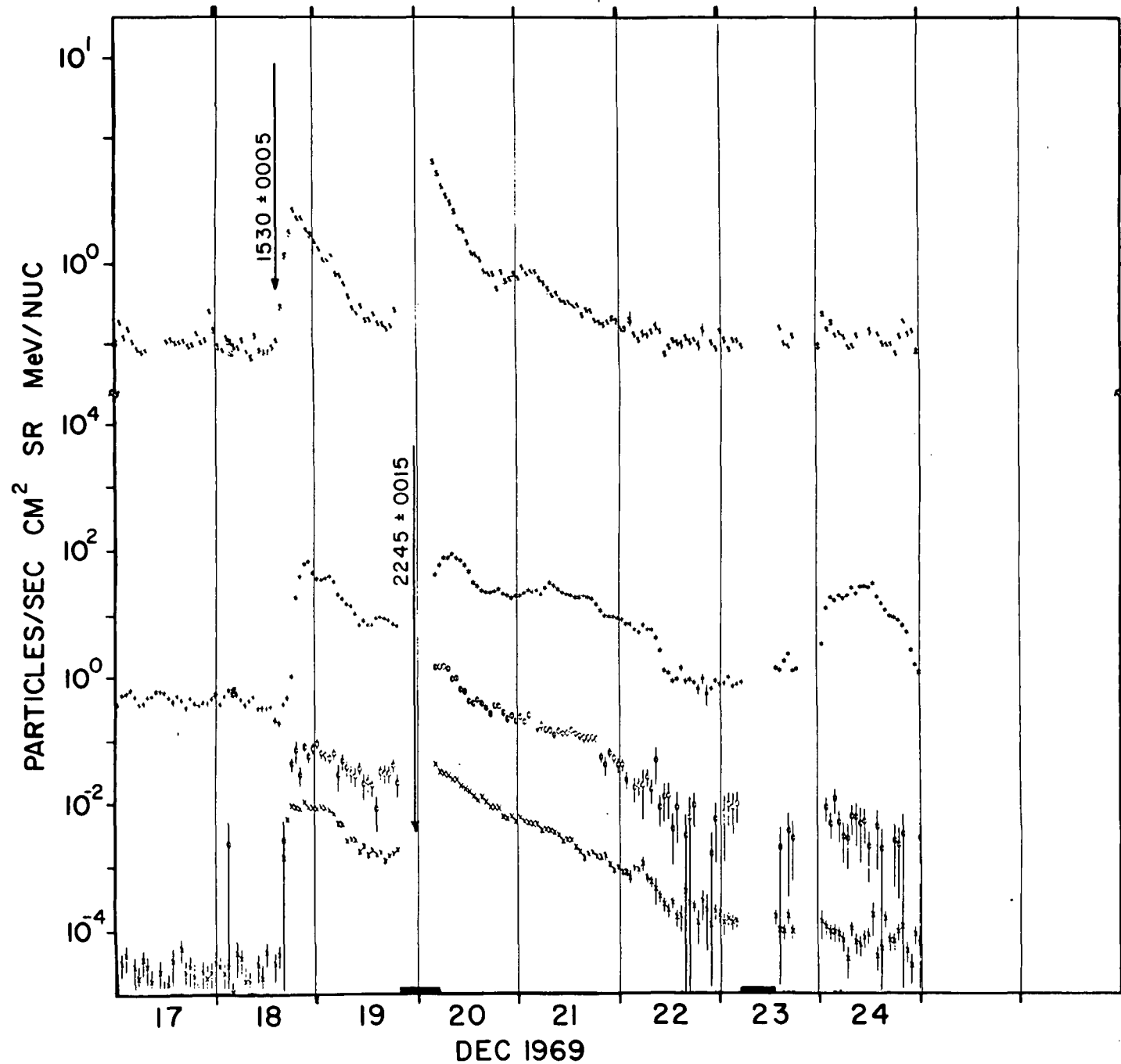
S .5-1.1 MeV ELECTRONS X .9-1.5 MeV PROTONS O 6-19 MeV PROTONS X 19-80 MeV PROTONS



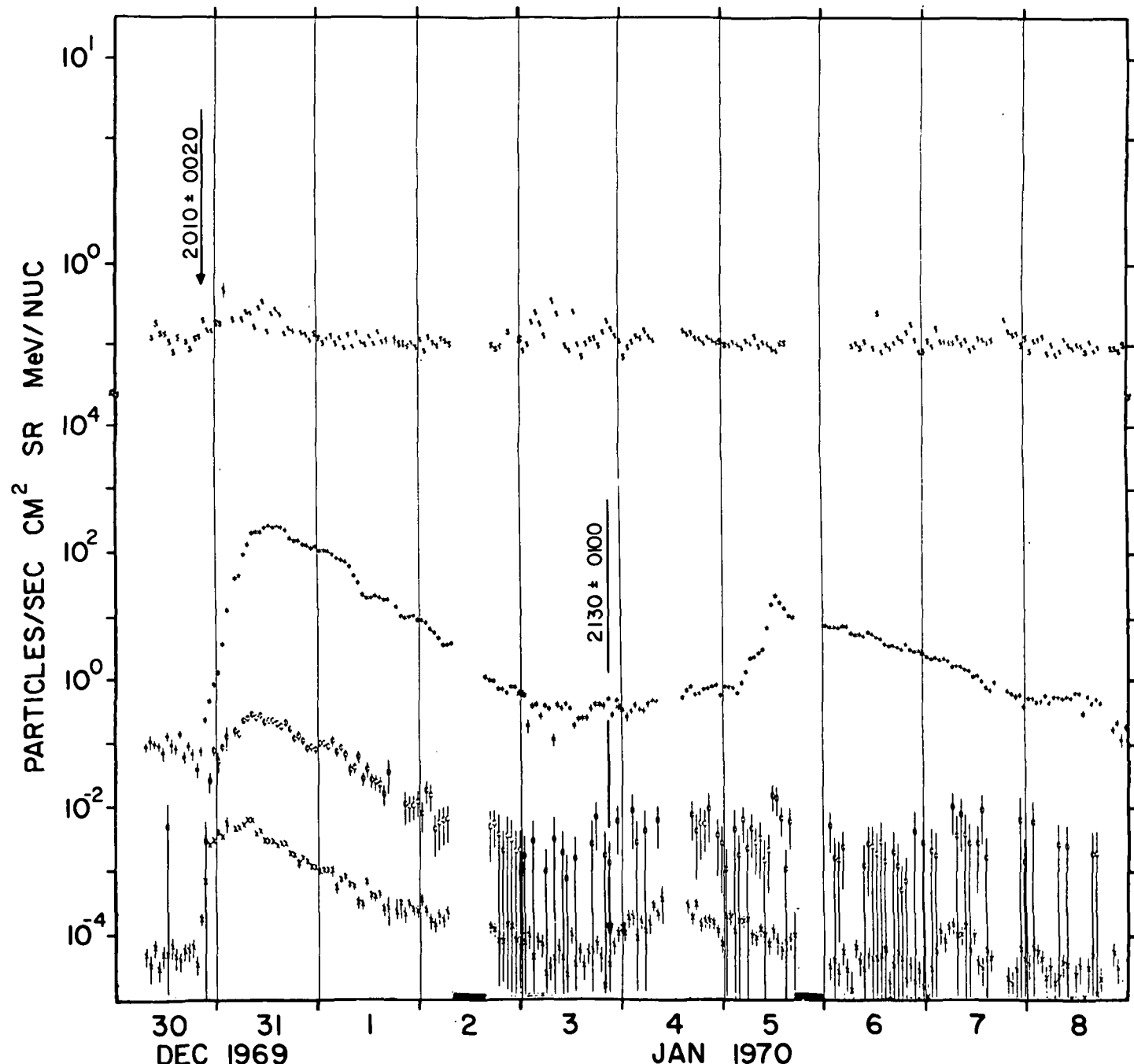
.5-1.1 MeV ELECTRONS X .9-1.5 MeV PROTONS Ø 6-19 MeV PROTONS X 19-80 MeV PROTONS



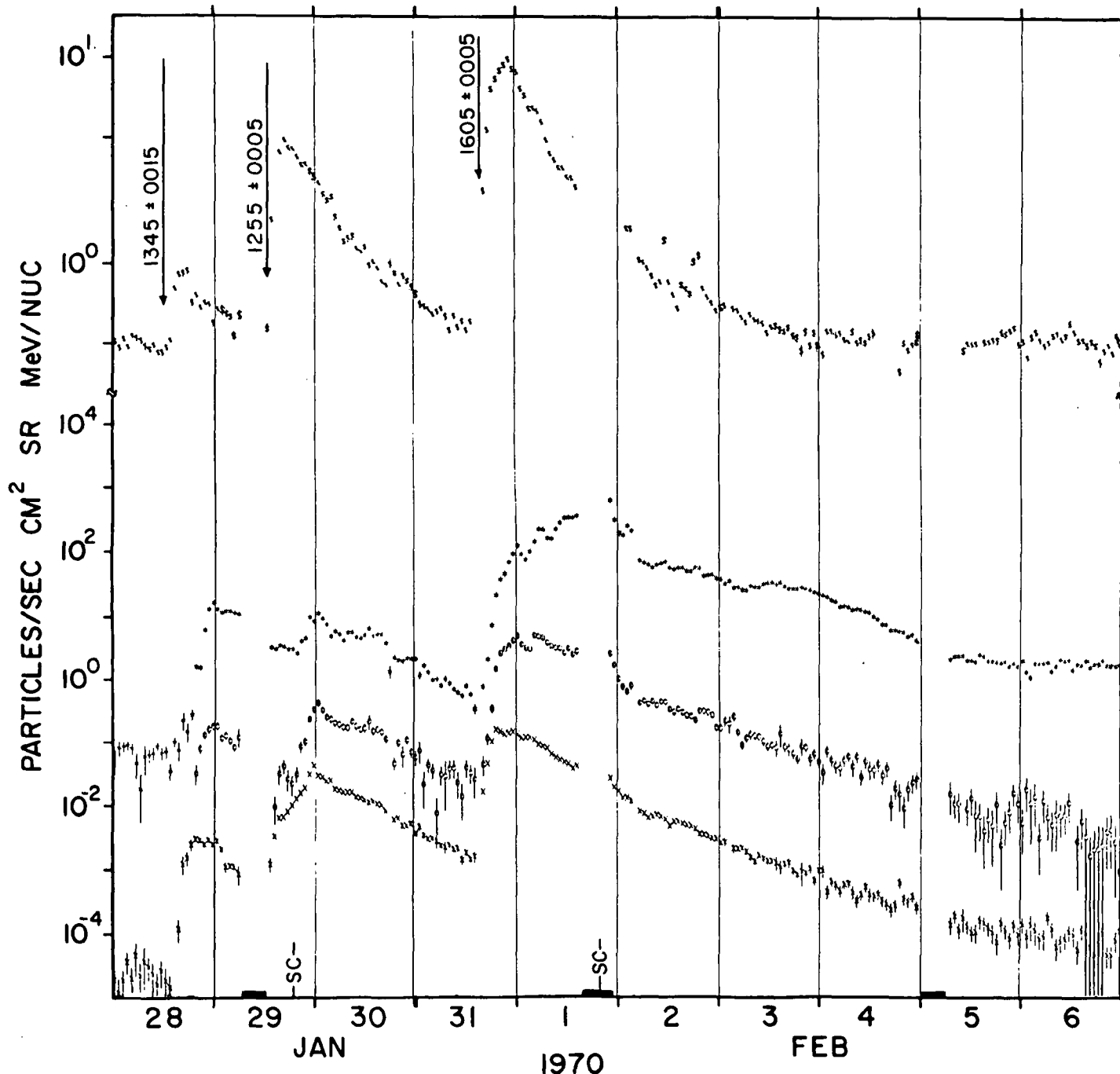
\$.5-1.1 MeV ELECTRONS X .9-1.5 MeV PROTONS O 6-19 MeV PROTONS X 19-80 MeV PROTONS



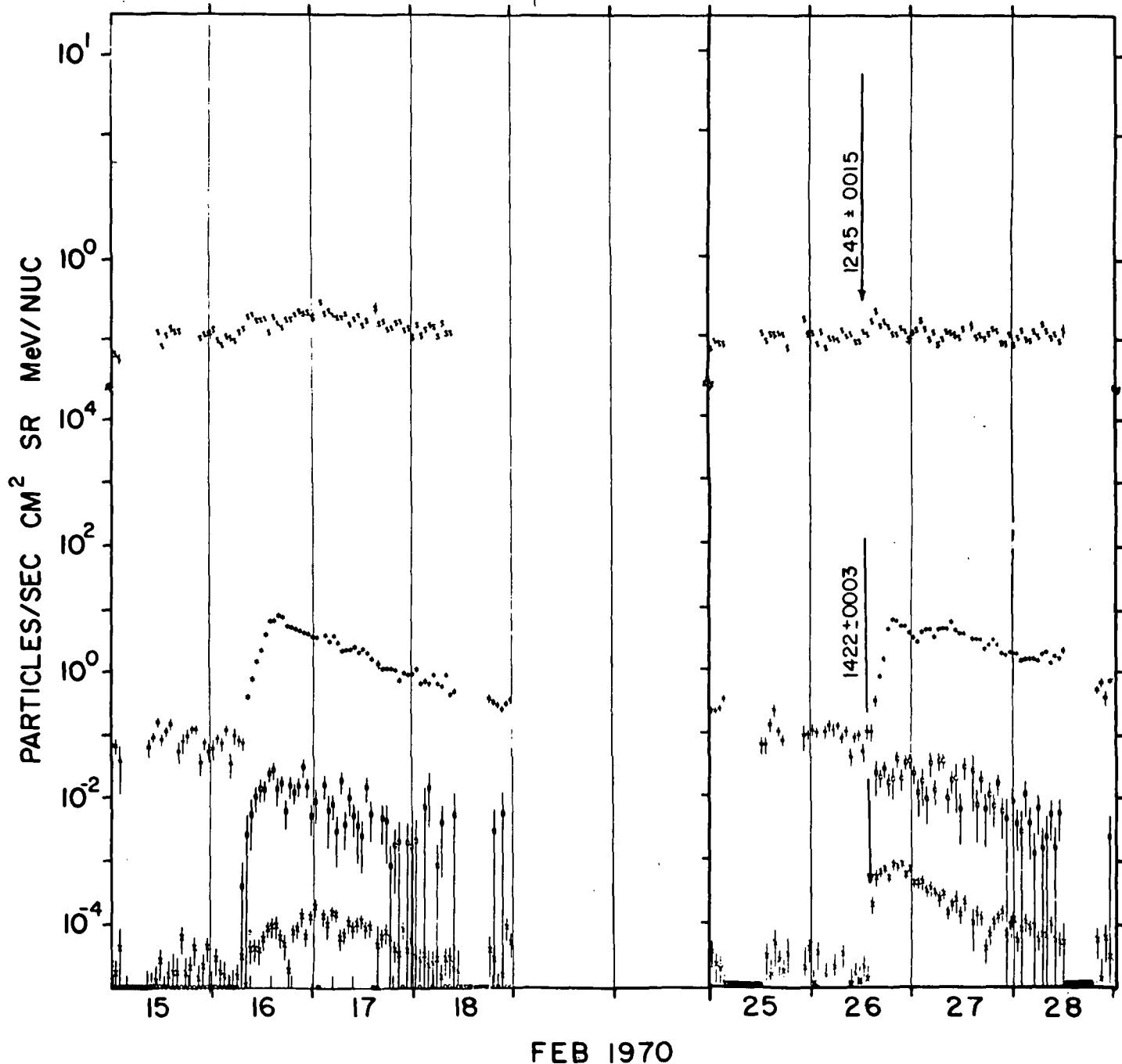
\$.5-1.1 MeV ELECTRONS X .9-1.5 MeV PROTONS 0 6-19 MeV PROTONS X 19-80 MeV PROTONS



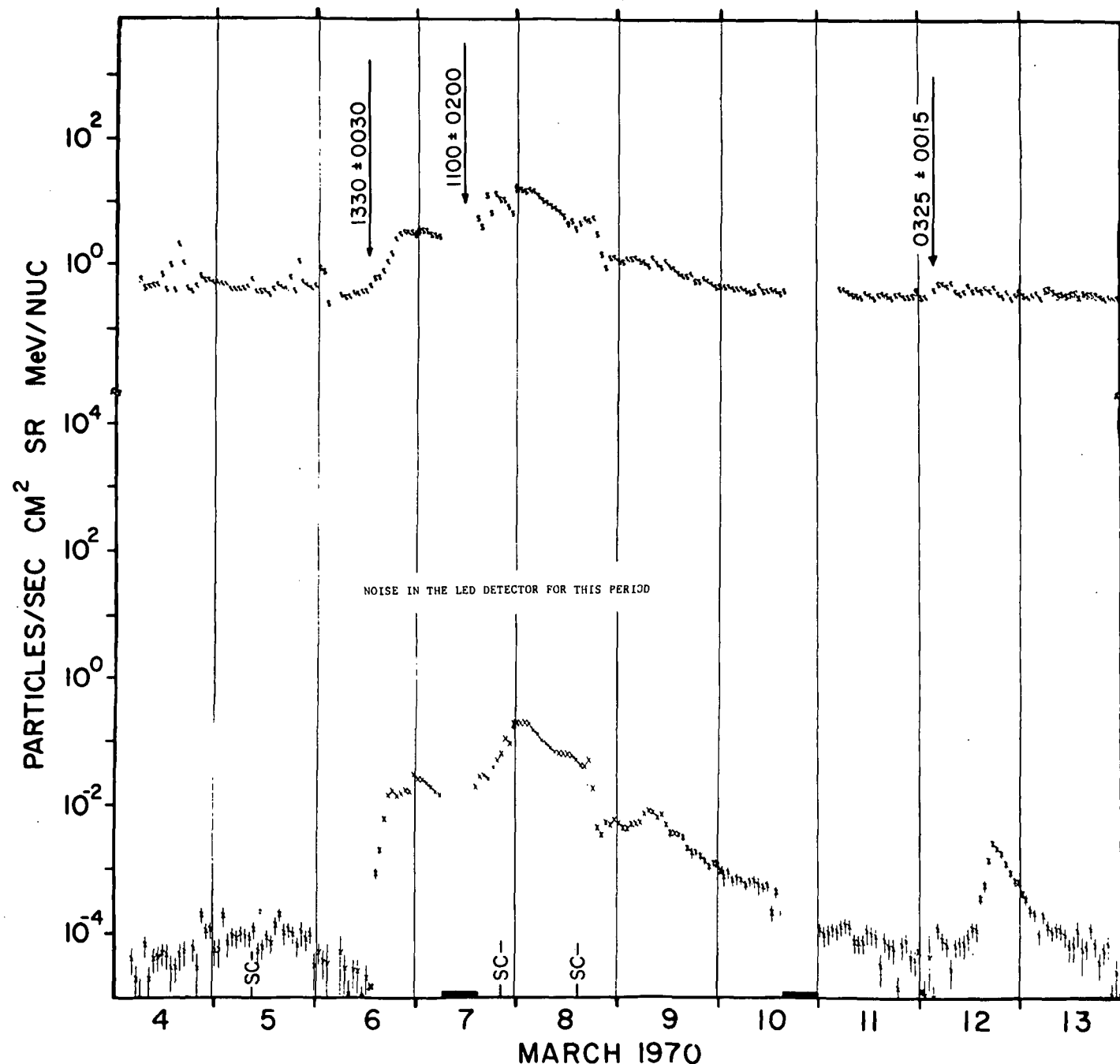
\$.5-1.1 MeV ELECTRONS X .9-1.5 MeV PROTONS \diamond 6-19 MeV PROTONS X 19-80 MeV PROTONS



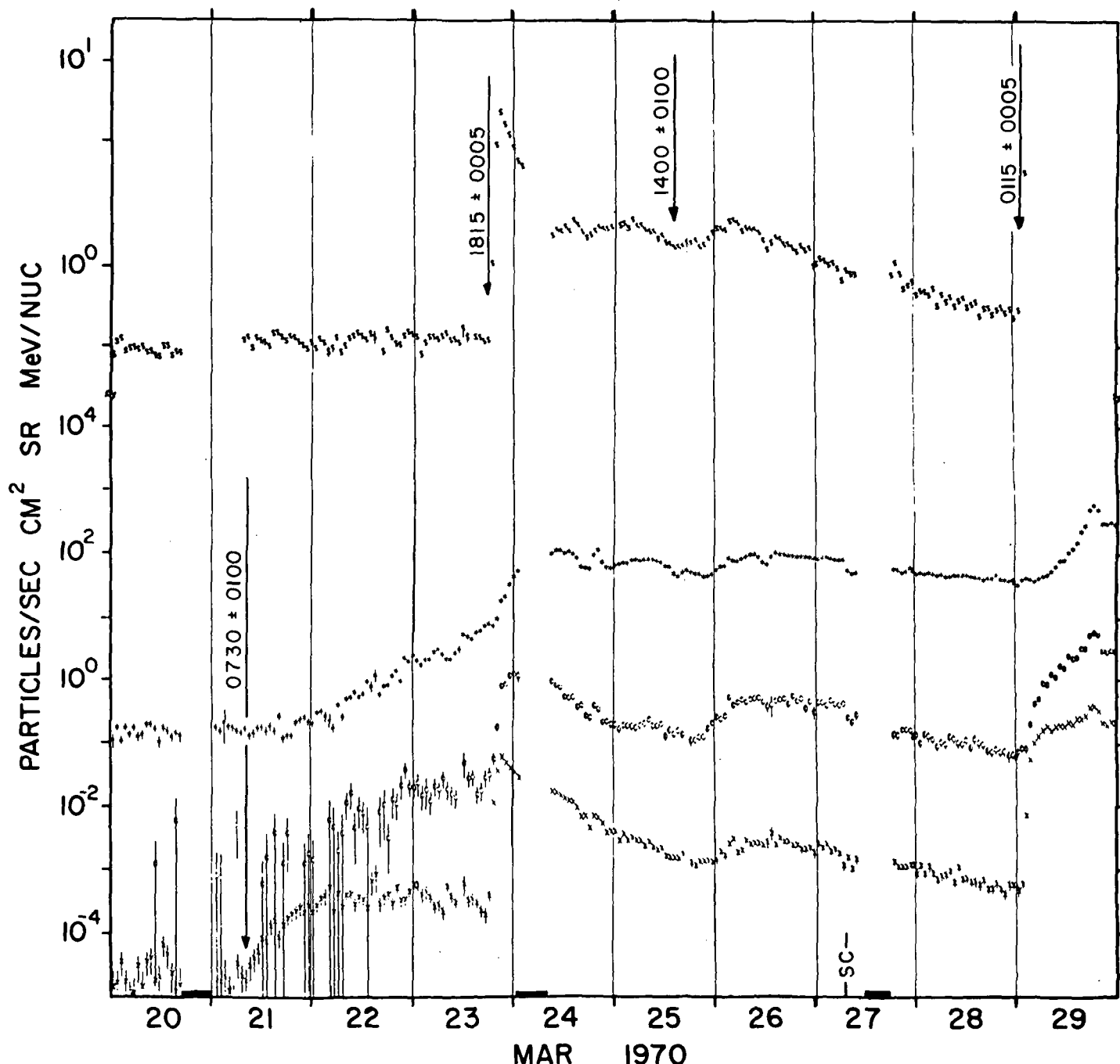
S .5-1.1 MeV ELECTRONS X .9-1.5 MeV PROTONS ϕ 6-19 MeV PROTONS X 19-80 MeV PROTONS



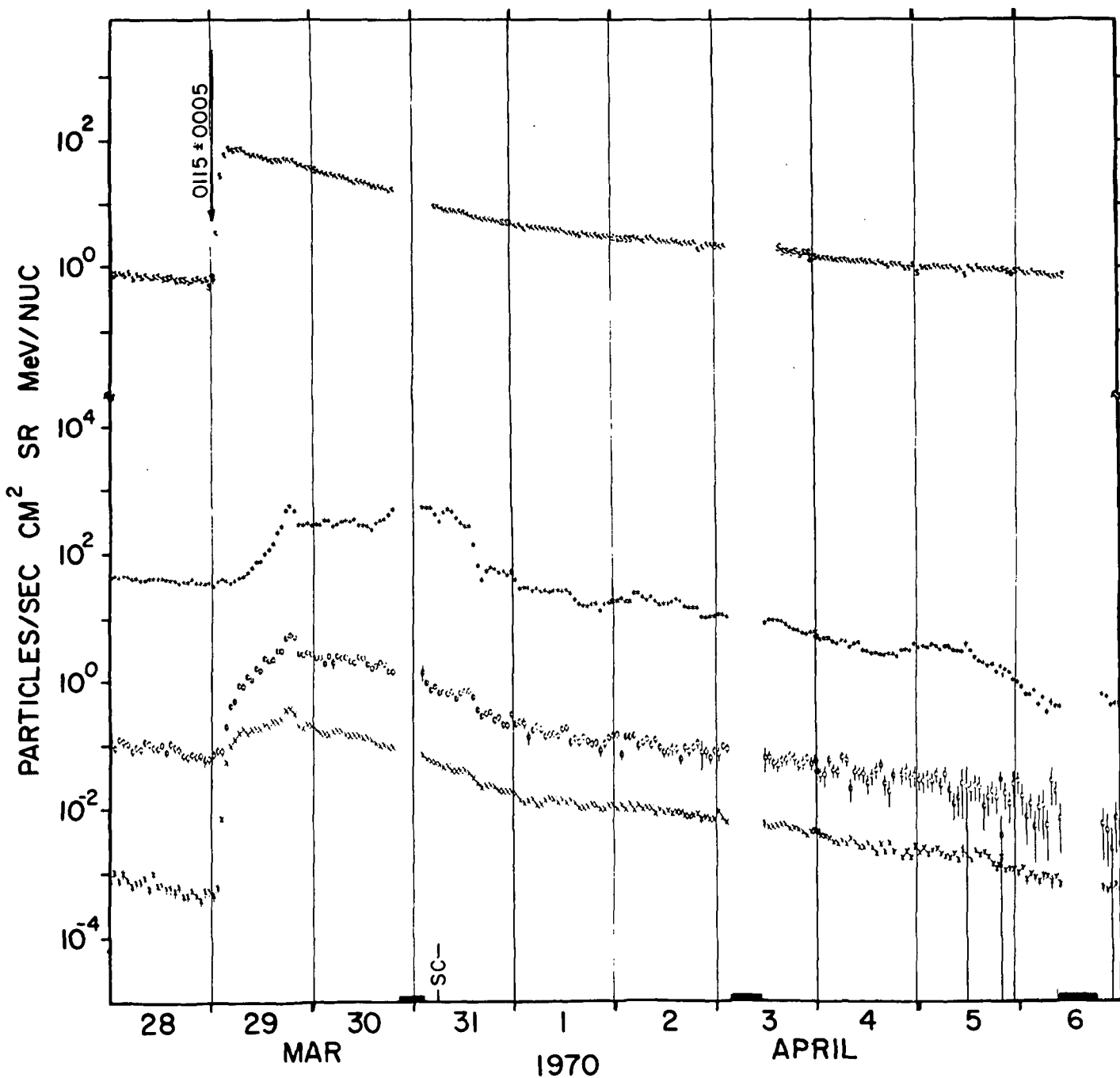
5.5-1.1 MeV ELECTRONS X 9-1.5 MeV PROTONS 0 6-19 MeV PROTONS X 19-80 MeV PROTONS



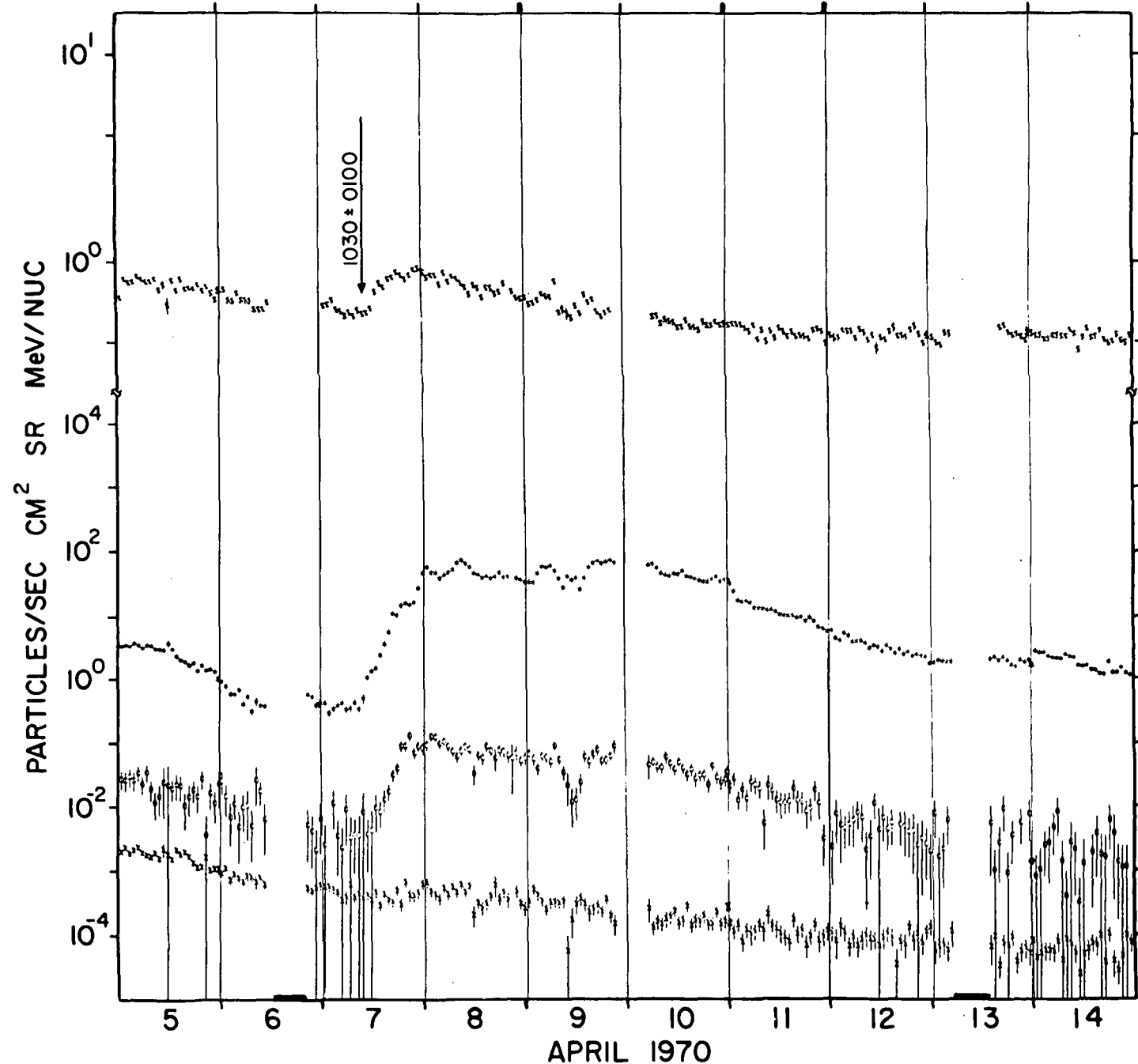
.5-1.1 MeV ELECTRONS X .9-1.5 MeV PROTONS @ 6-19 MeV PROTONS X 19-80 MeV PROTONS



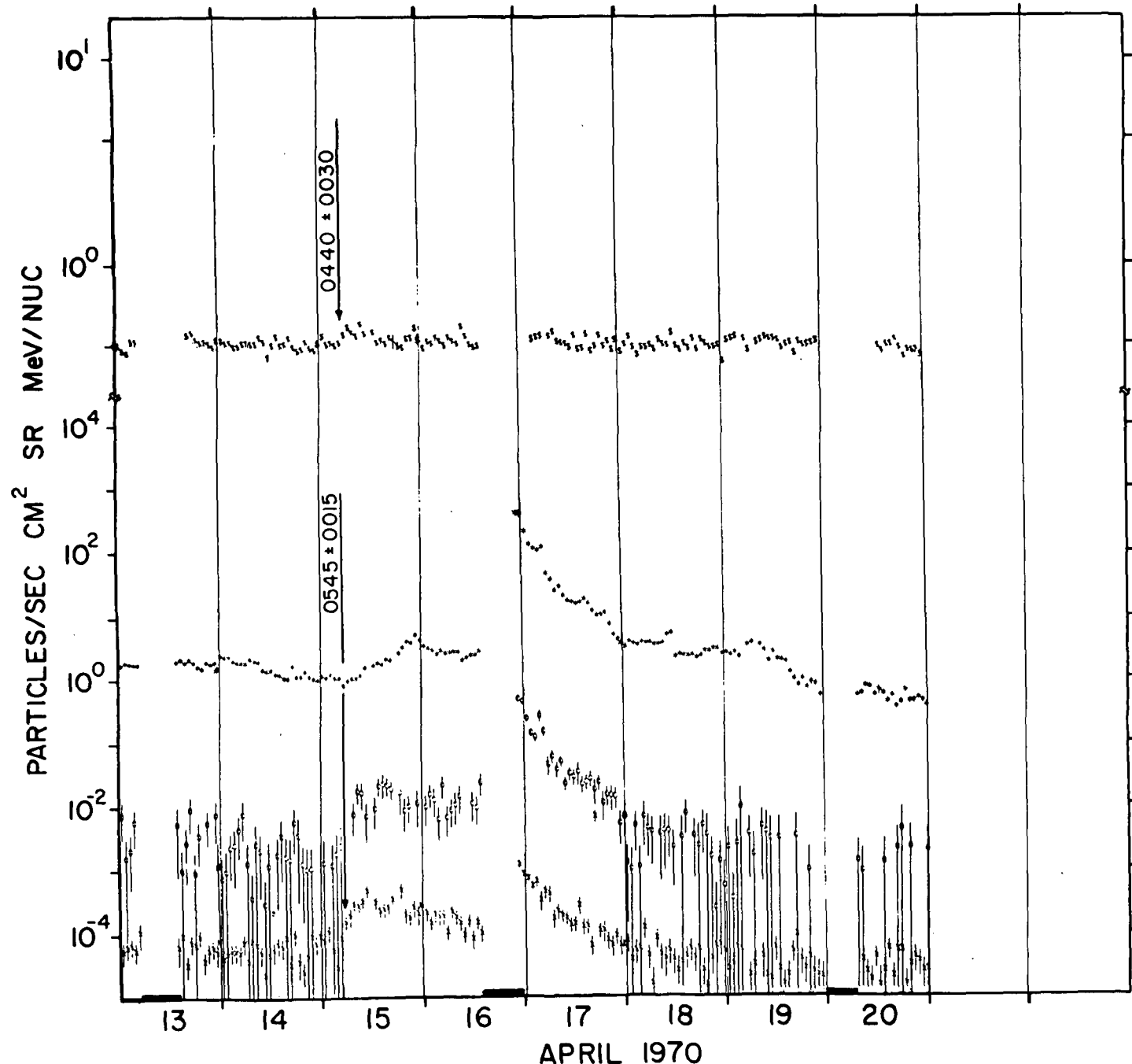
.5-1.1 MeV ELECTRONS X .9-1.5 MeV PROTONS O 6-19 MeV PROTONS X 19-80 MeV PROTONS



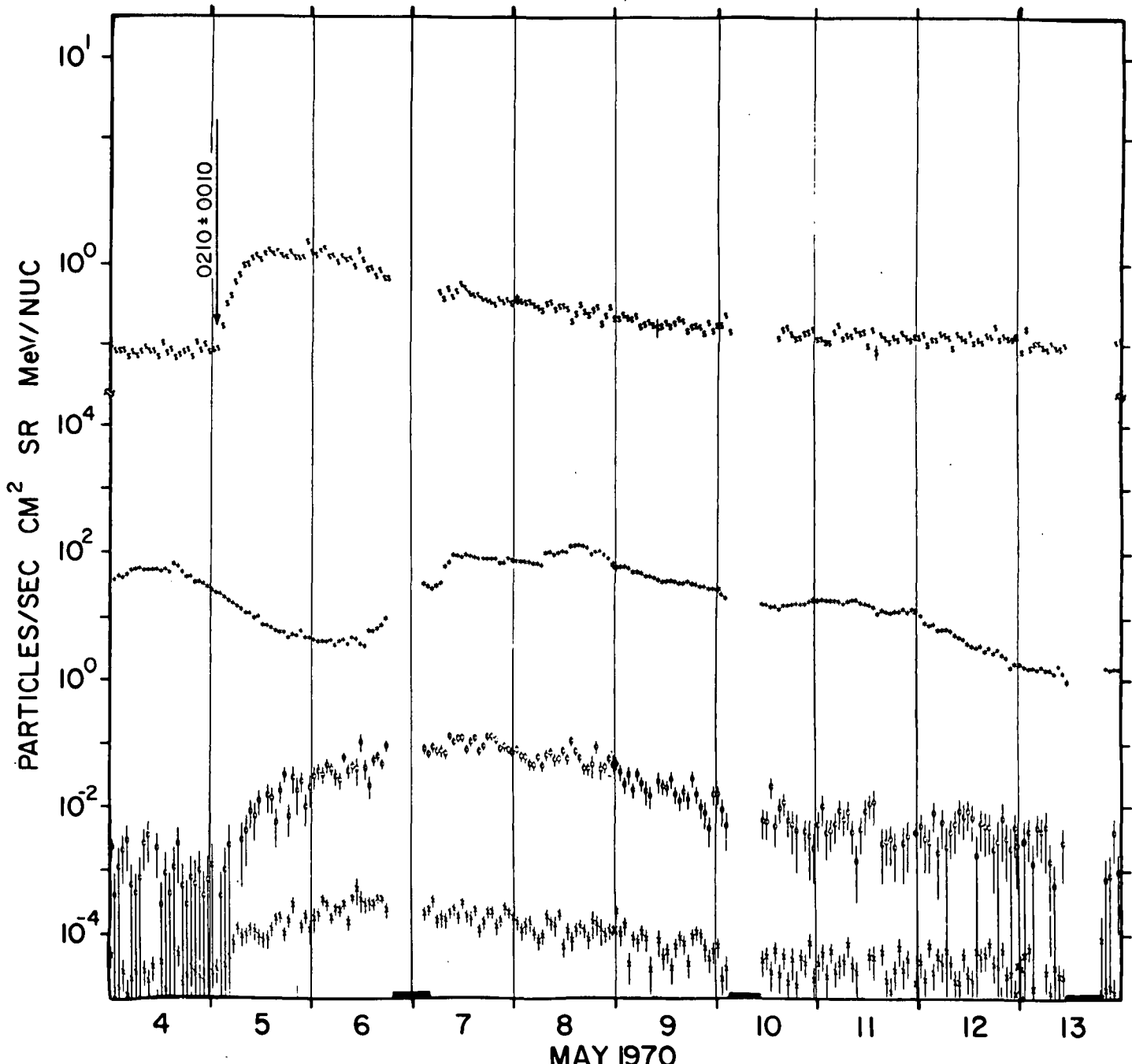
.5-1.1 MeV ELECTRONS X .9-1.5 MeV PROTONS \diamond 6-19 MeV PROTONS X 19-80 MeV PROTONS



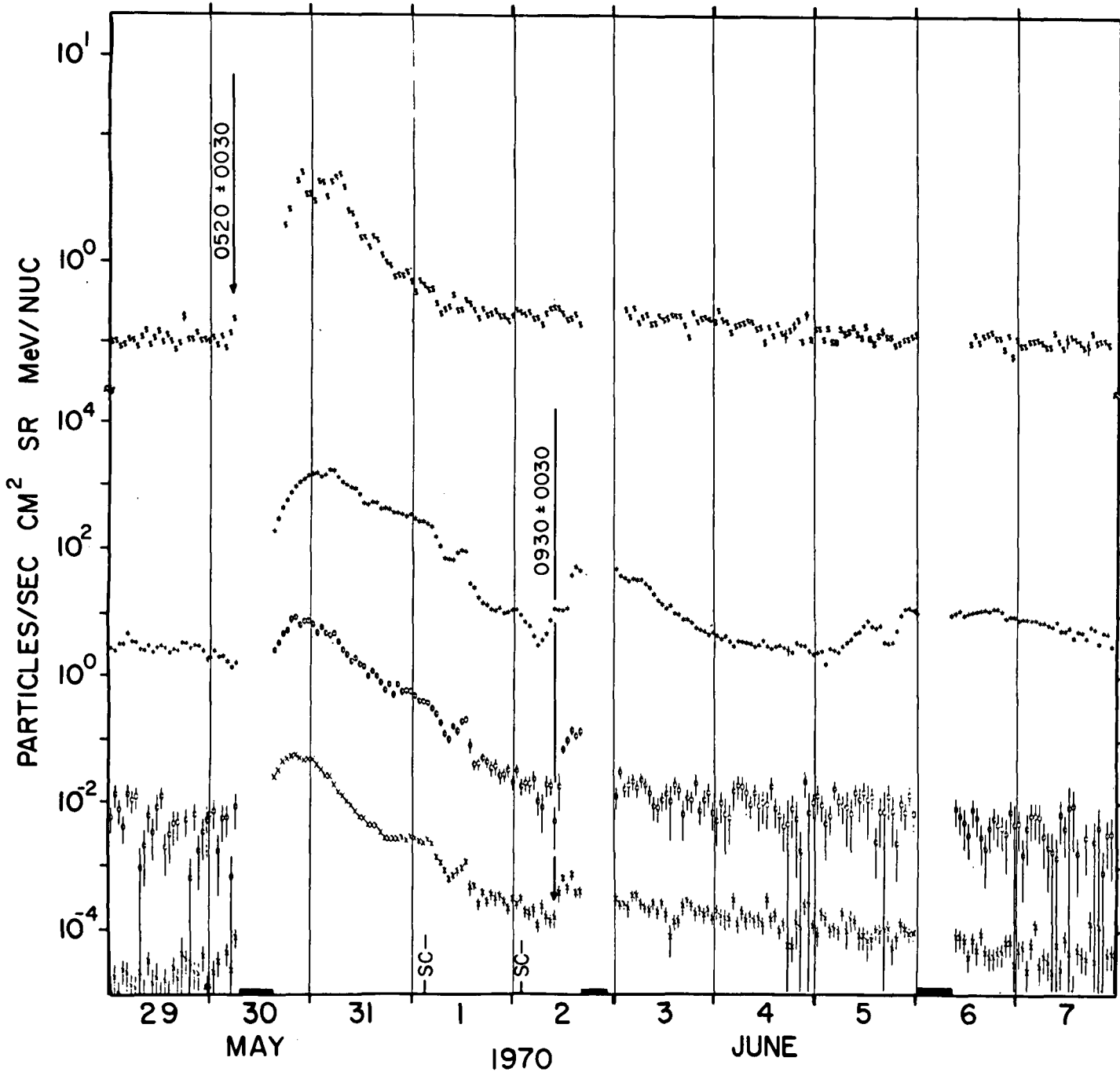
\$.5-1.1 MeV ELECTRONS X .9-1.5 MeV PROTONS O 6-19 MeV PROTONS X 19-80 MeV PROTONS



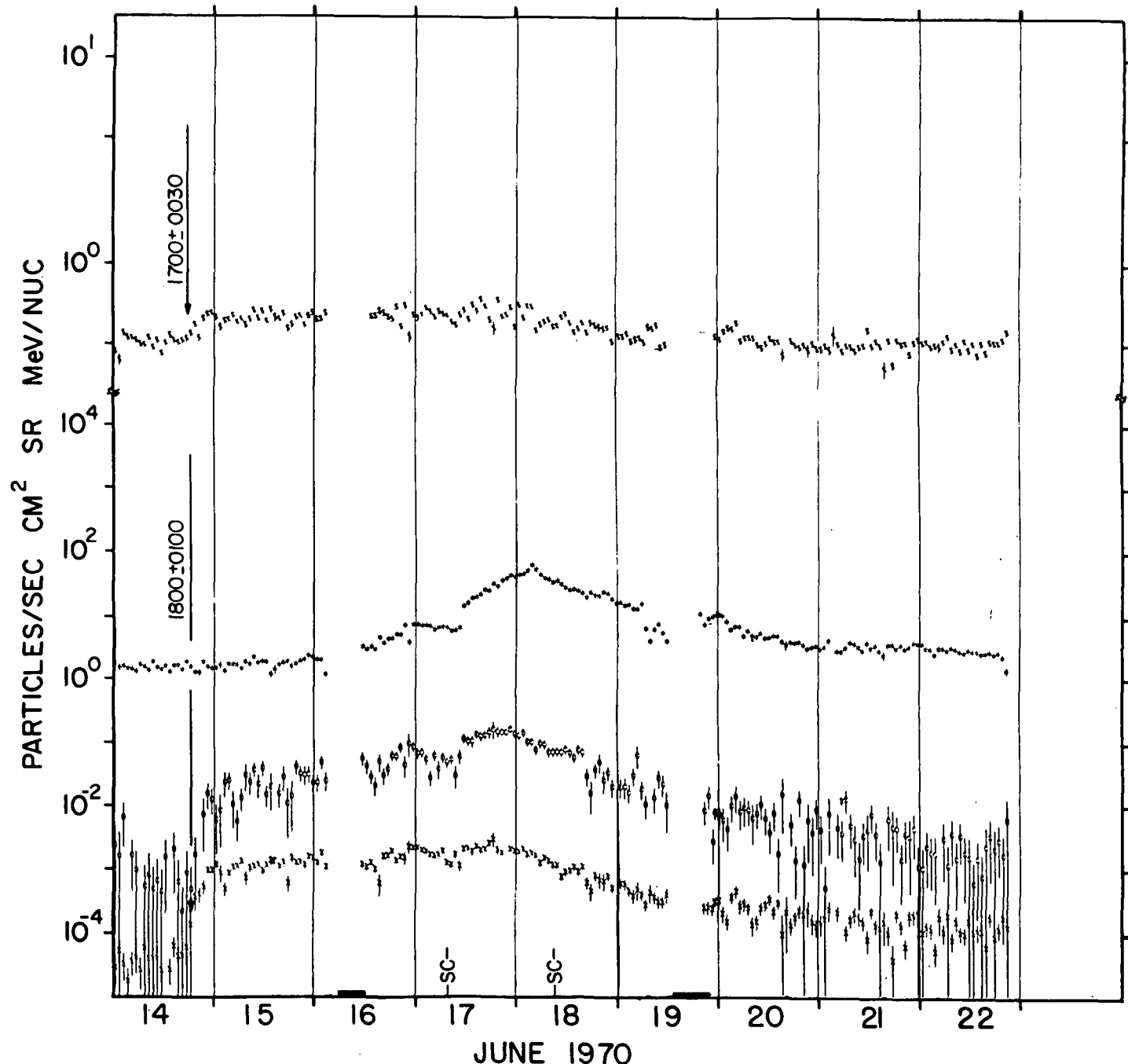
\$.5-1.1 MeV ELECTRONS X .9-1.5 MeV PROTONS \oplus 6-19 MeV PROTONS \times 19-80 MeV PROTONS



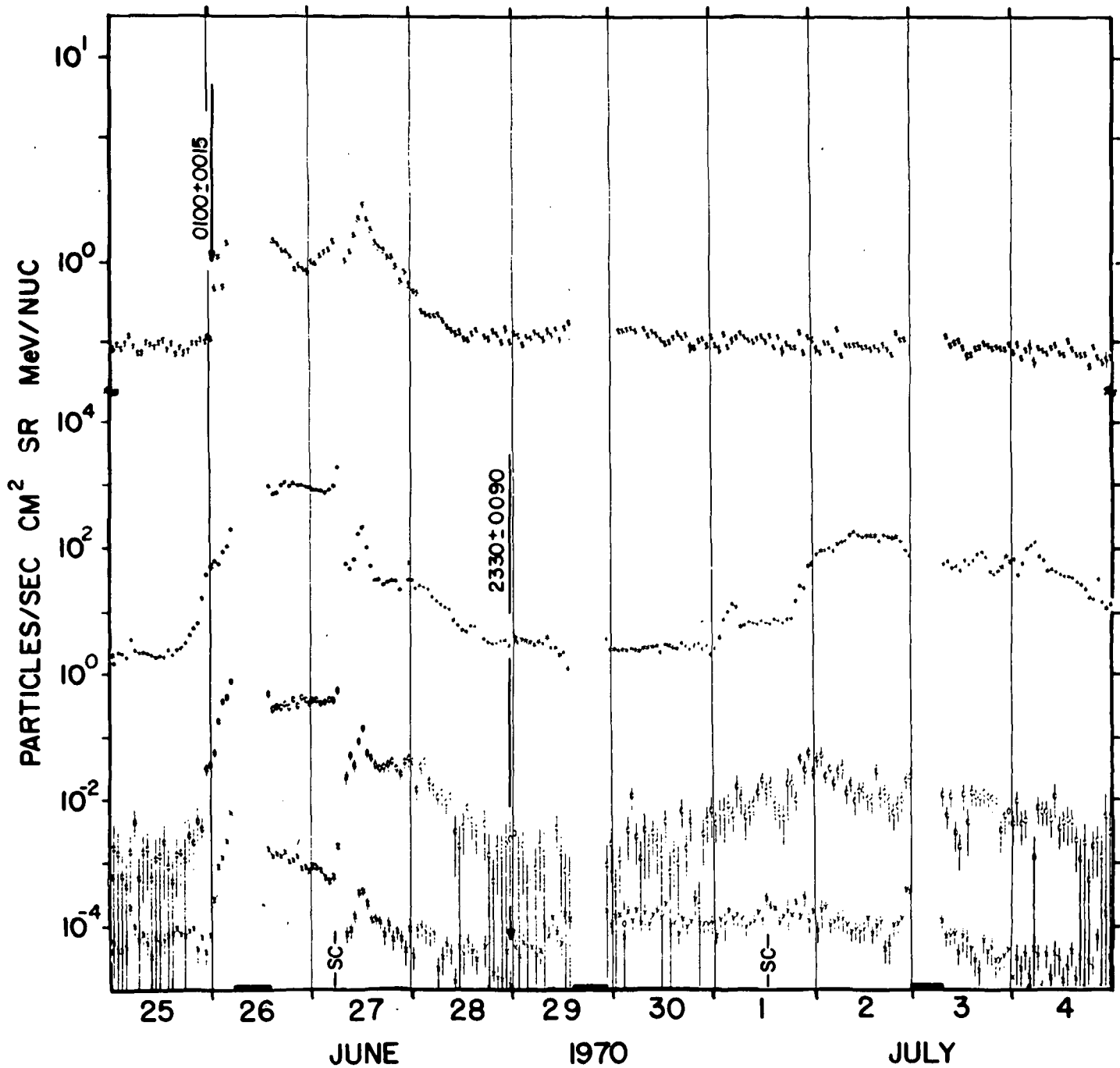
\$.5-1.1 MeV ELECTRONS X .9-1.5 MeV PROTONS 0 6-19 MeV PROTONS X 19-80 MeV PROTONS



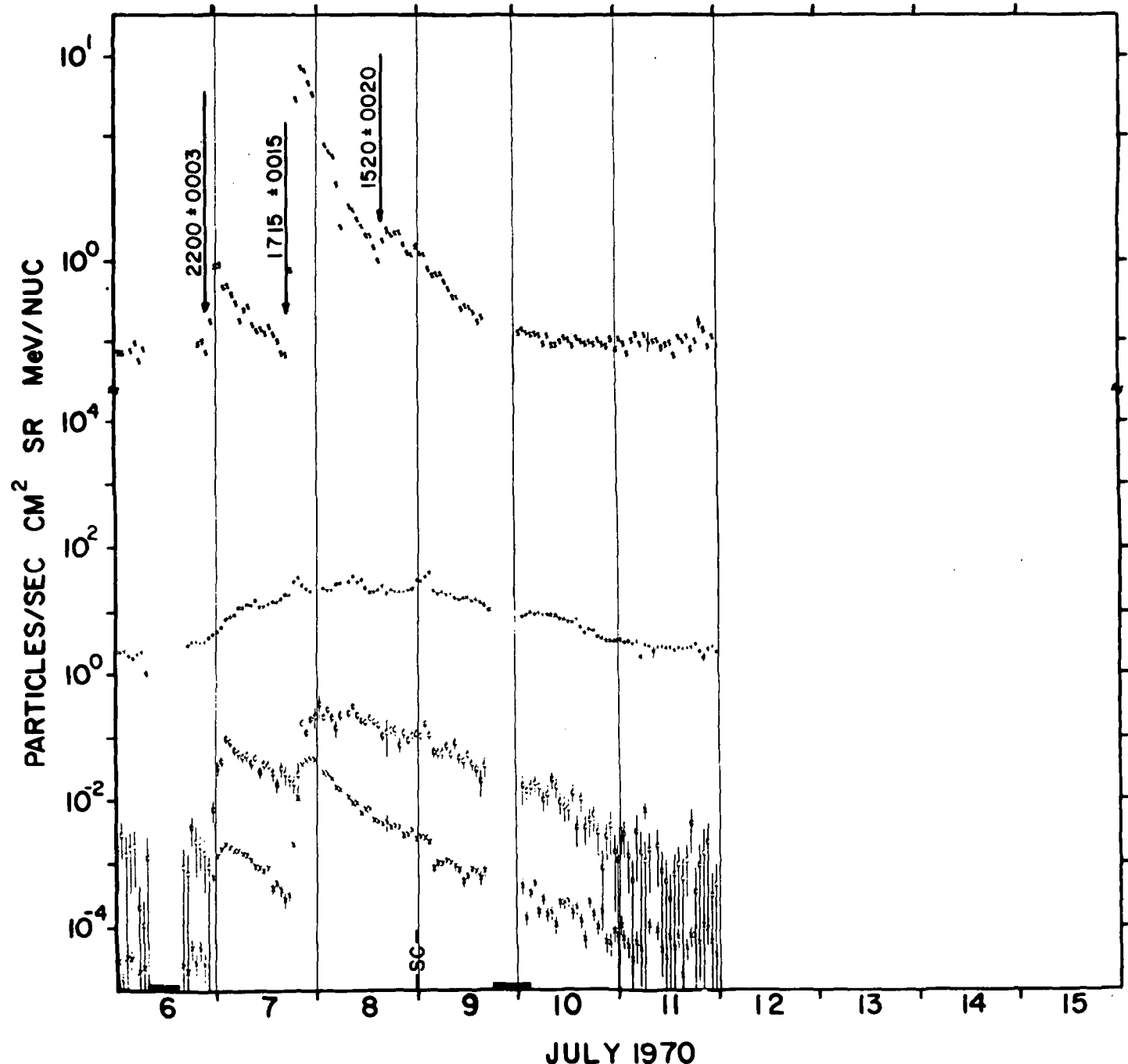
.5-1.1 MeV ELECTRONS X .9-1.5 MeV PROTONS 0.6-1.9 MeV PROTONS X 1.9-80 MeV PROTONS



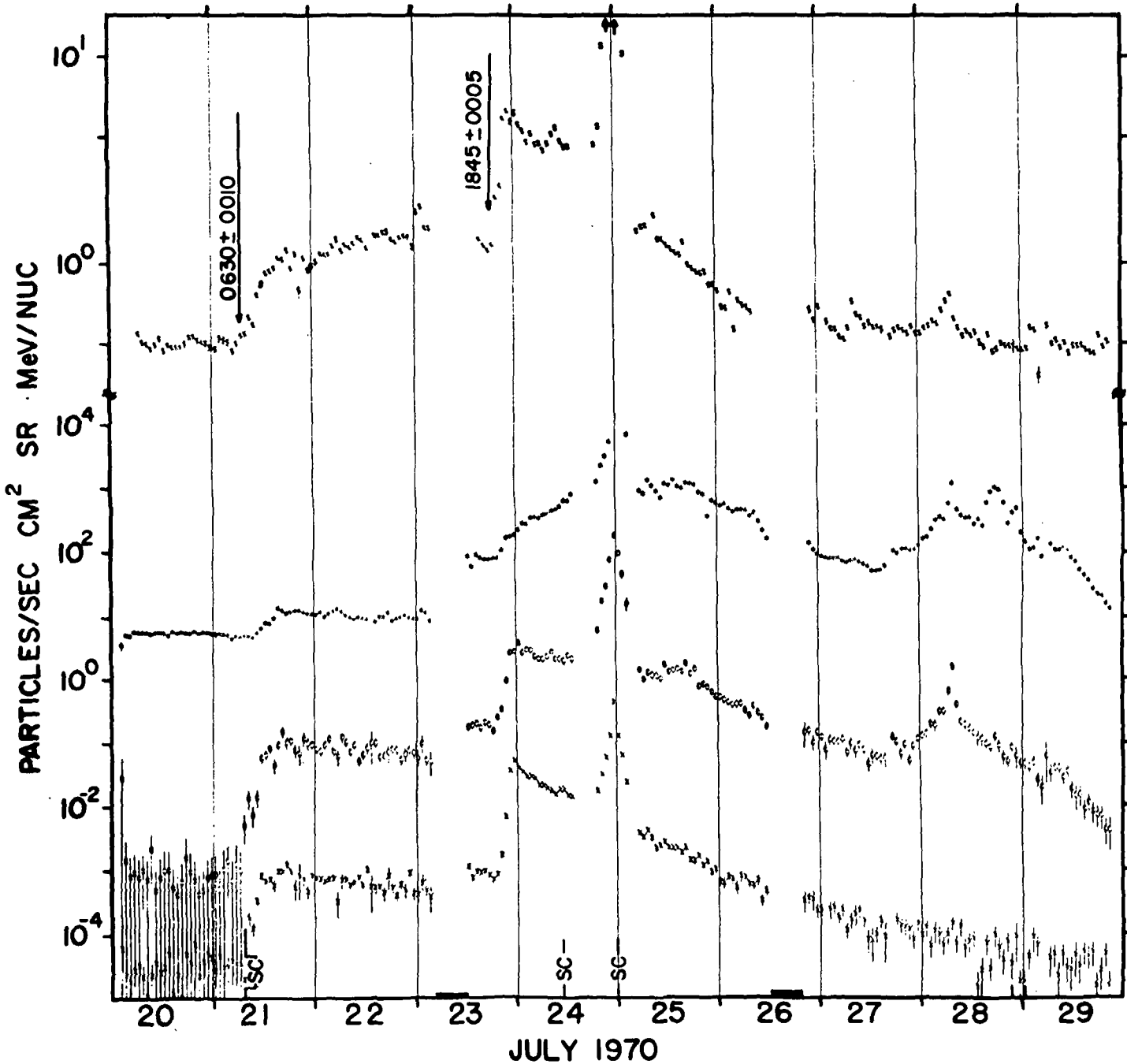
S .5-1.1 MeV ELECTRONS X .9-1.5 MeV PROTONS 0 6-19 MeV PROTONS X19-80 MeV PROTONS



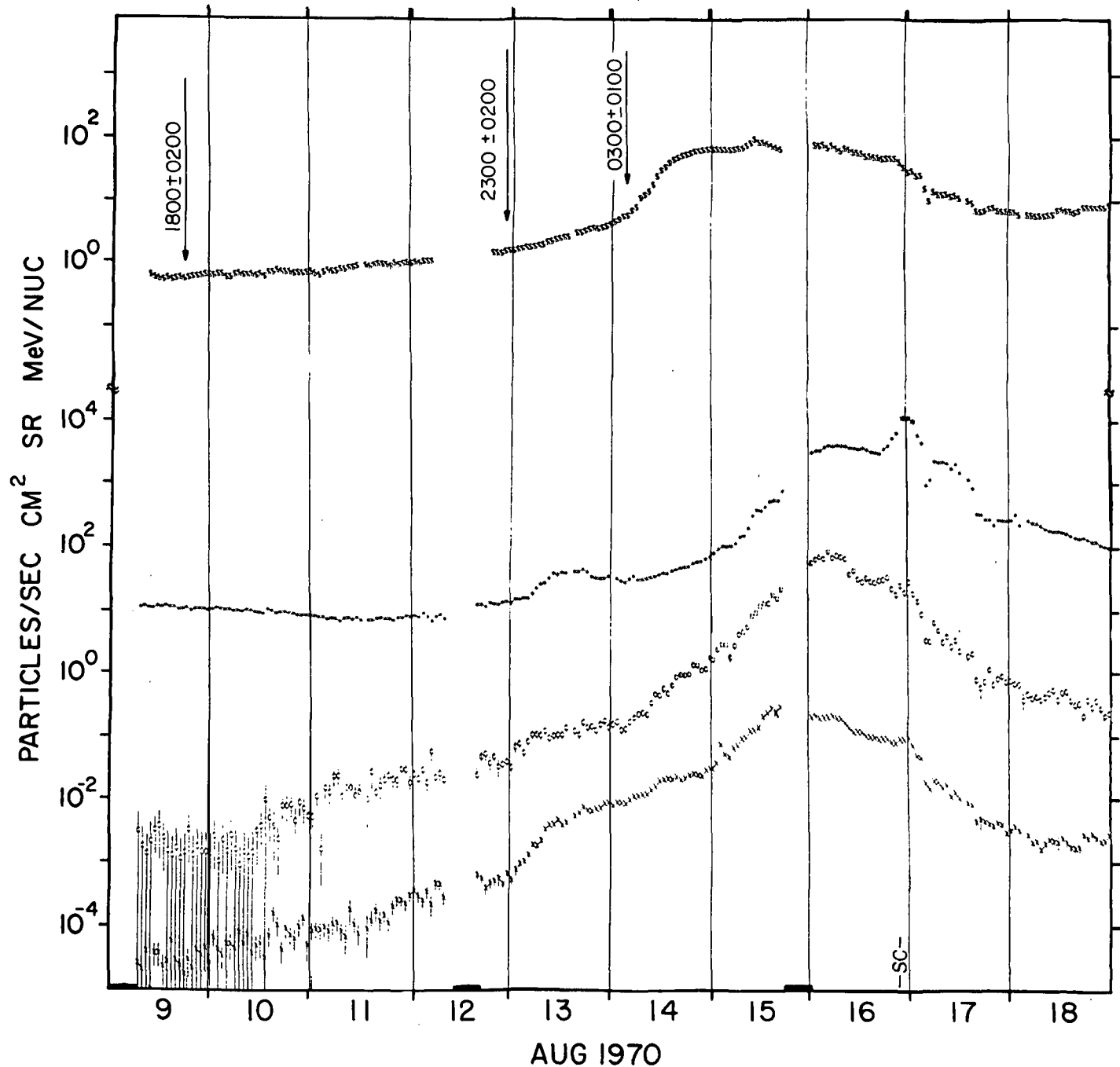
3.5-1.1 MeV ELECTRONS X .9-1.5 MeV PROTONS 6-19 MeV PROTONS X 19-80 MeV PROTONS



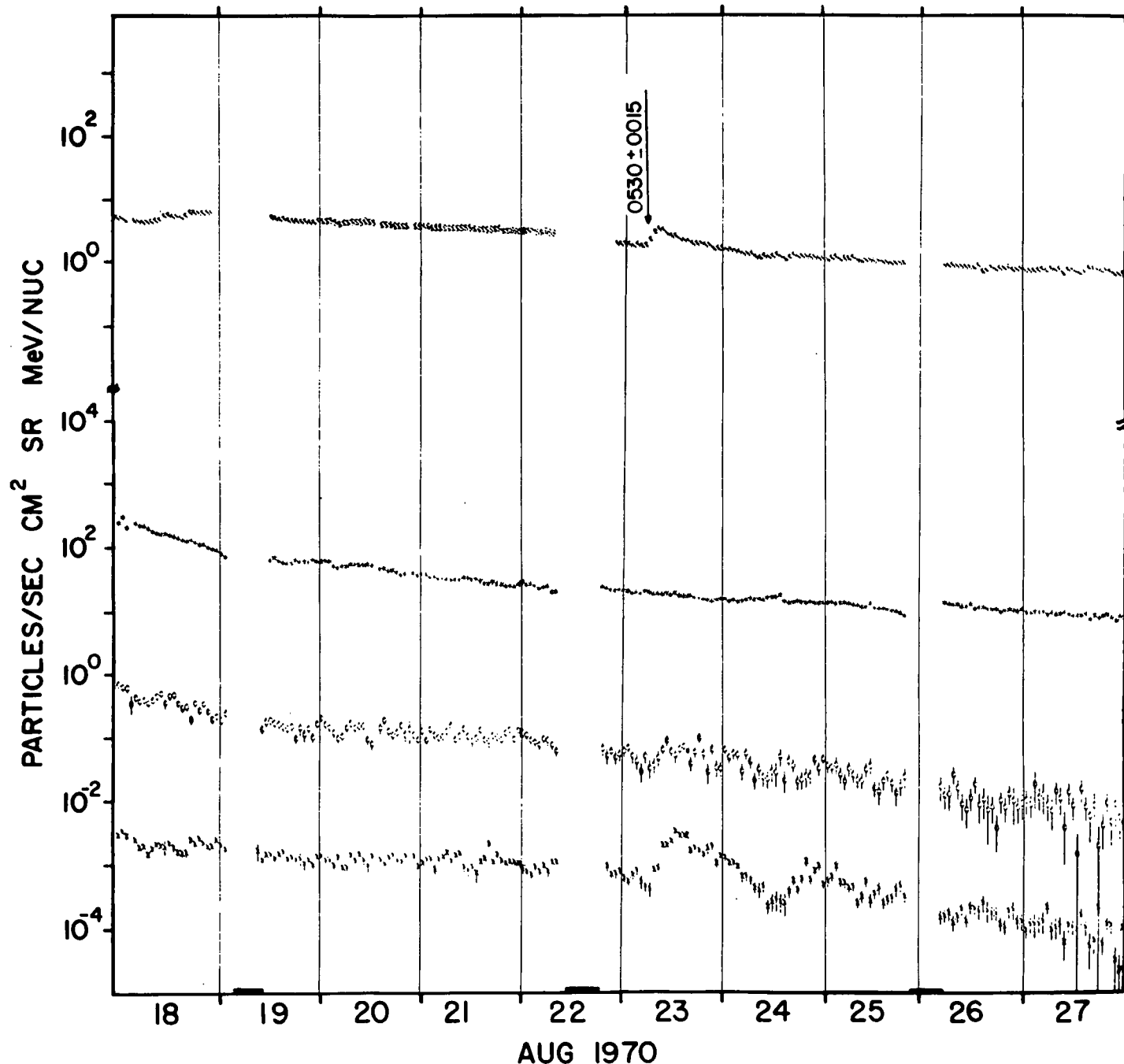
5.5-1.1 MeV ELECTRONS X .9-1.5 MeV PROTONS 0 6-19 MeV PROTONS X 19-80 MeV PROTONS



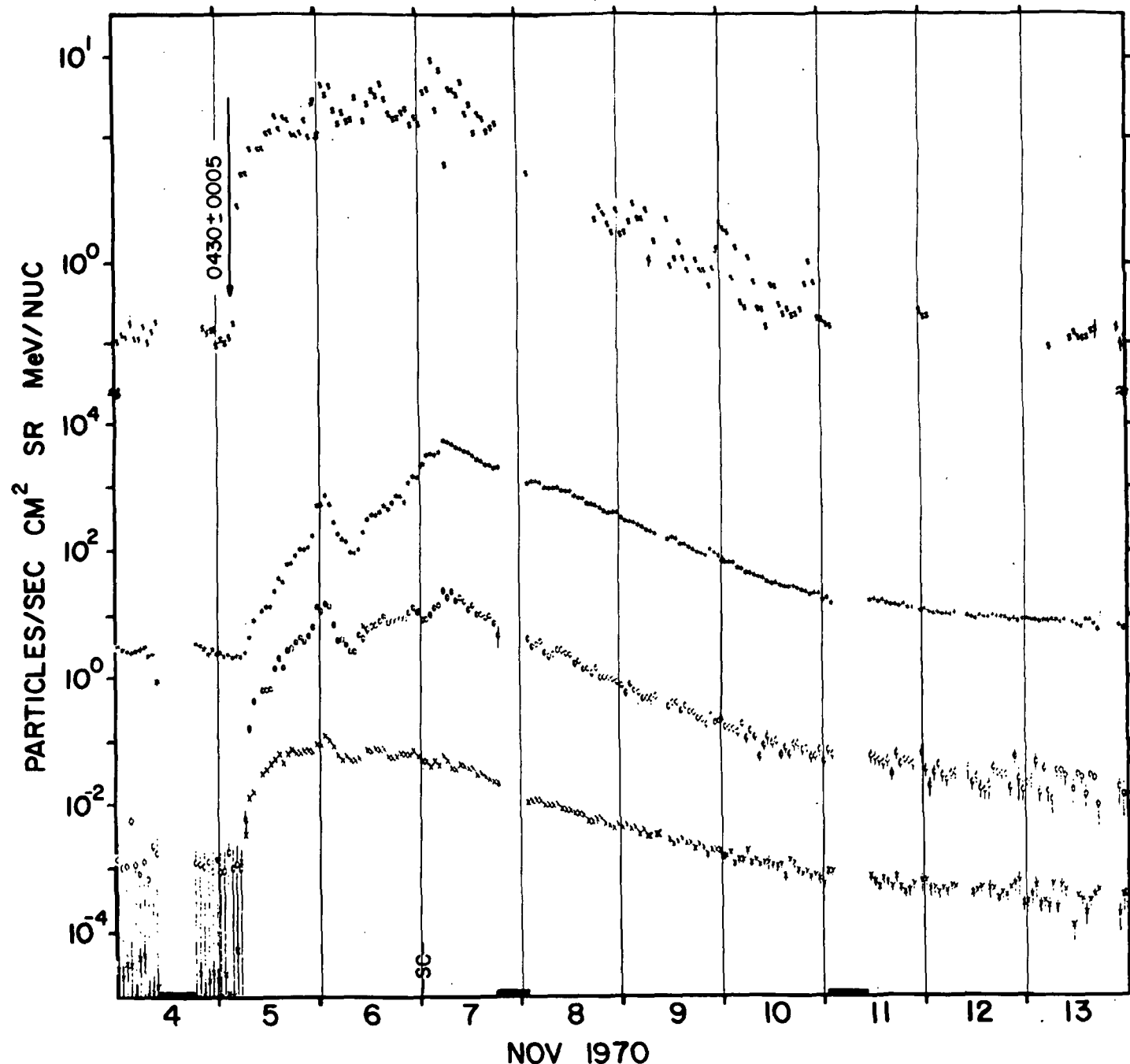
\$.5-1.1 MeV ELECTRONS \times .9-1.5 MeV PROTONS ϕ 6-19 MeV PROTONS \times 19-80 MeV PROTONS



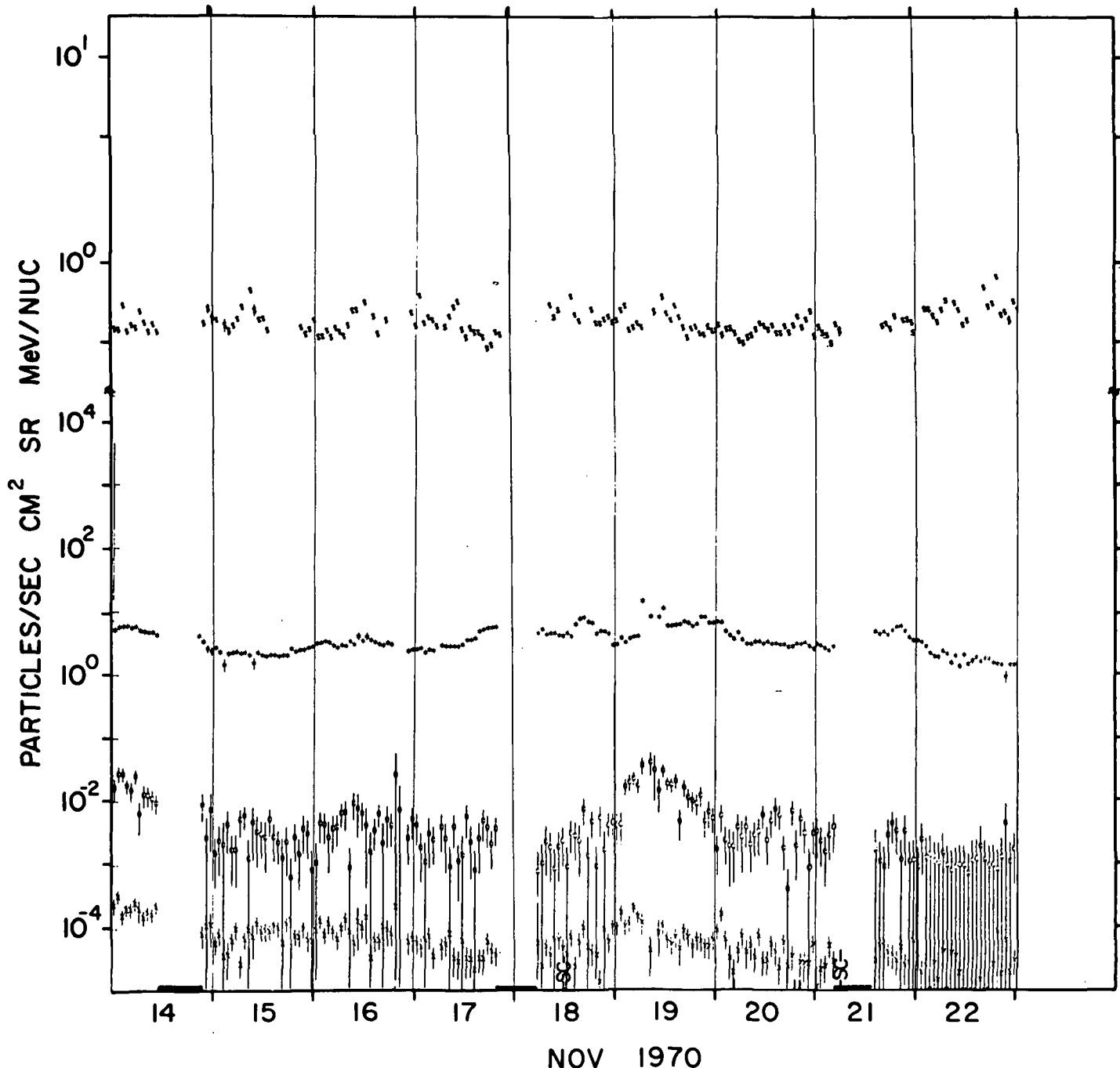
5.5-1.1 MeV ELECTRONS X .9-1.5 MeV PROTONS O 6-19 MeV PROTONS X 19-80 MeV PROTONS



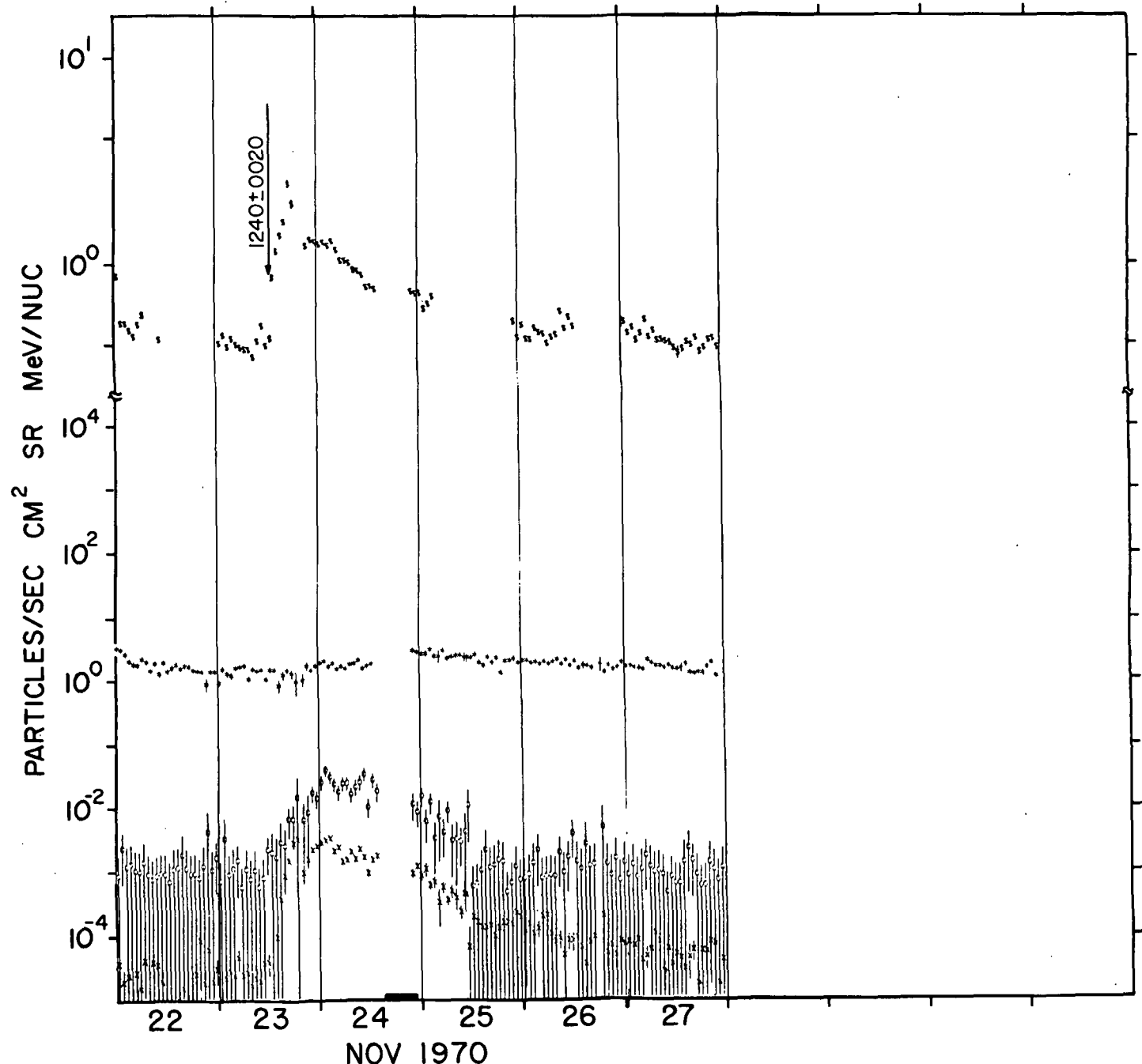
S .5-1.1 MeV ELECTRONS X .9-1.5 MeV PROTONS O 6-19 MeV PROTONS X 19-80 MeV PROTONS



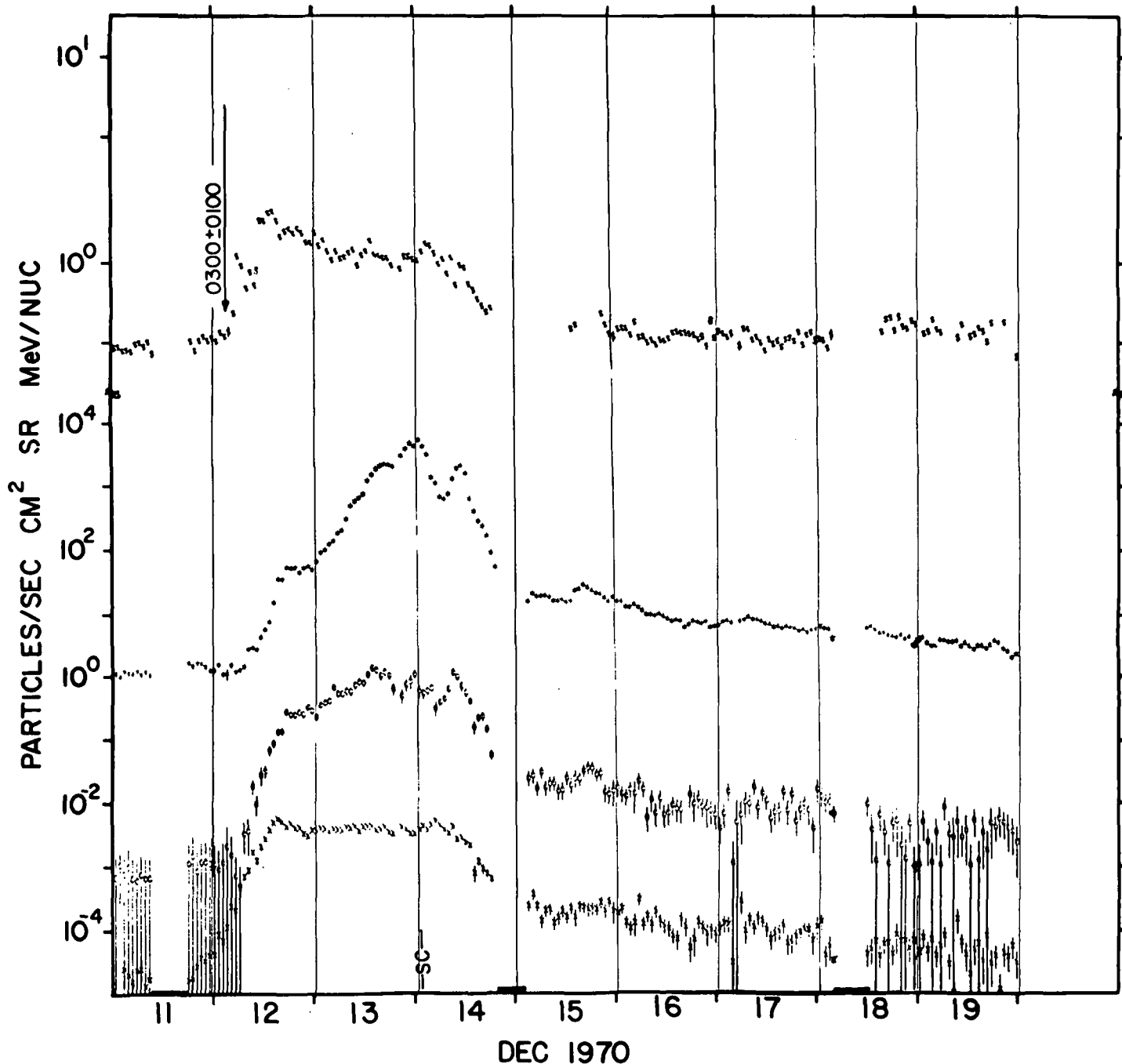
\$.5-1.1 MeV ELECTRONS X .9-1.5 MeV PROTONS ϕ 6-19 MeV PROTONS X 19-80 MeV PROTONS

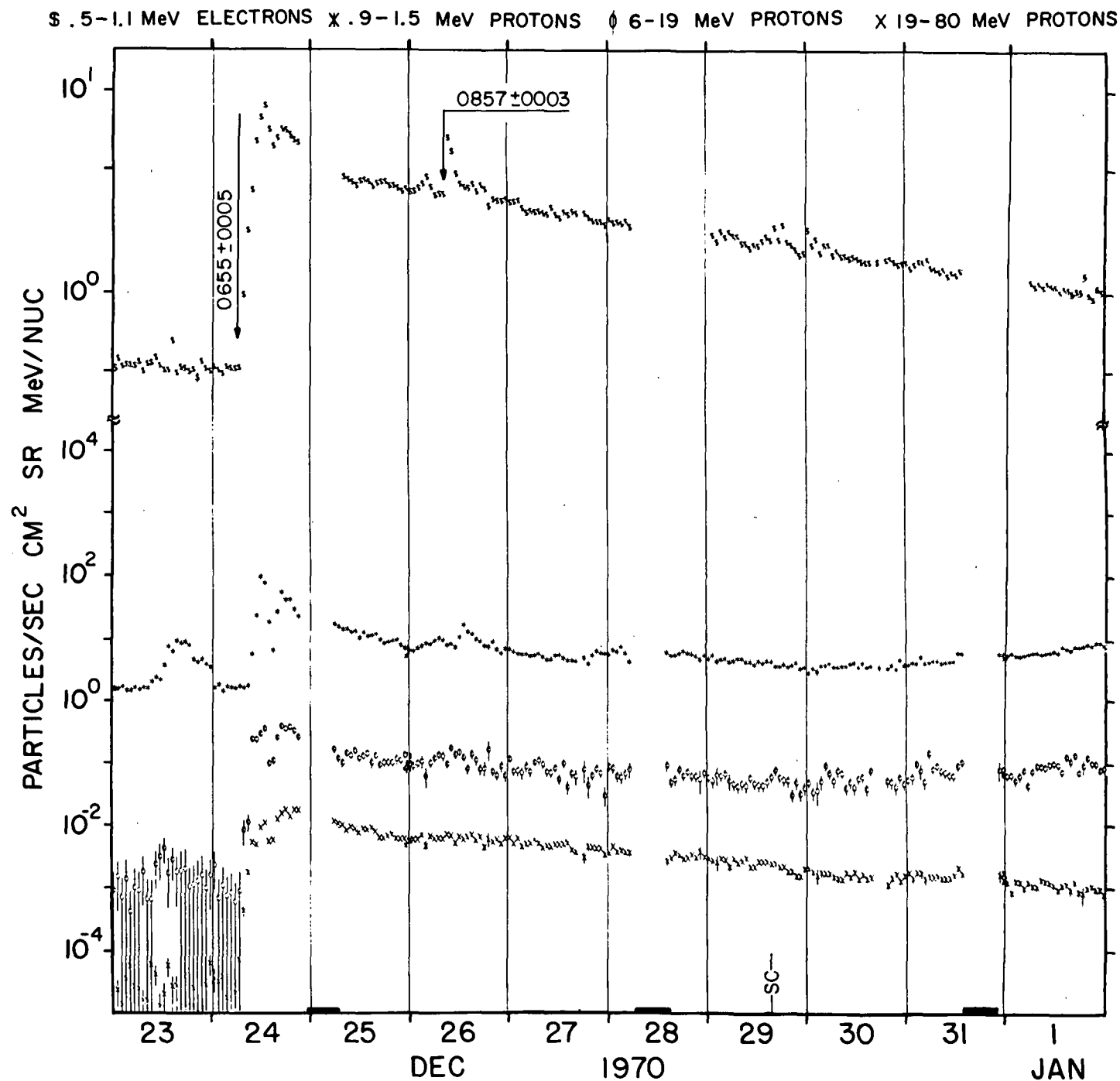


.5-1.1 MeV ELECTRONS X .9-1.5 MeV PROTONS ϕ 6-19 MeV PROTONS X 19-80 MeV PROTONS

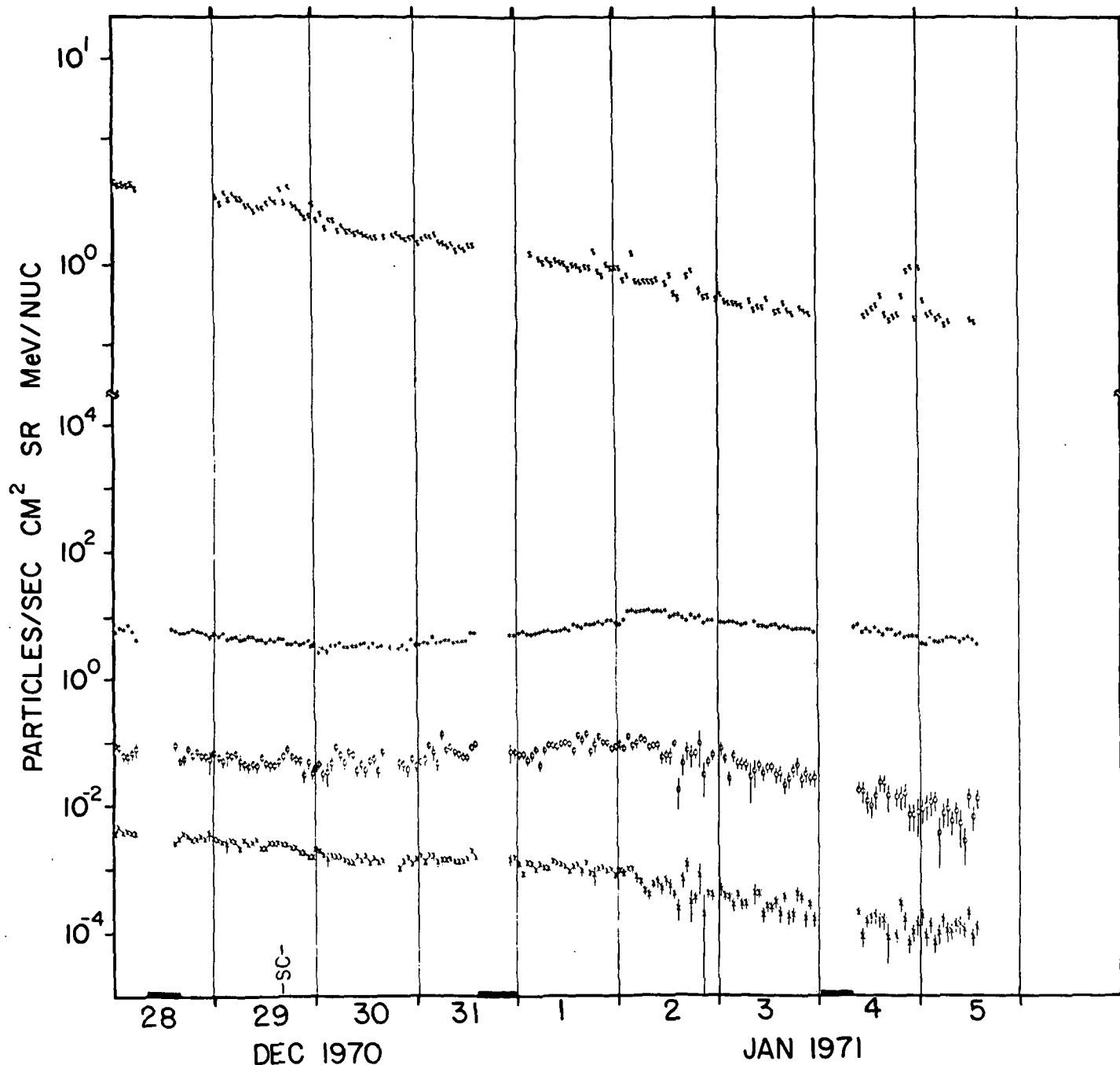


\$.5-1.1 MeV ELECTRONS X .9-1.5 MeV PROTONS O 6-19 MeV PROTONS X 19-80 MeV PROTONS

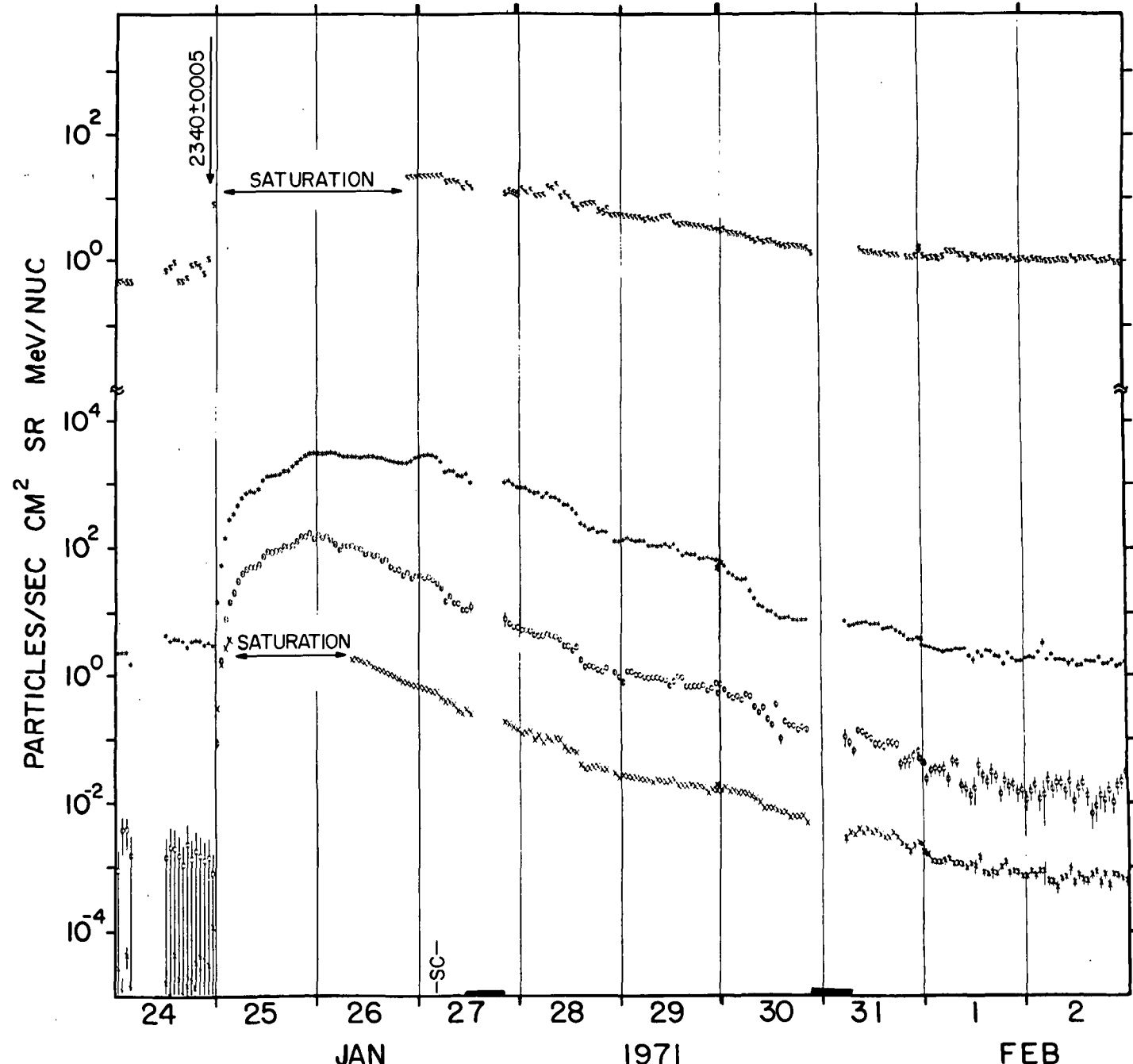




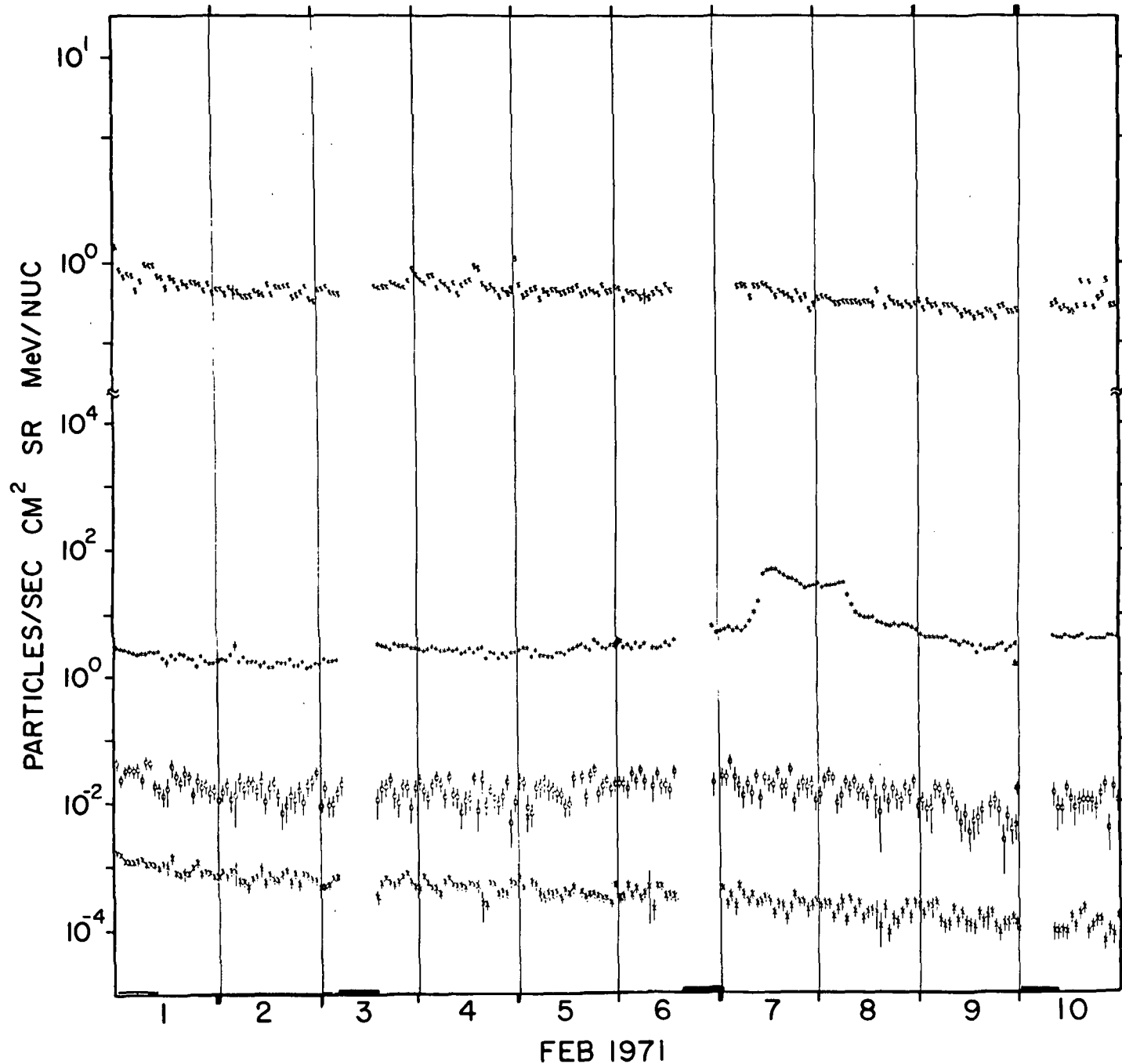
\$.5-1.1 MeV ELECTRONS X .9-1.5 MeV PROTONS O 6-19 MeV PROTONS X 19-80 MeV PROTONS



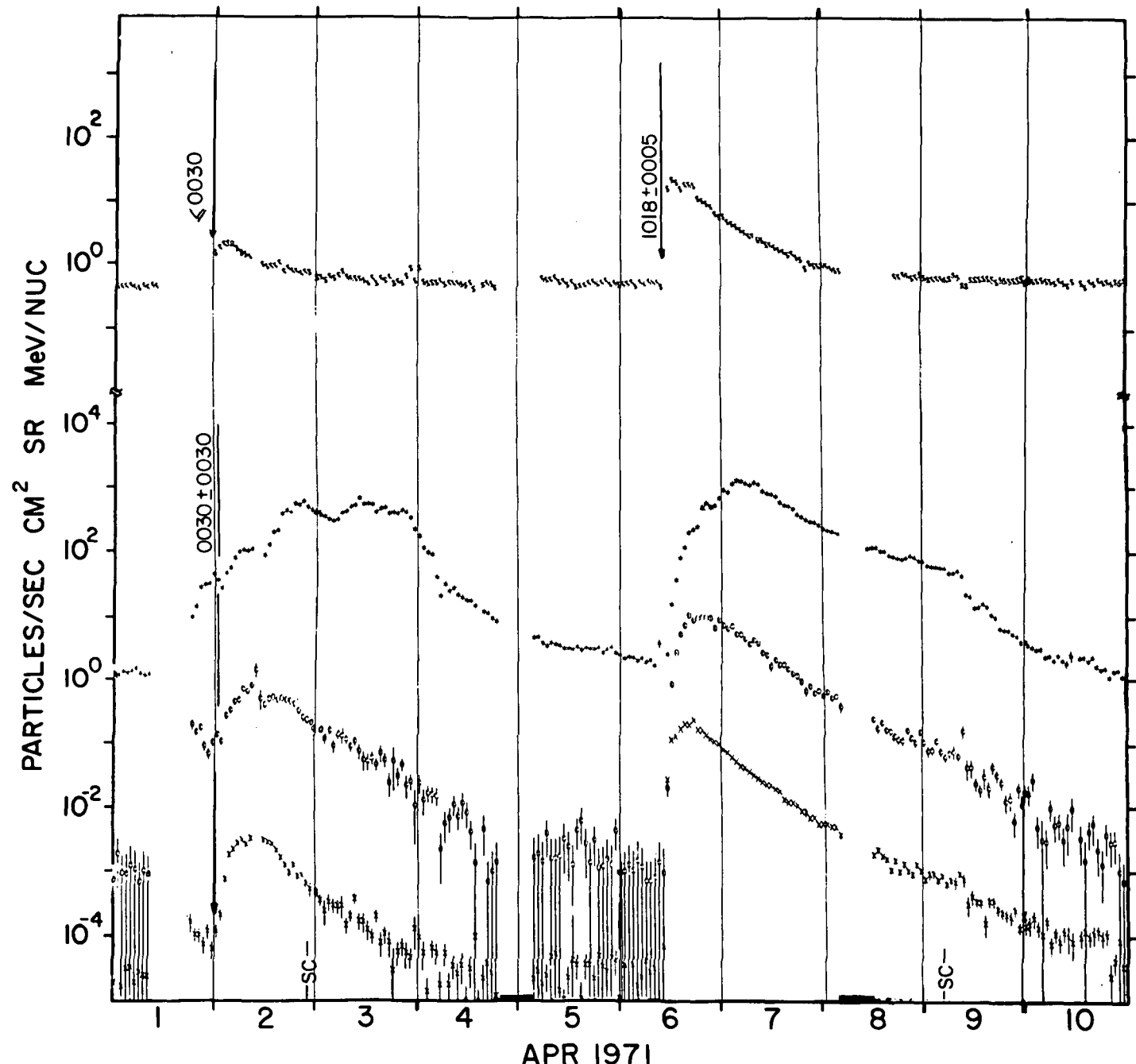
\$.5-1.1 MeV ELECTRONS X .9-1.5 MeV PROTONS ϕ 6-19 MeV PROTONS X 19-80 MeV PROTONS



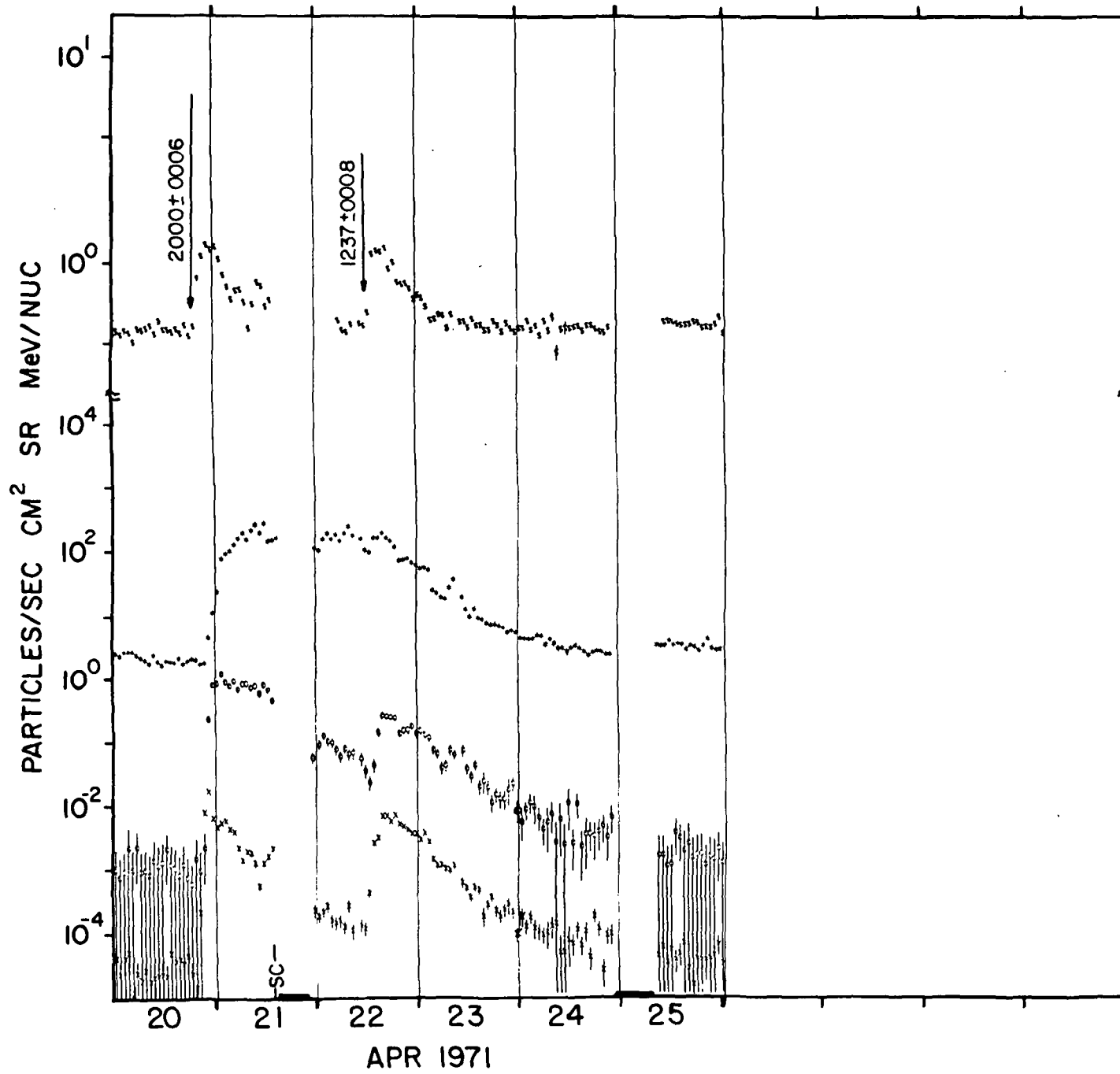
.5-1.1 MeV ELECTRONS X .9-1.5 MeV PROTONS \circ 6-19 MeV PROTONS X 19-80 MeV PROTONS



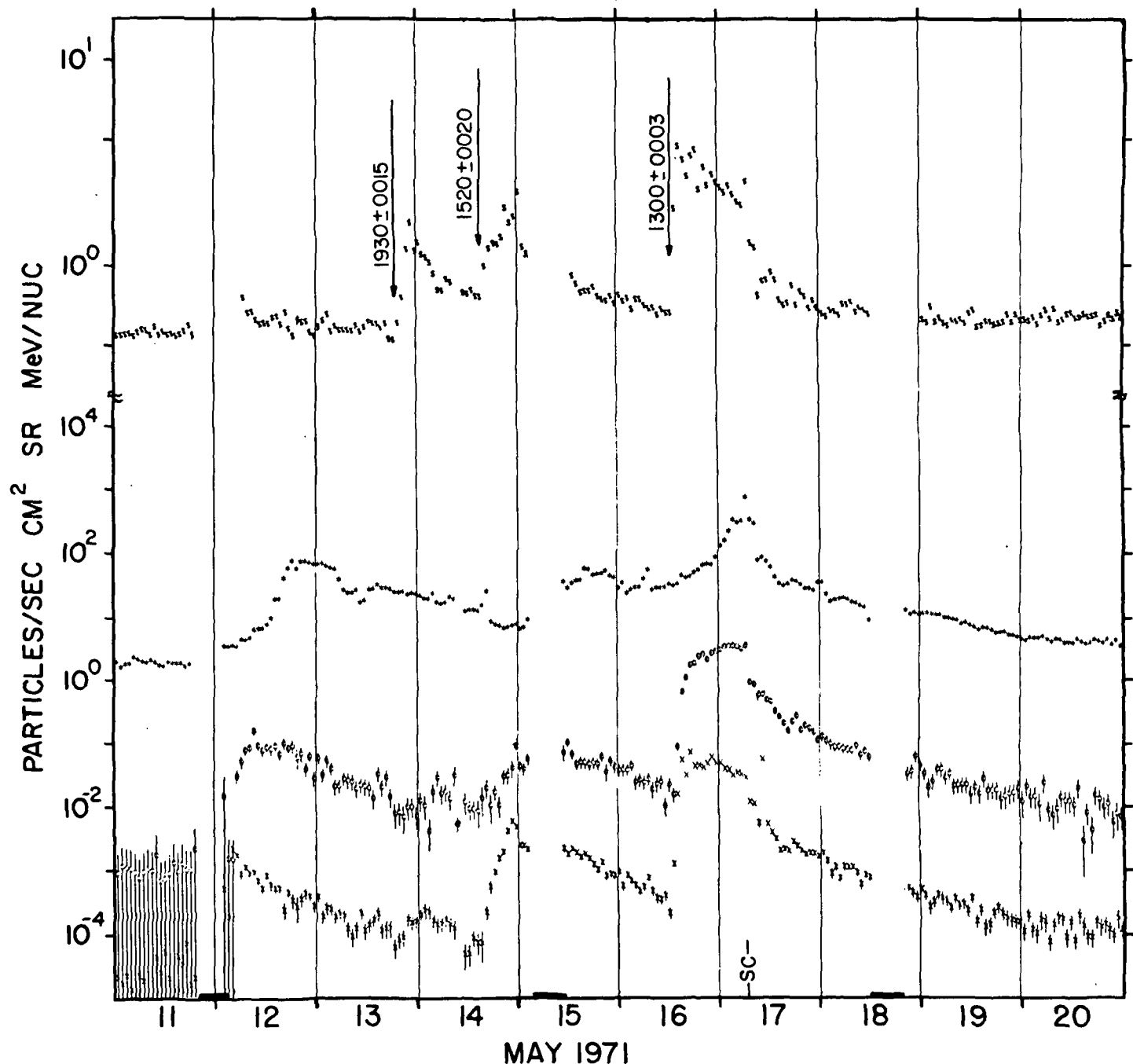
\$.5-1.1 MeV ELECTRONS X .9-1.5 MeV PROTONS \diamond 6-19 MeV PROTONS X 19-80 MeV PROTONS



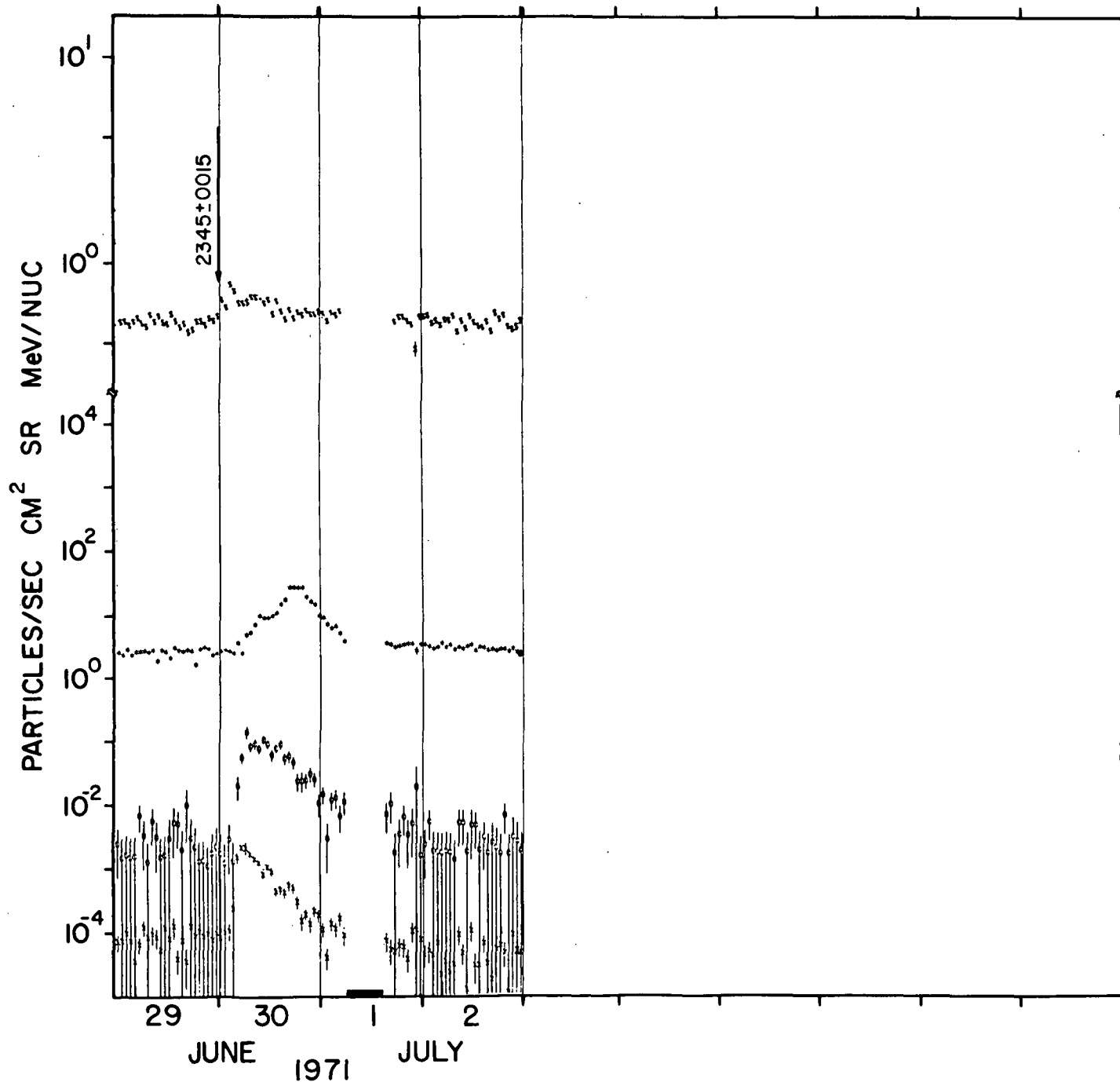
\$.5-1.1 MeV ELECTRONS X .9-1.5 MeV PROTONS O 6-19 MeV PROTONS X 19-80 MeV PROTONS



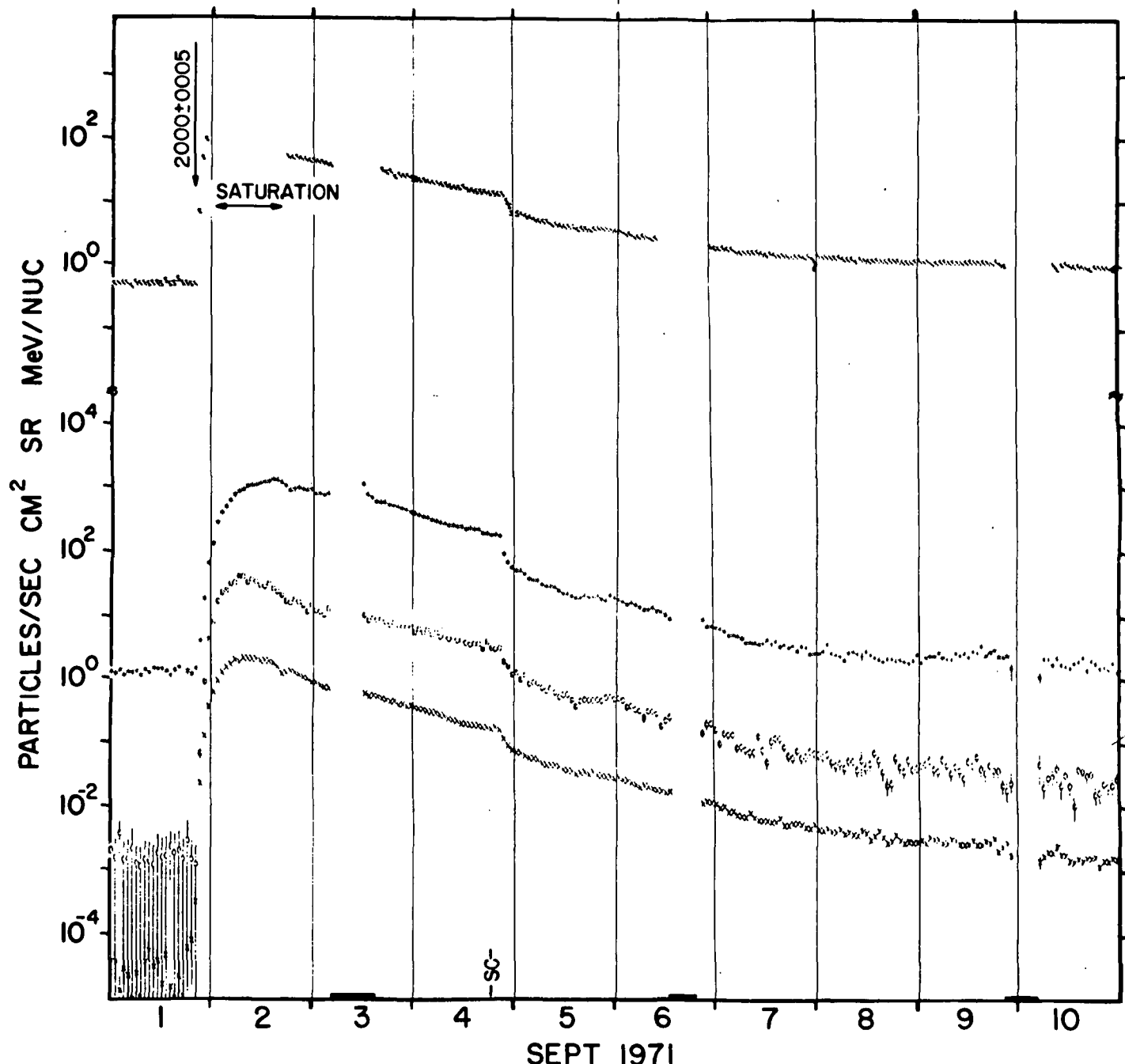
\$.5-1.1 MeV ELECTRONS X .9-1.5 MeV PROTONS O 6-19 MeV PROTONS X 19-80 MeV PROTONS



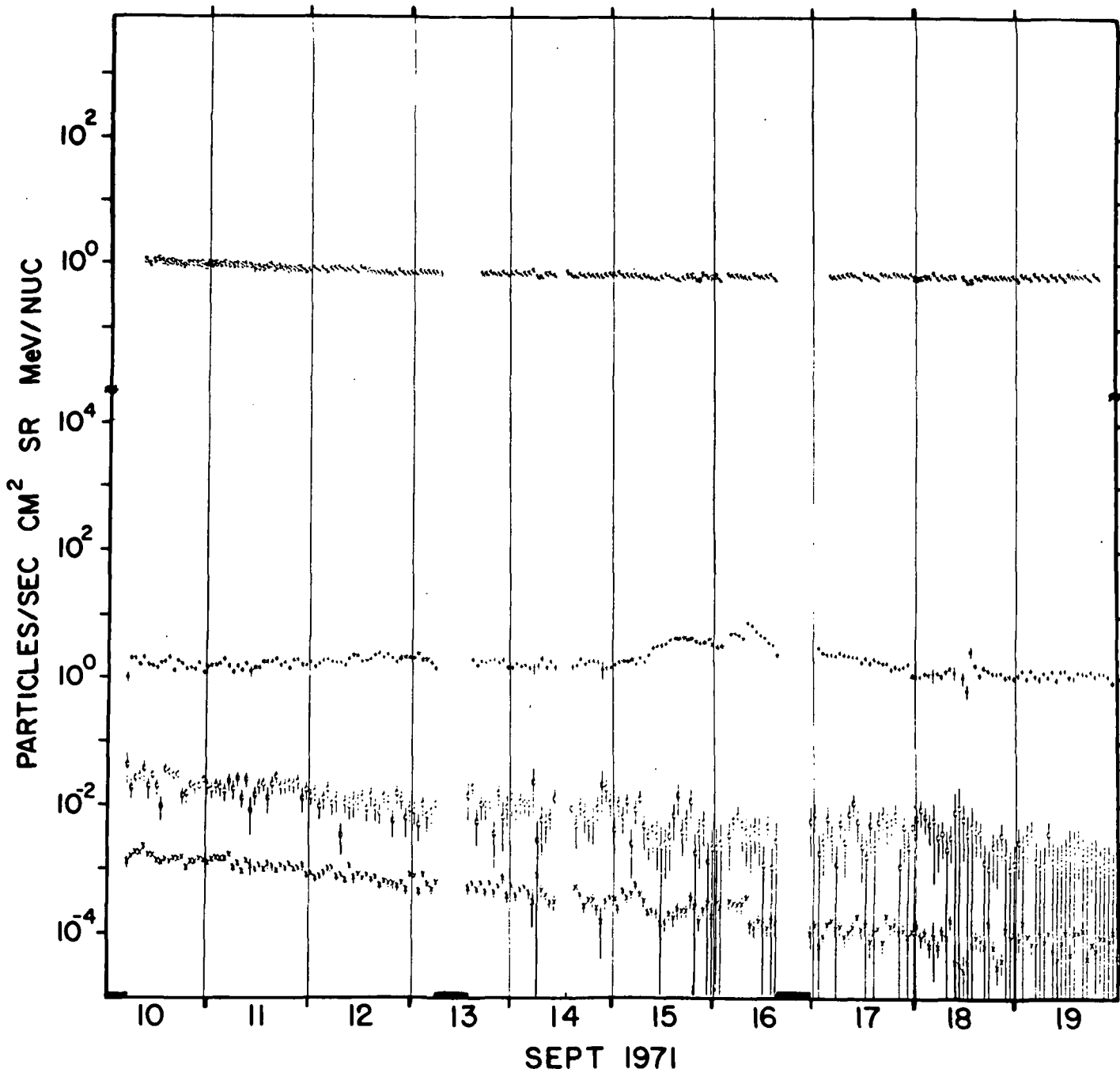
\$.5-1.1 MeV ELECTRONS X .9-1.5 MeV PROTONS \oplus 6-19 MeV PROTONS X 19-80 MeV PROTONS



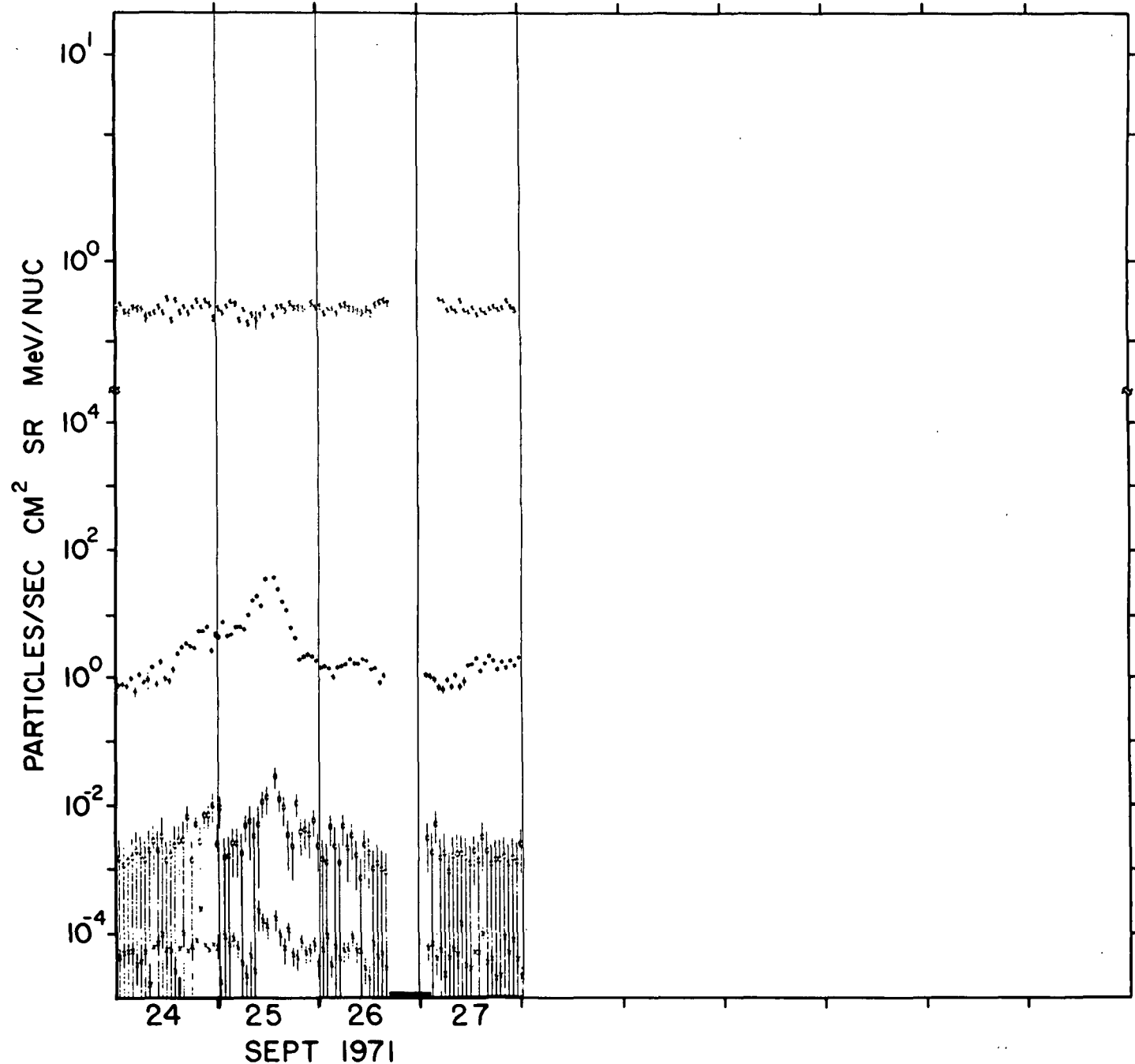
.5-1.1 MeV ELECTRONS \times .9-1.5 MeV PROTONS \circ 6-19 MeV PROTONS \times 19-80 MeV PROTONS



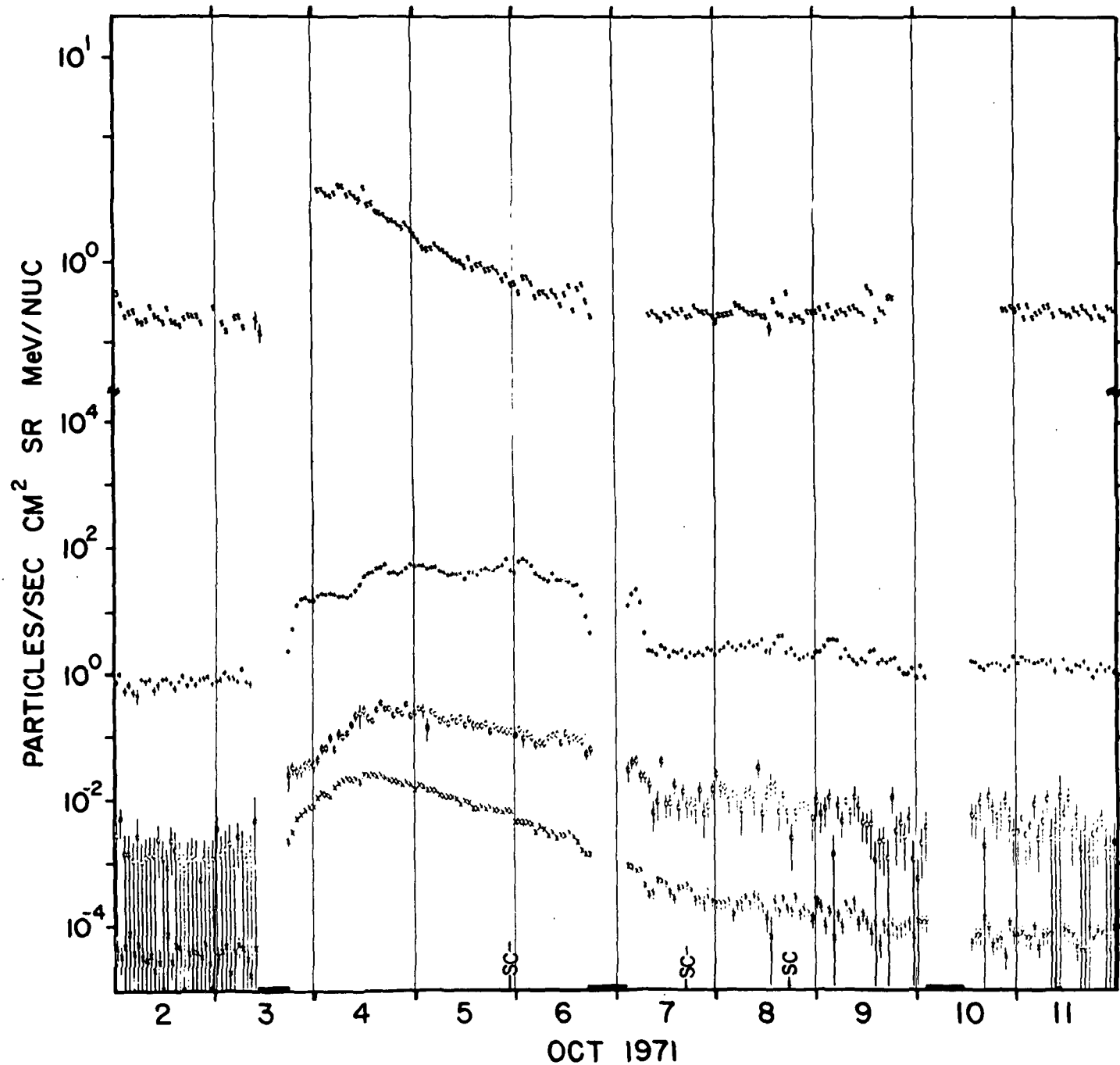
S .5-1.1 MeV ELECTRONS X .9-1.5 MeV PROTONS @ 6-19 MeV PROTONS X 19-80 MeV PROTONS



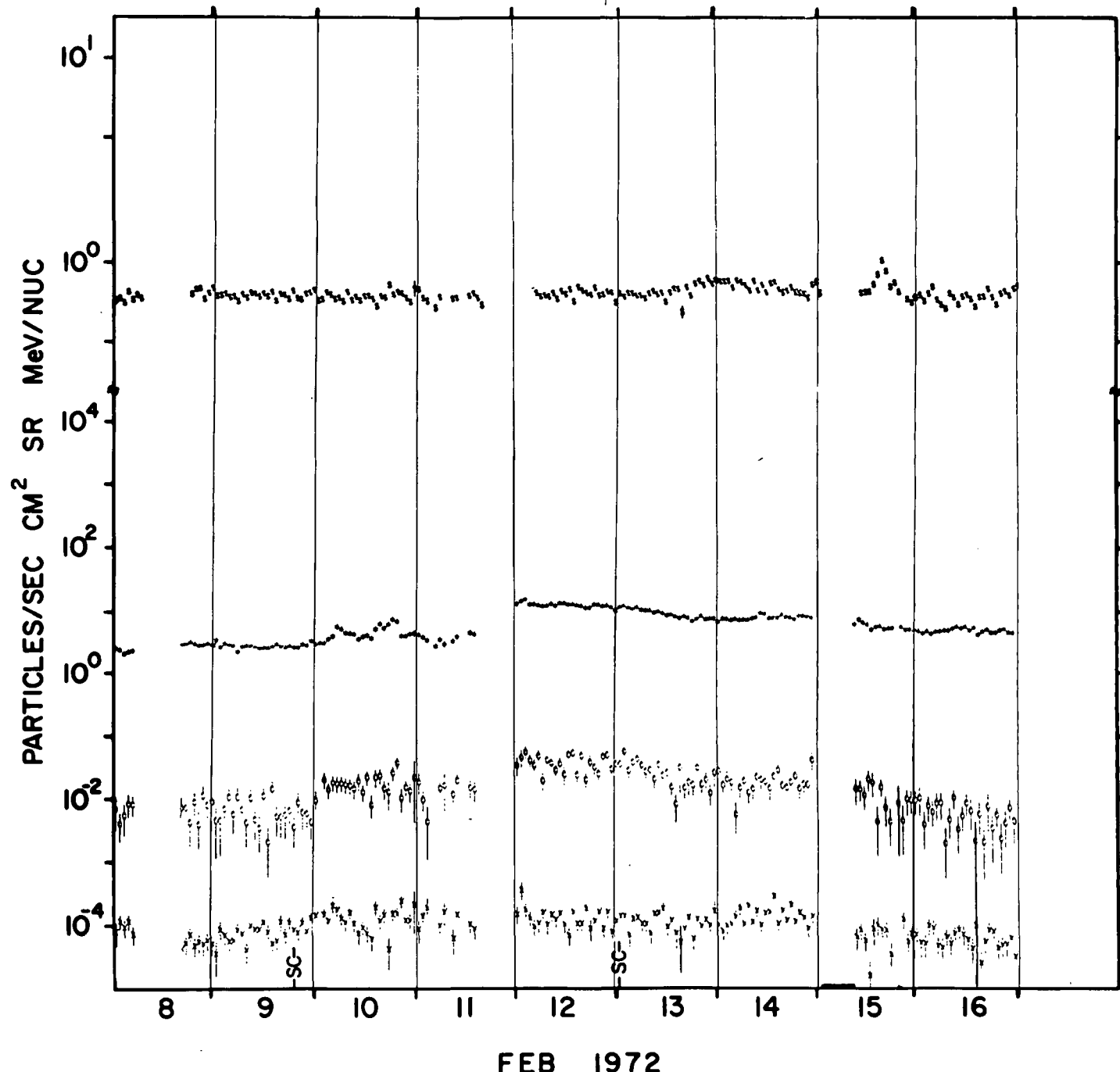
.5-1.1 MeV ELECTRONS X .9-1.5 MeV PROTONS ϕ 6-19 MeV PROTONS X 19-80 MeV PROTONS



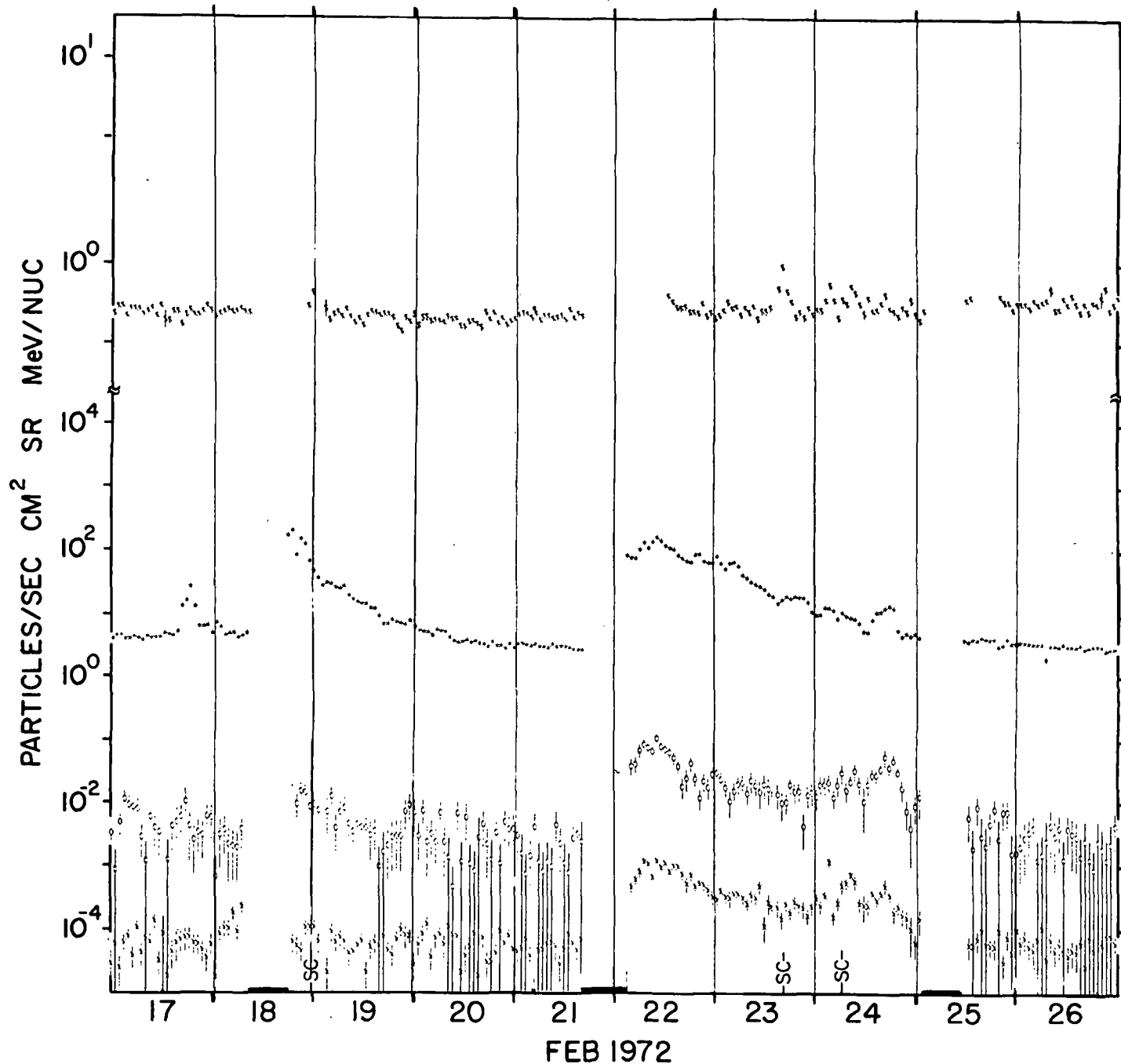
.5-1.1 MeV ELECTRONS X .9-1.5 MeV PROTONS O 6-19 MeV PROTONS X 19-80 MeV PROTONS



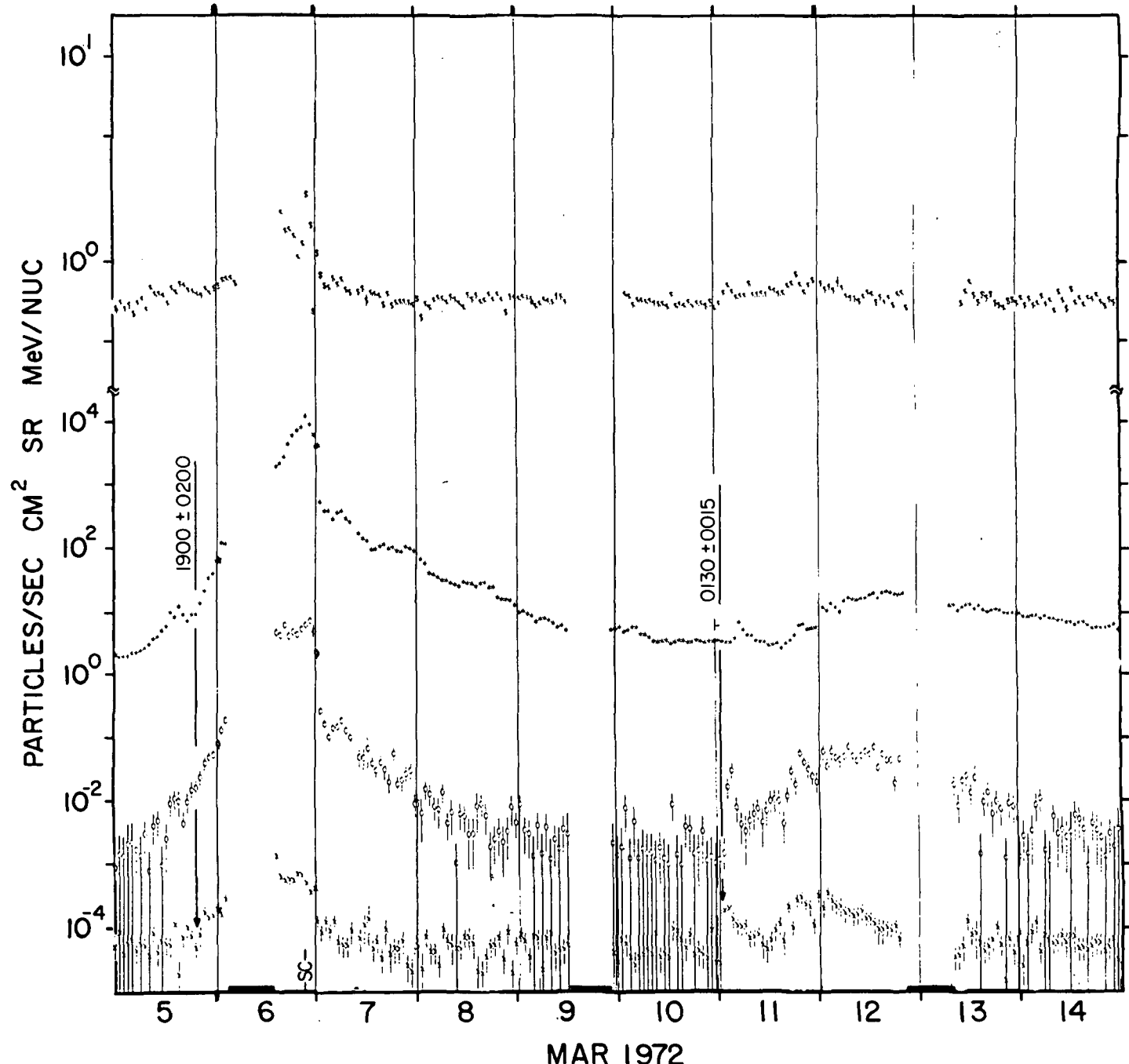
S .5-1.1 MeV ELECTRONS X .9-1.5 MeV PROTONS Ø 6-19 MeV PROTONS X 19-80 MeV PROTONS



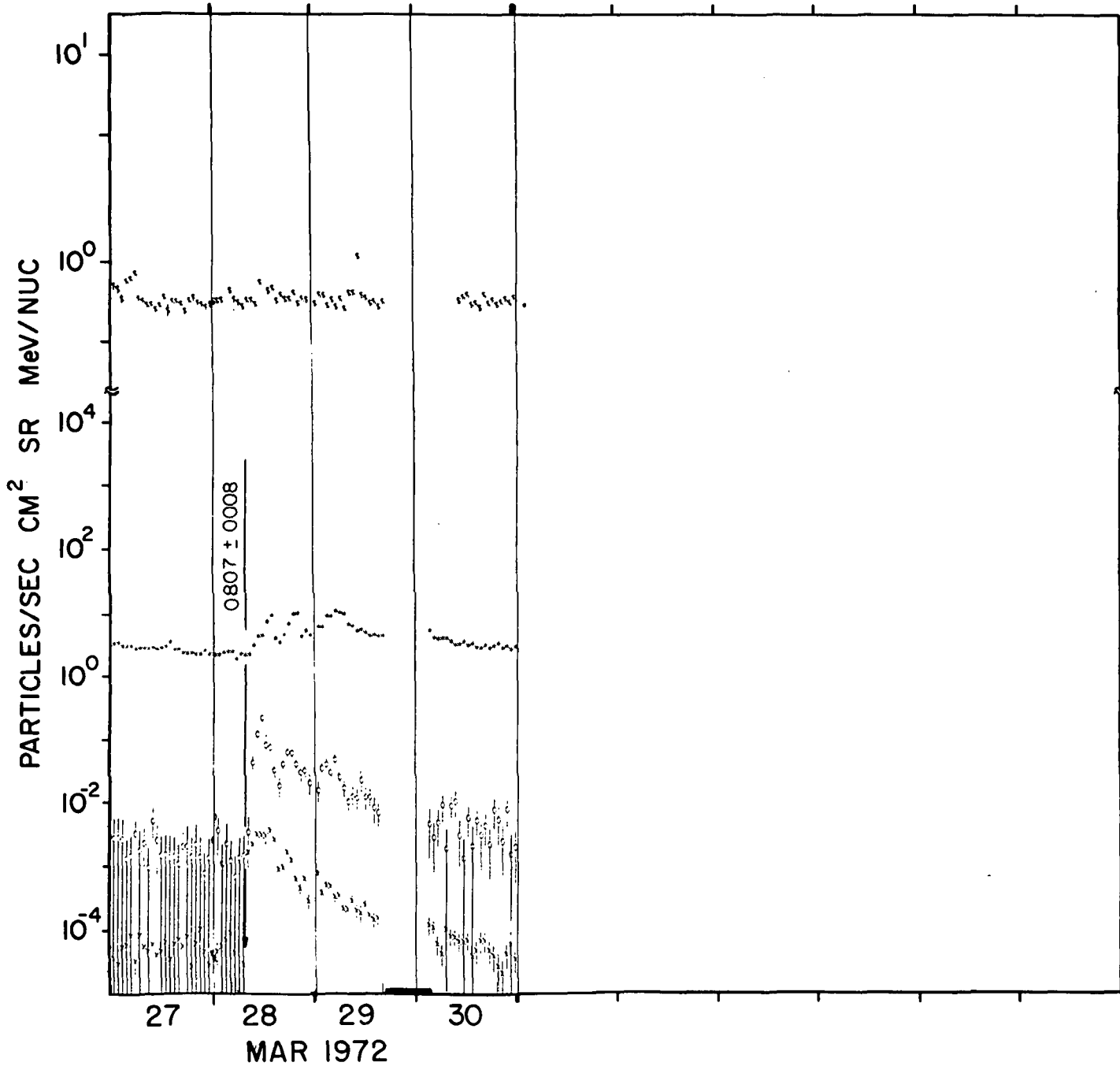
- 89 -
\$.5-1.1 MeV ELECTRONS X .9-1.5 MeV PROTONS O 6-19 MeV PROTONS X 19-80 MeV PROTONS



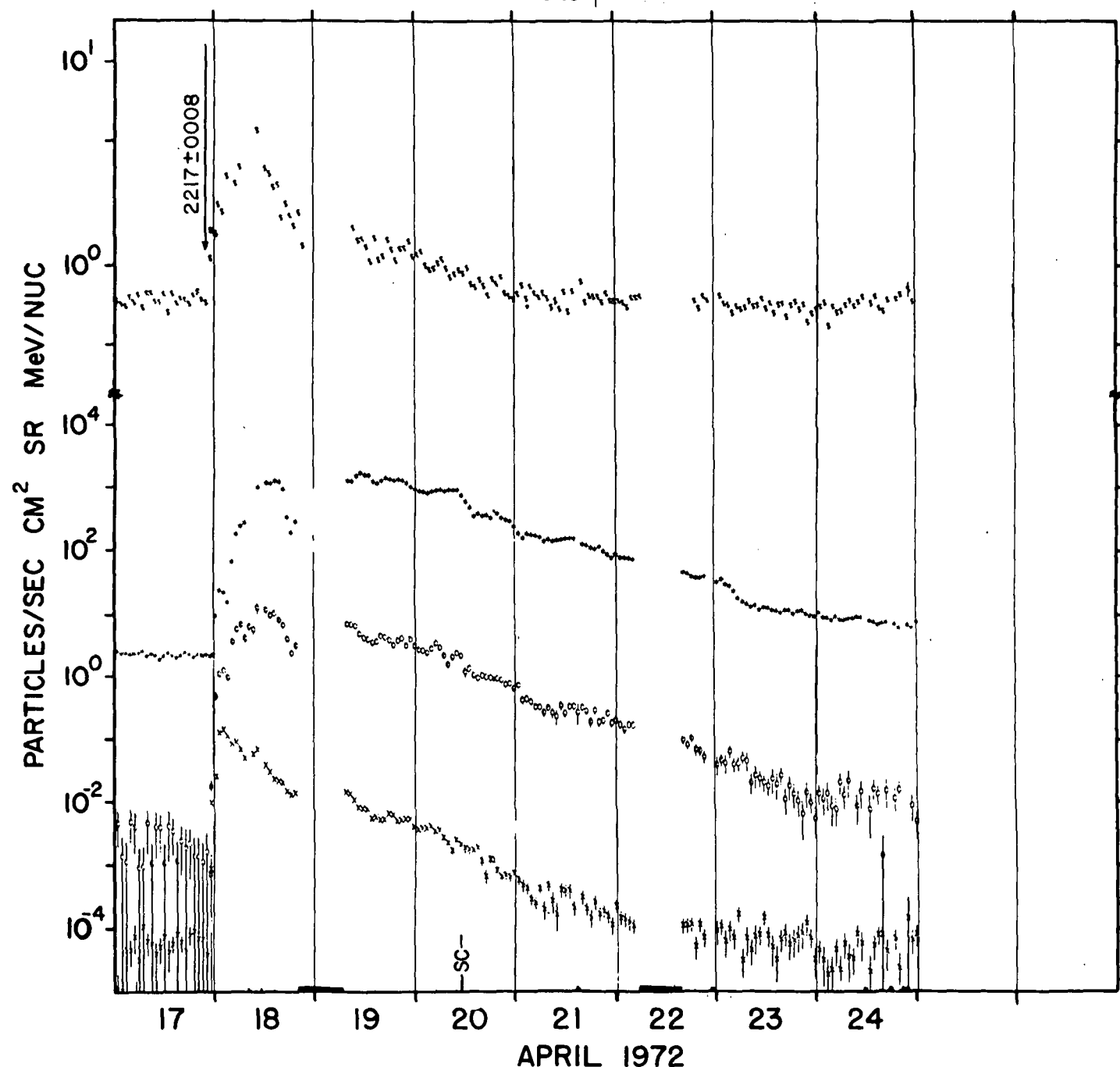
\$.5-1.1 MeV ELECTRONS X .9-1.5 MeV PROTONS O 6-19 MeV PROTONS X 19-80 MeV PROTONS



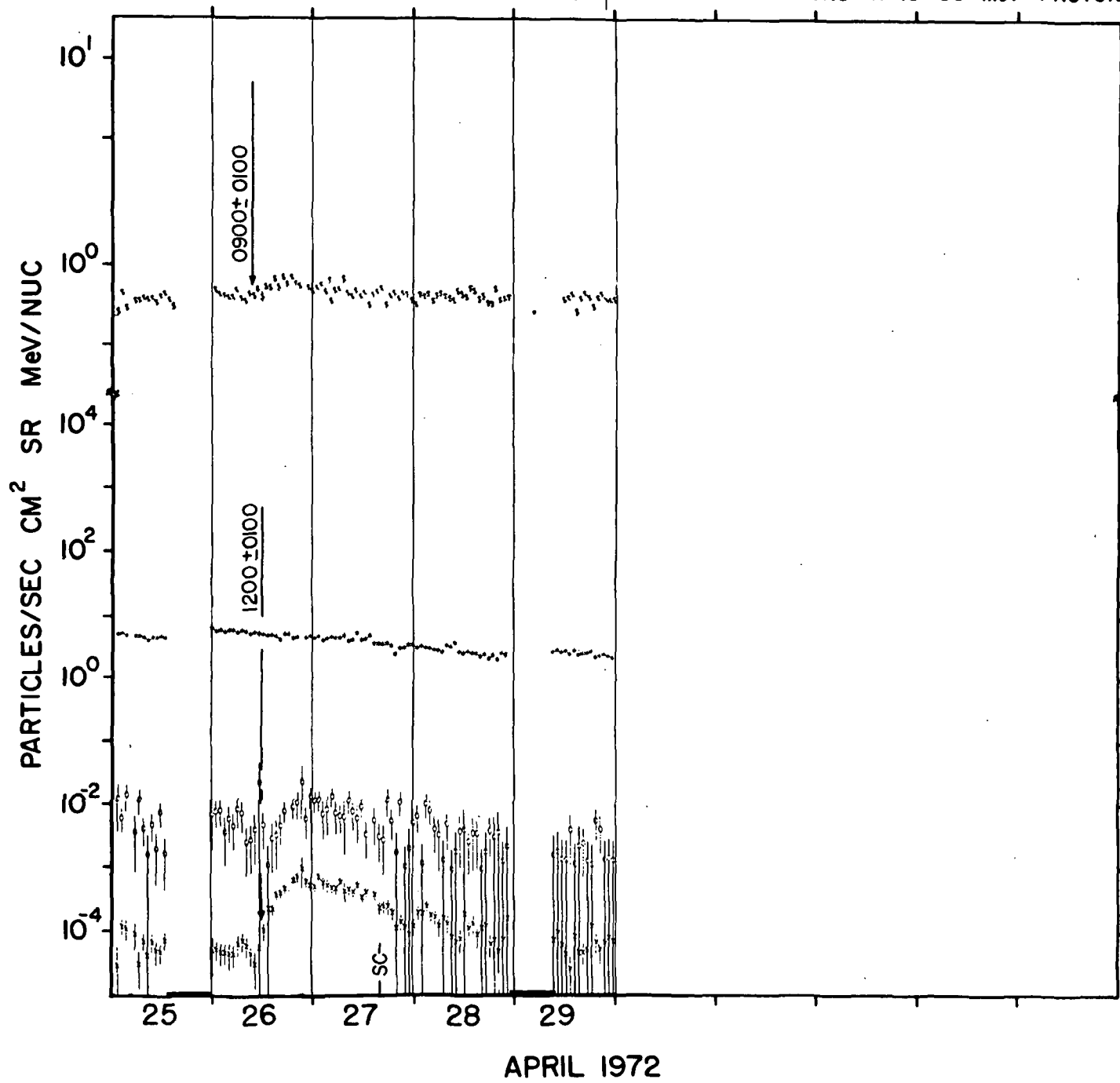
- 91 -
\$.5 - 1.1 MeV ELECTRONS X .9 - 1.5 MeV PROTONS ϕ 6 - 19 MeV PROTONS X 19 - 80 MeV PROTONS



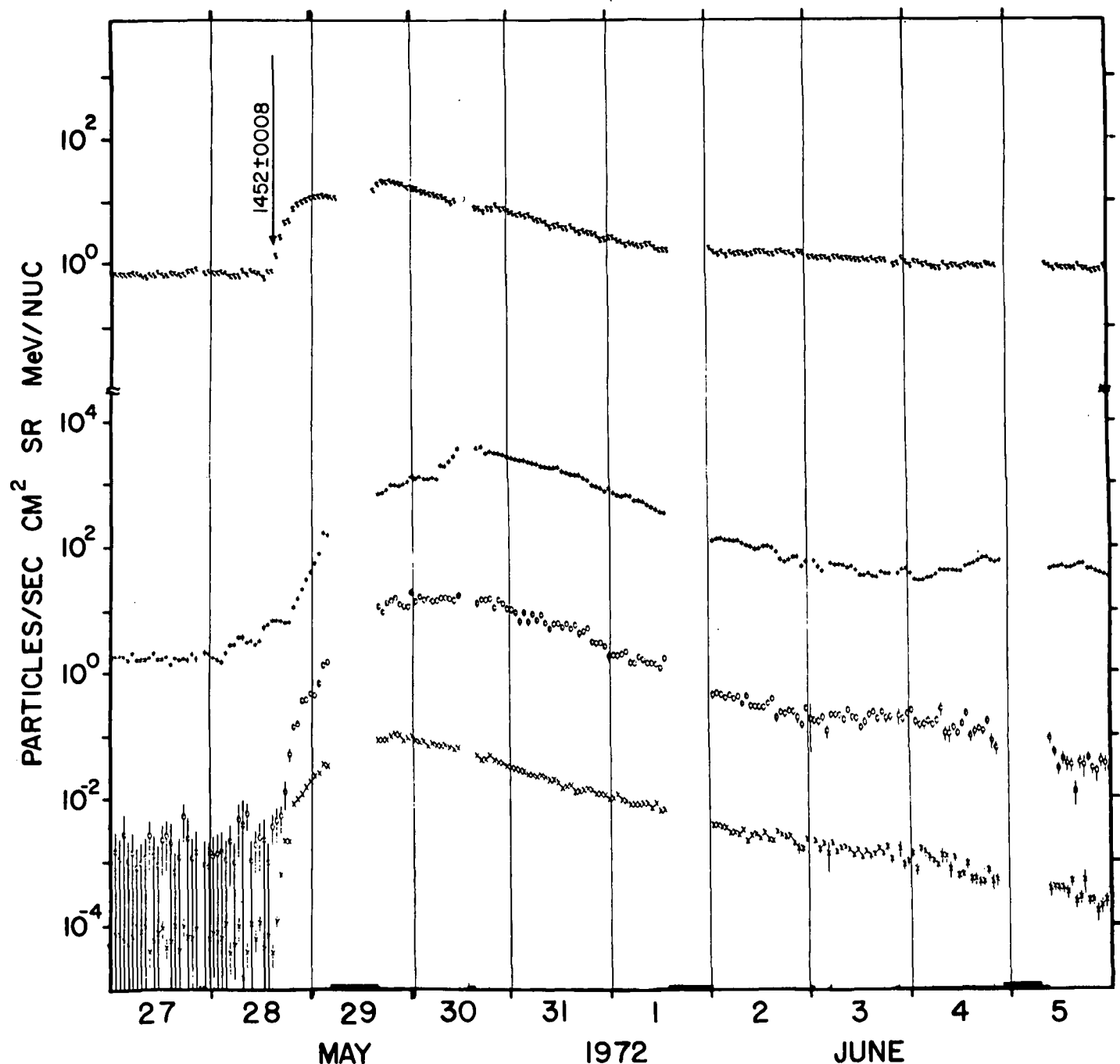
\$.5-1.1 MeV ELECTRONS X .9-1.5 MeV PROTONS o 6-19 MeV PROTONS X 19-80 MeV PROTONS



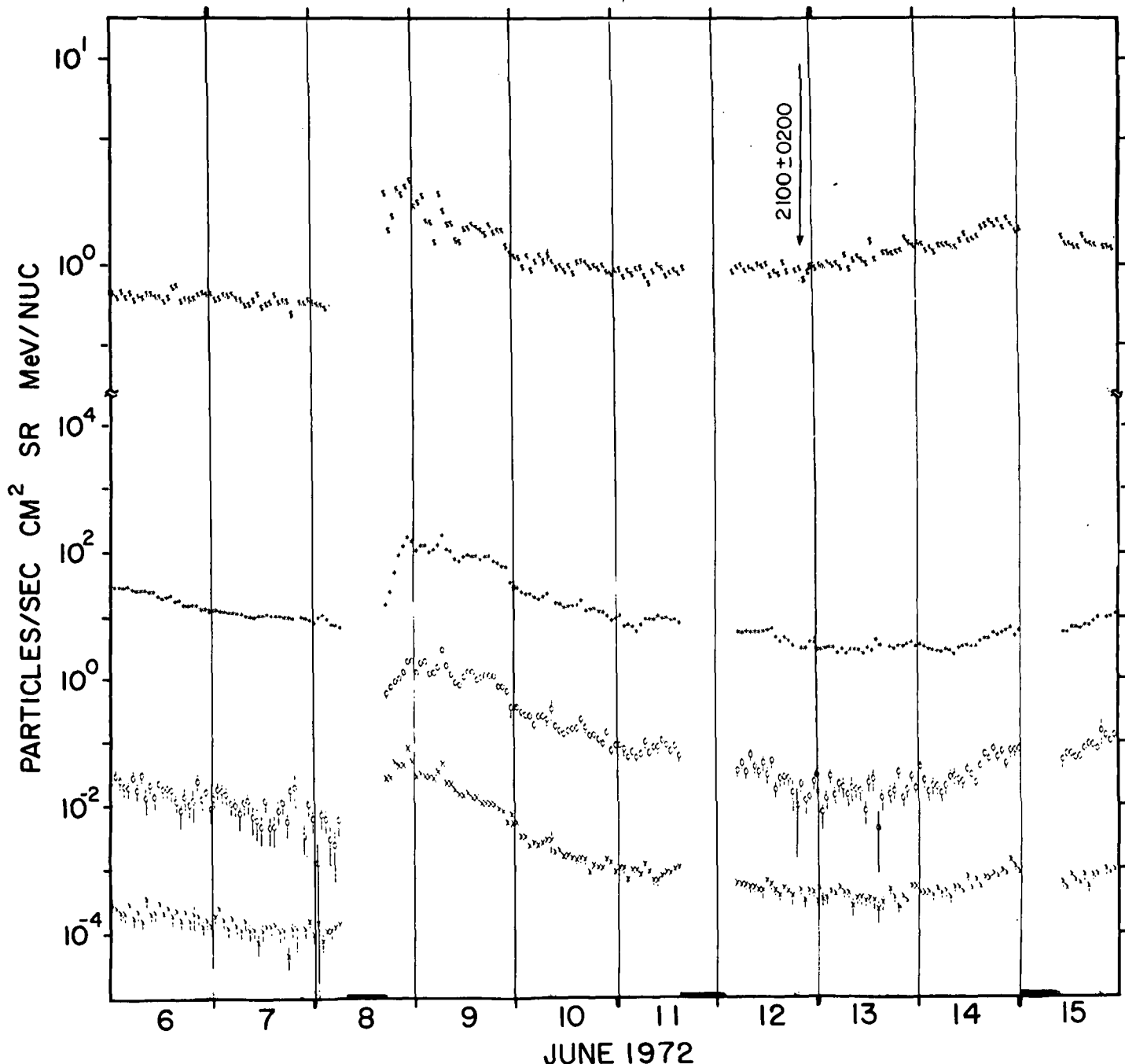
- 93 -
\$.5-1.1 MeV ELECTRONS X .9-1.5 MeV PROTONS + 6-19 MeV PROTONS X 19-80 MeV PROTONS



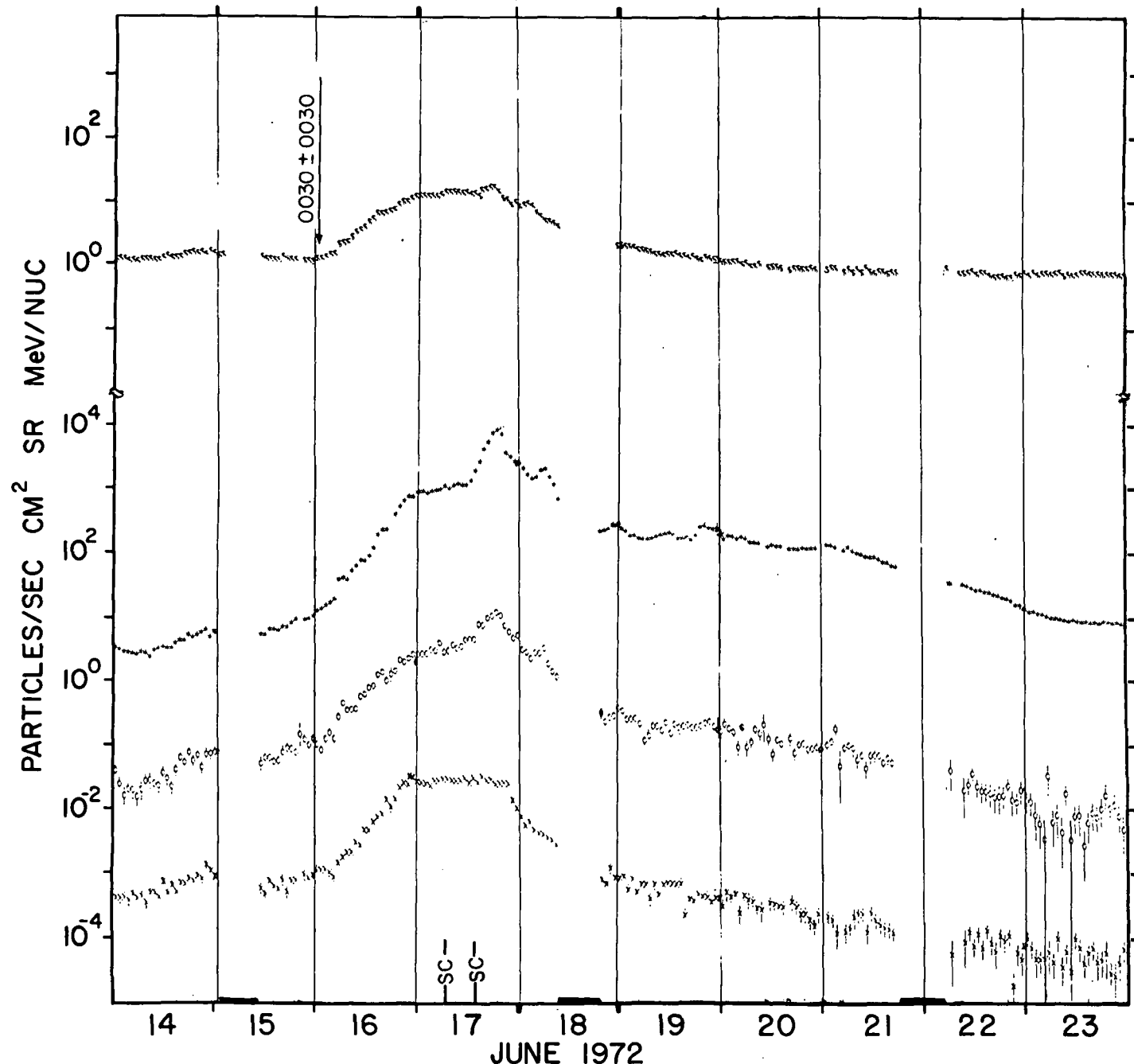
- 94 -
\$.5-1.1 MeV ELECTRONS X .9-1.5 MeV PROTONS O 6-19 MeV PROTONS X 19-80 MeV PROTONS



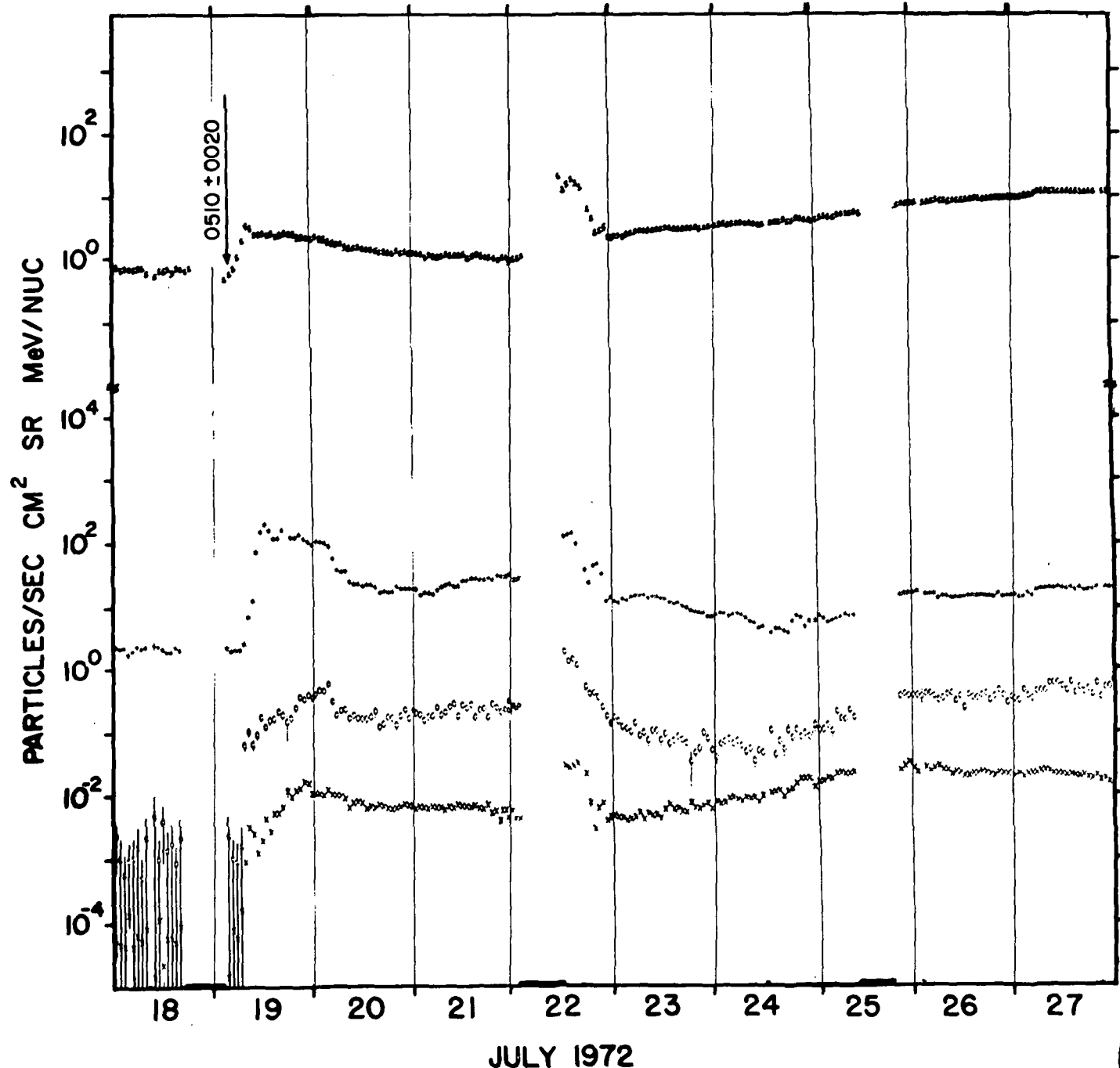
\$.5-.11 MeV ELECTRONS X .9-.15 MeV PROTONS O 6-19 MeV PROTONS X 19-80 MeV PROTONS



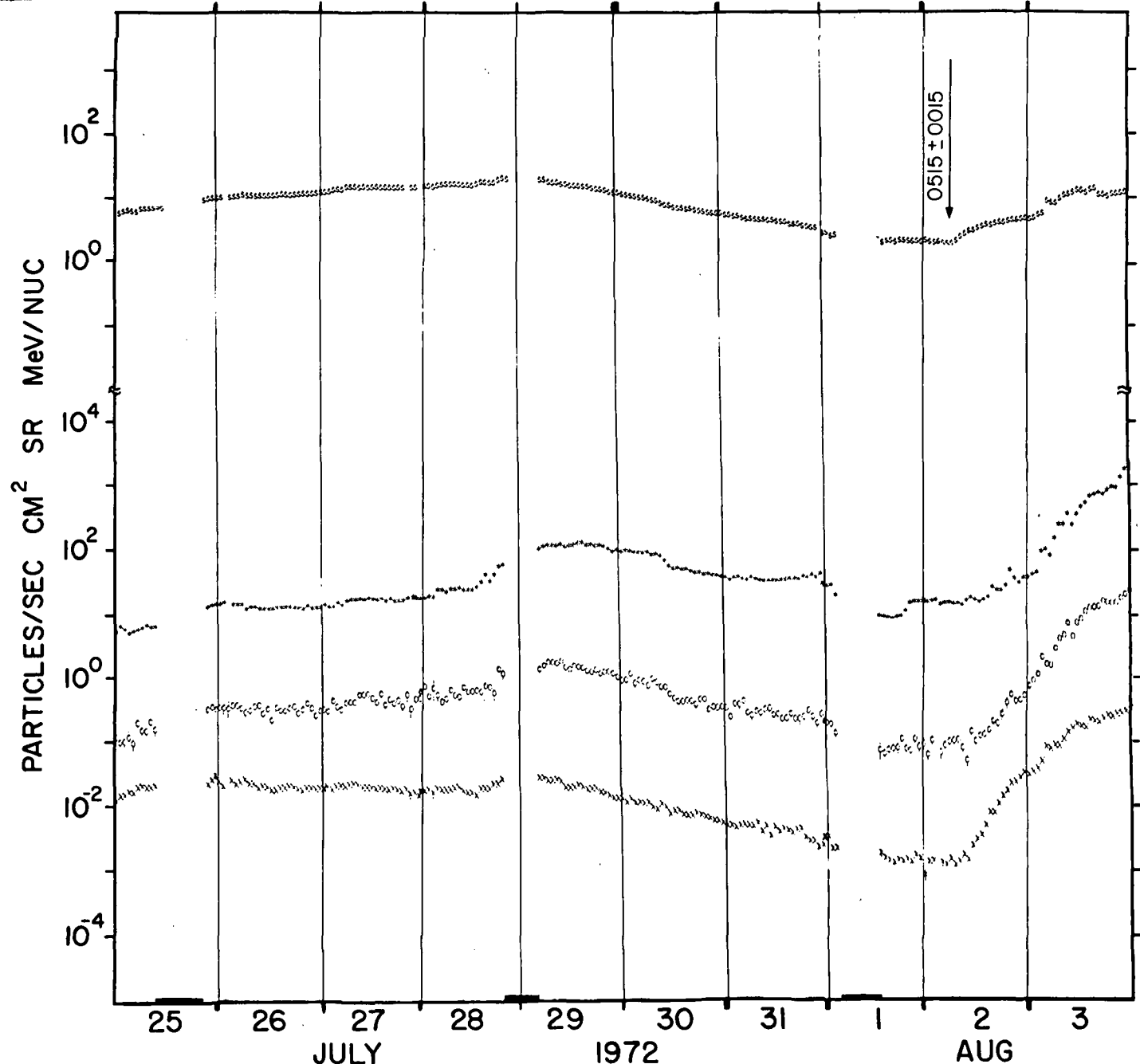
- 96 -
\$.5-1.1 MeV ELECTRONS X .9-1.5 MeV PROTONS O 6-19 MeV PROTONS X 19-80 MeV PROTONS



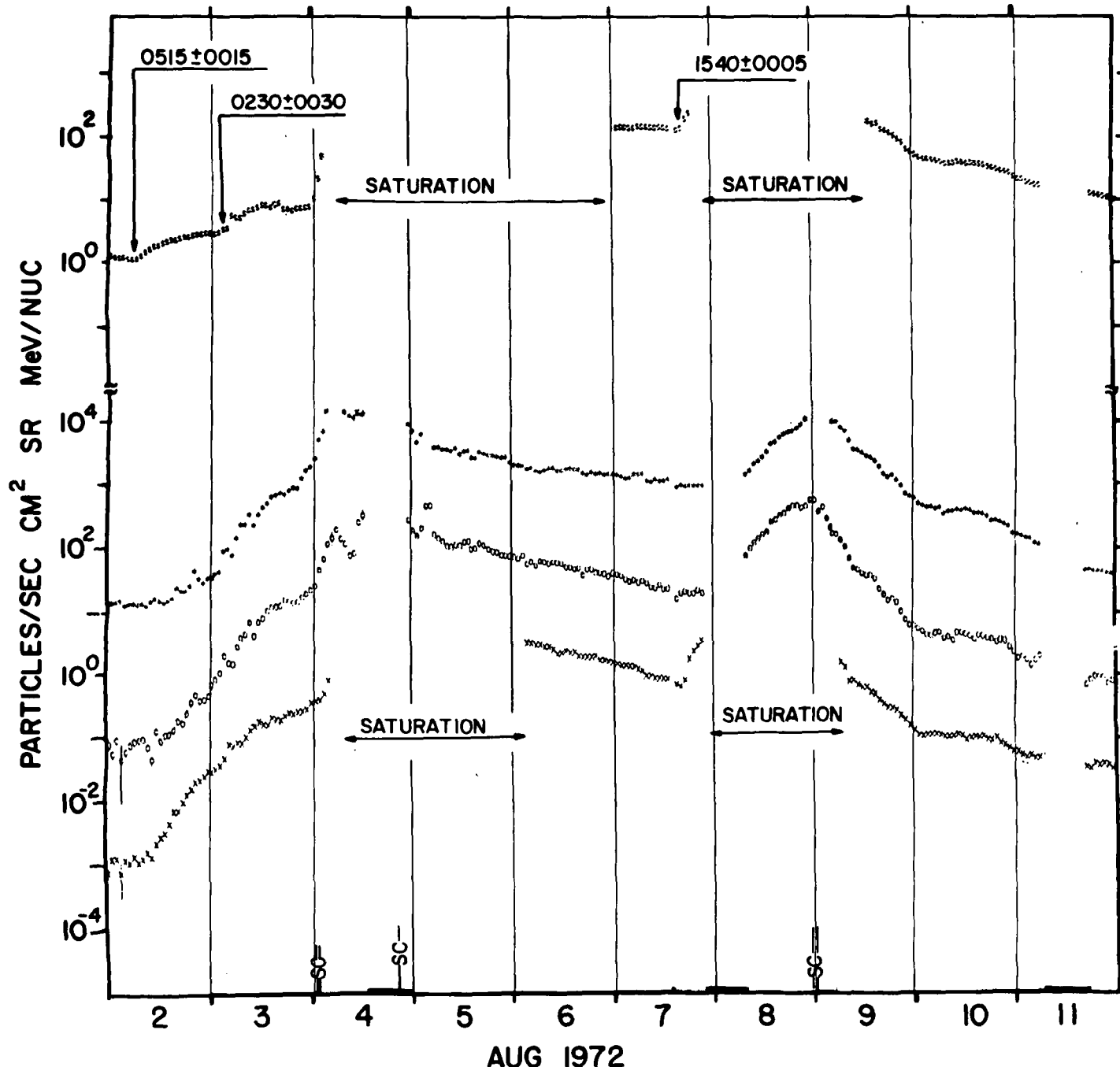
S.5-1.1 MeV ELECTRONS X .9-1.5 MeV PROTONS + 6-19 MeV PROTONS X 19-80 MeV PROTONS



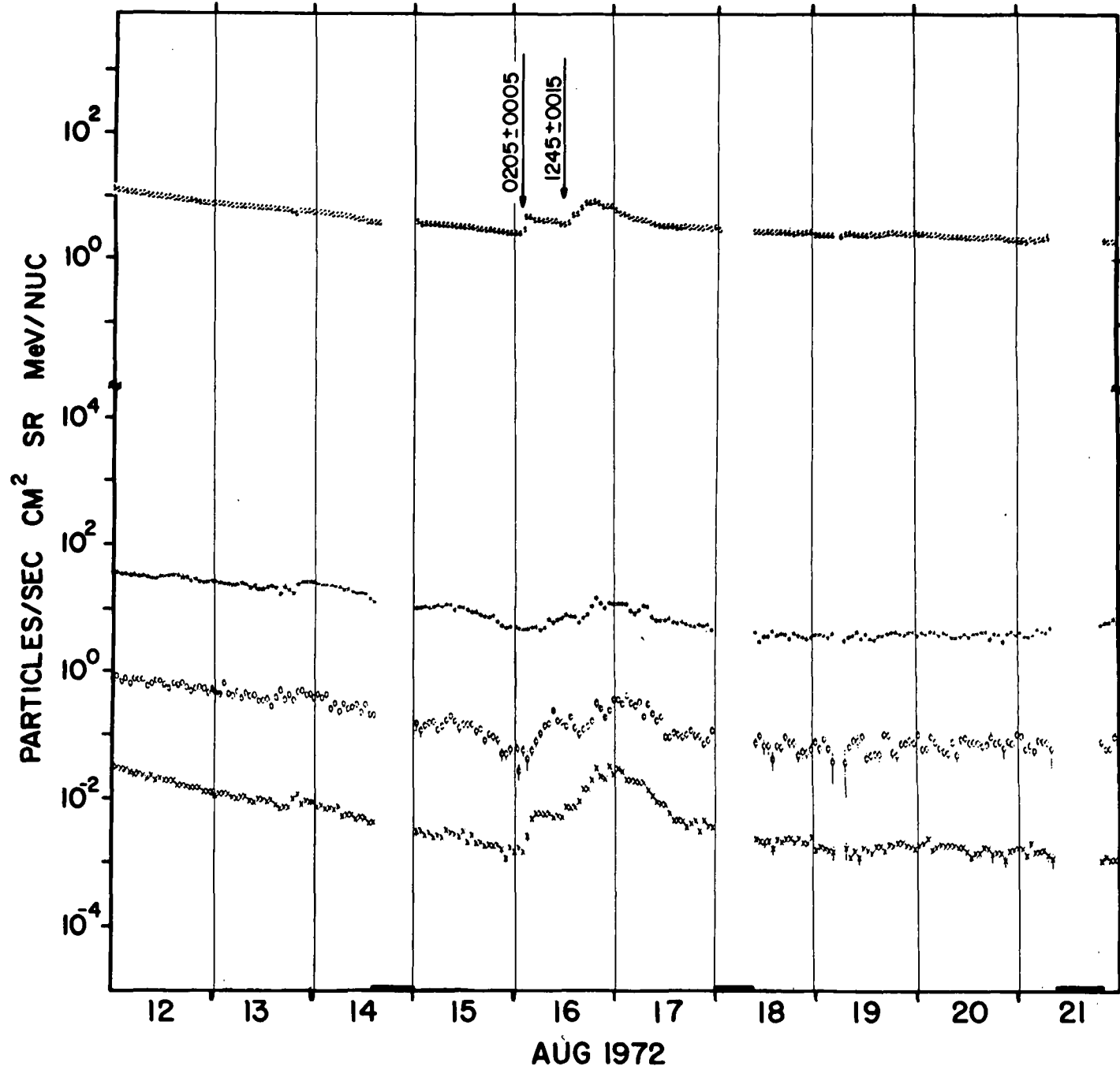
.5-1.1 MeV ELECTRONS X .9-1.5 MeV PROTONS \diamond 6-19 MeV PROTONS X 19-80 MeV PROTONS



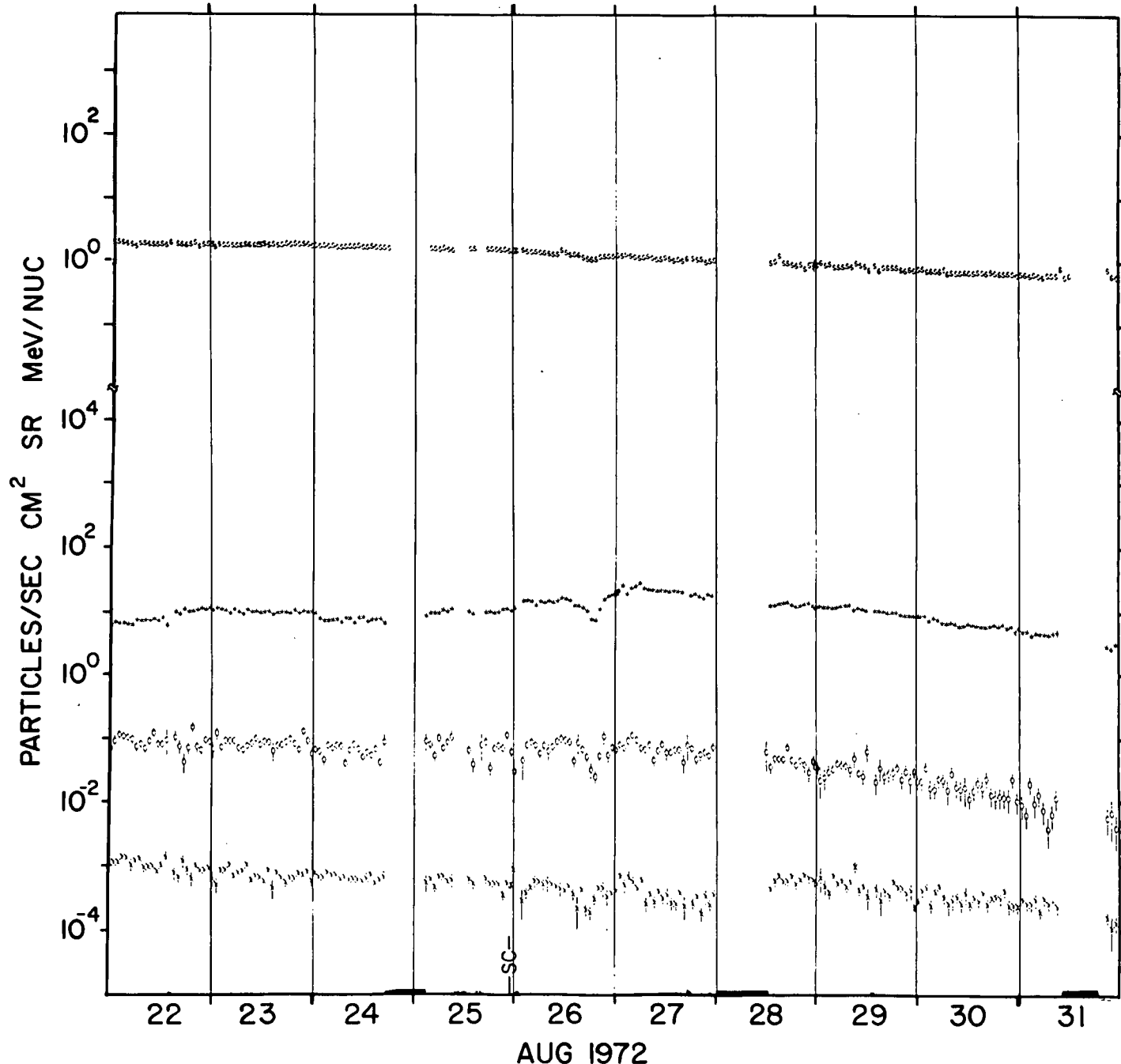
5.5-1.1 MeV ELECTRONS X .9-1.5 MeV PROTONS + 6-19 MeV PROTONS X 19-80 MeV PROTONS



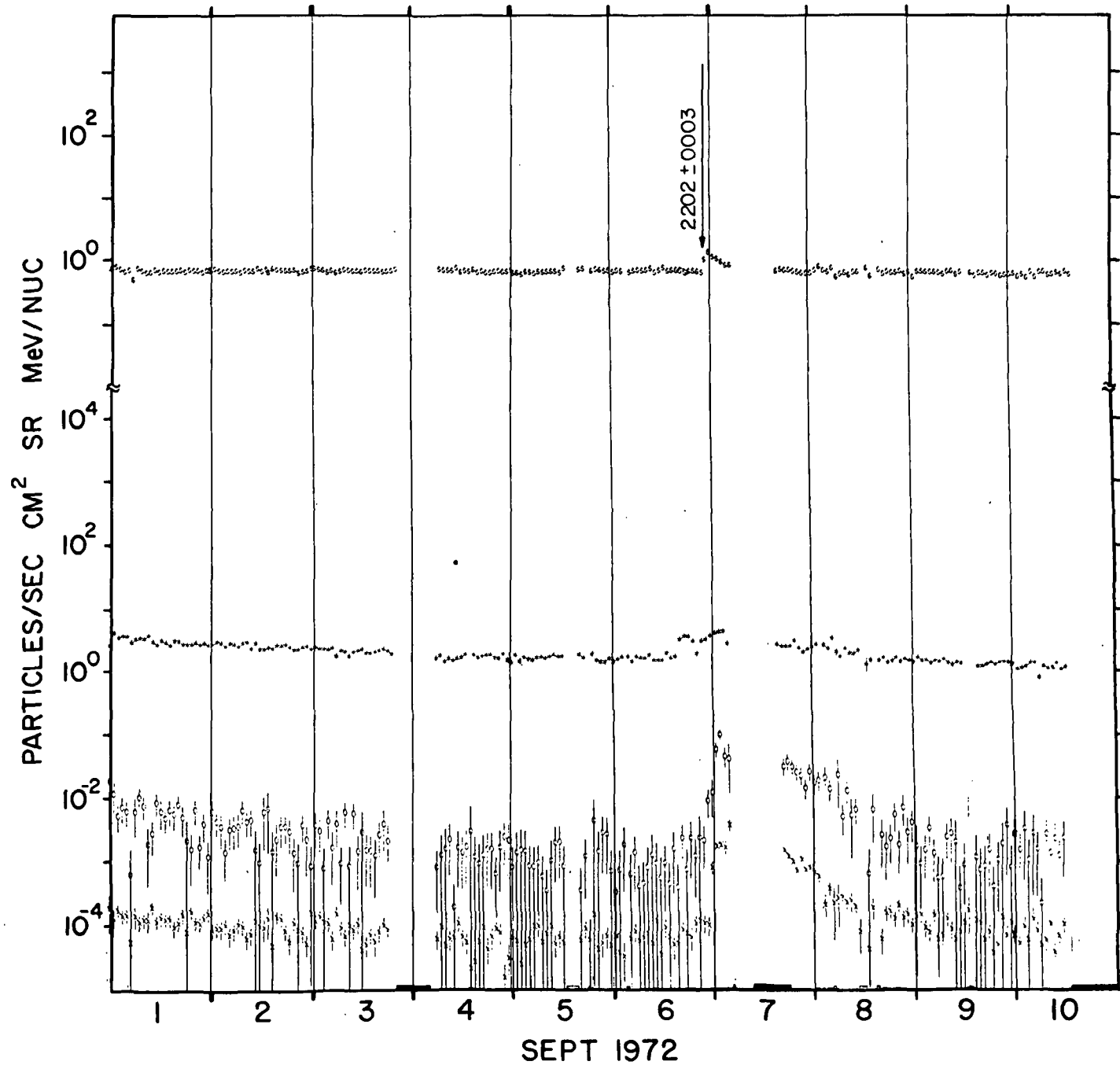
\$.5-1.1 MeV ELECTRONS X .9-1.5 MeV PROTONS ♦ 6-19 MeV PROTONS X 19-80 MeV PROTONS



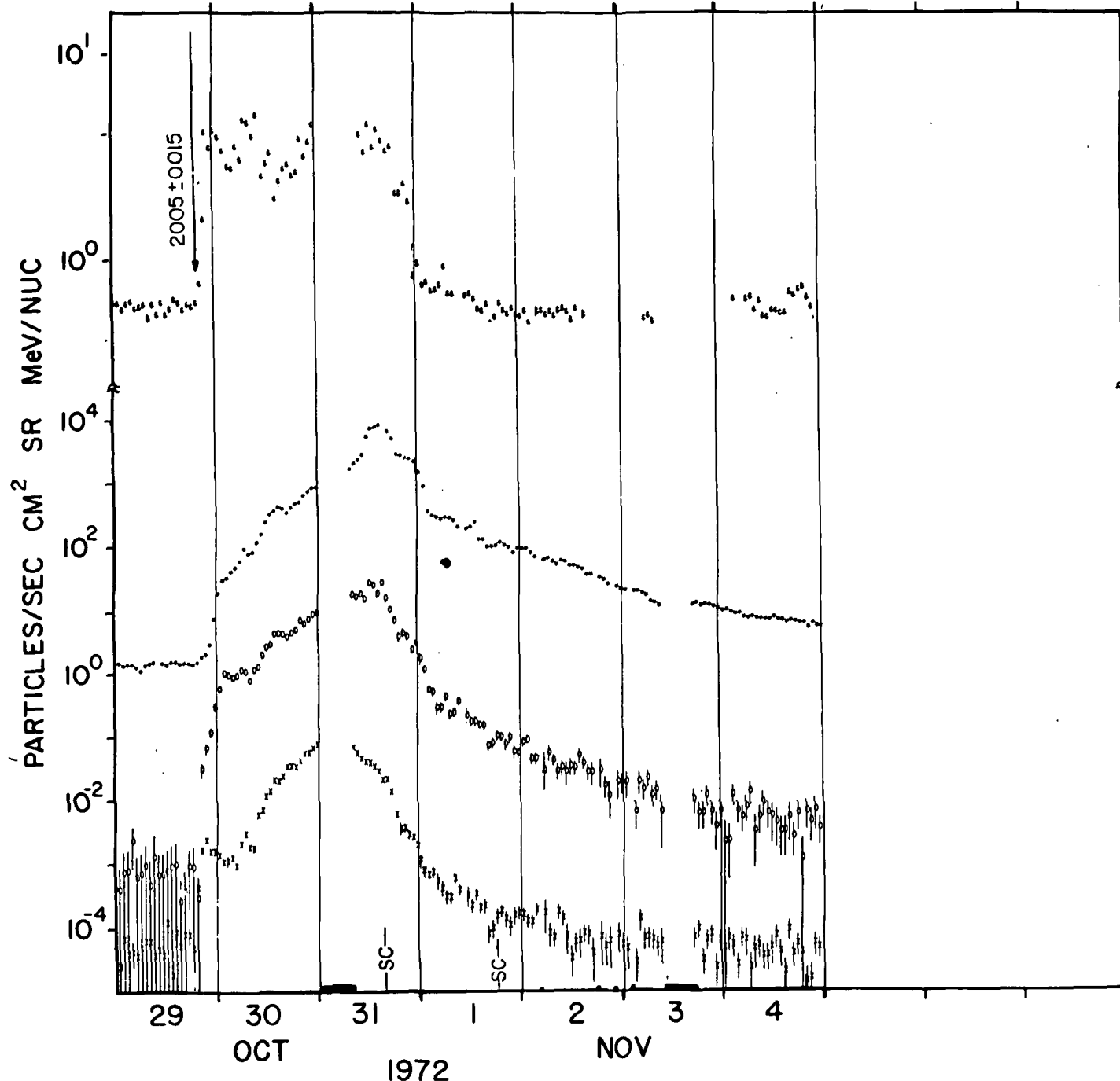
\$.5-1.1 MeV ELECTRONS X .9-1.5 MeV PROTONS Ø 6-19 MeV PROTONS X 19-80 MeV PROTONS



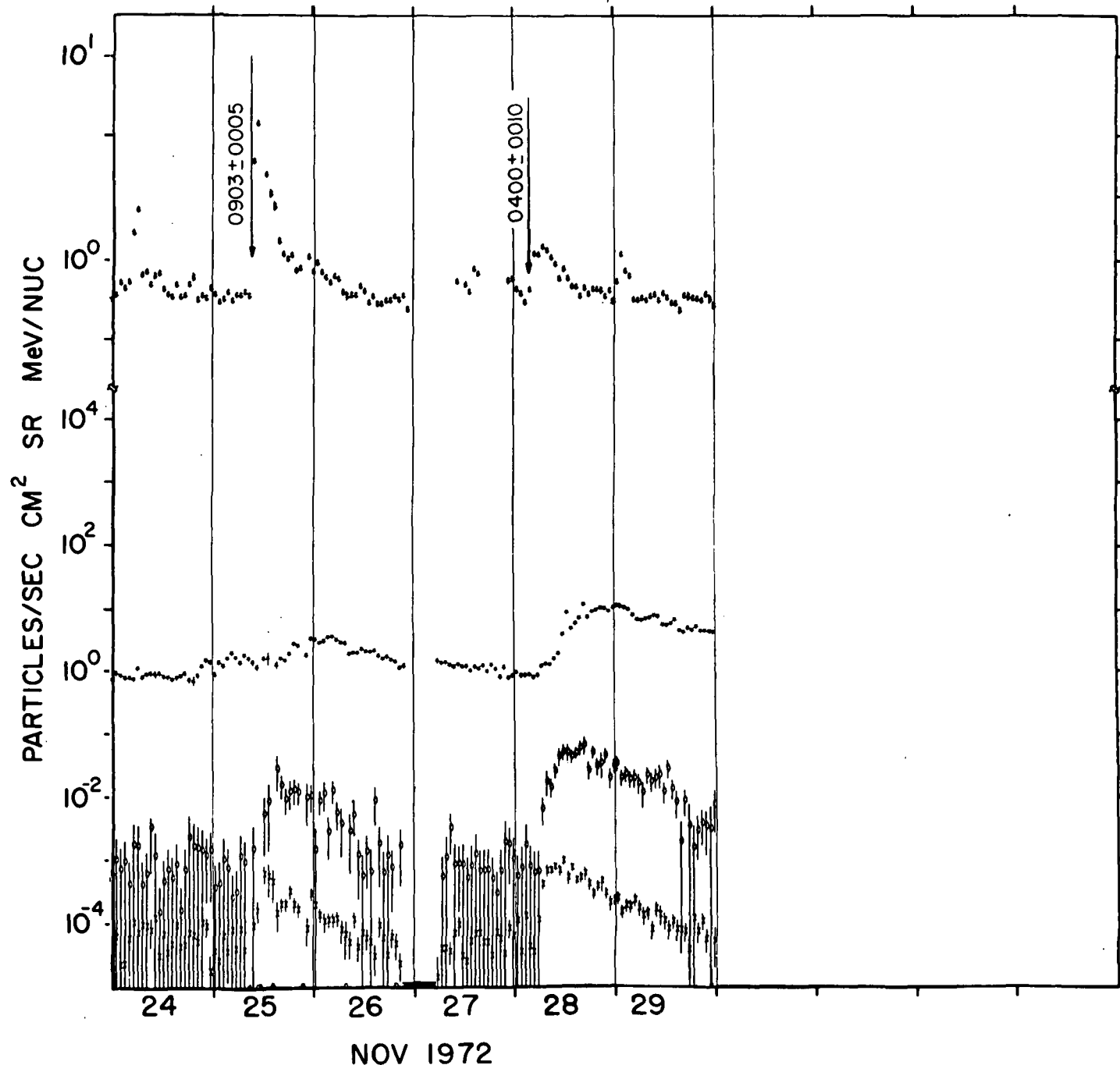
.5-1.1 MeV ELECTRONS X .9-1.5 MeV PROTONS 6-19 MeV PROTONS X 19-80 MeV PROTONS



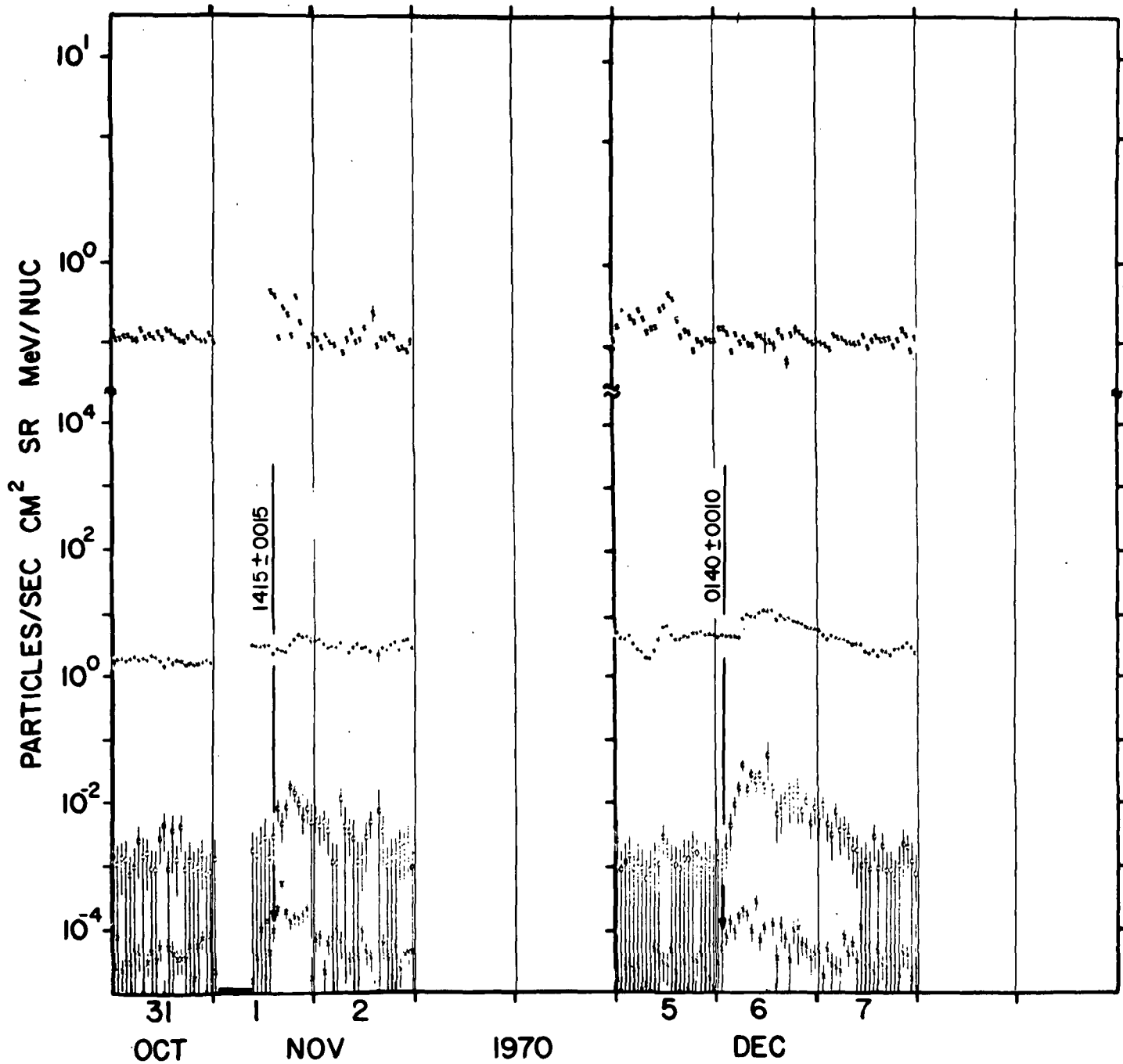
- 103 -
\$.5-1.1 MeV ELECTRONS X .9-1.5 MeV PROTONS 6-19 MeV PROTONS X 19-80 MeV PROTONS



\$.5-1.1 MeV ELECTRONS X .9-1.5 MeV PROTONS • 6-19 MeV PROTONS X 19-80 MeV PROTONS



5.5-1.1 MeV ELECTRONS X 9-1.5 MeV PROTONS 0 6-19 MeV PROTONS X 19-80 MeV PROTONS



\$.5-1.1 MeV ELECTRONS X .9-1.5 MeV PROTONS O 6-19 MeV PROTONS X 19-80 MeV PROTONS

